Analysis and design of Piezoelectric sonar transducers.

Rodrigo, Gerard Christopher

For additional information about this publication click this link.
http://qmro.qmul.ac.uk/jspui/handle/123456789/1712

ANALYSIS AND DESIGN
OF
PIEZOELECTRIC SONAR TRANSDUCERS

Gerard Christopher Rodrigo
Department of Electrical and Electronic
Engineering,
Queen Mary College,
London E.1.

Thesis presented for
the Degree of Doctor of Philosophy
of the
University of London

August 1970

ABSTRACT

In this study techniques are developed for the analysis and design of piezoelectric sonar transducers based on equivalent circuit representations.

For the purposes of analysis, equivalent circuits capable of accurately representing every element of a transducer in the full operating frequency range, are developed. The most convenient fashion in which these equivalents could be derived is also discussed. For the purposes of design the accurate equivalents are approximated by L-C-R circuits. The limits of both representations are discussed in detail.

The technique of analysis developed is capable of determining the frequency characteristics as well as the transient response to any electrical or acoustic input which can be specified analytically or numerically in the time domain.

The design technique is based on the formulation of a ladder-type generalized circuit incorporating the essential components of any transducer. The generalised circuit is then used to extract particular bandpass filter designs which possess wide passbands and which are mechanically realizable. By this procedure it is found possible to design transducers exhibiting bandwidths of around 100%.

The performance of a 'test' transducer constructed to verify both analysis and design theories is also discussed.

ACKNOWLEDGEMENTS

CONTENTS

LIST OF MAIN SYMBOLS

a	Radius of radiating face
A	Cross-sectional area normal to the direction of propagation of longitudinal waves
B	Inverse of the bandwidth β
c	Velocity of longitudinal waves
$c_e =$	$c(1-k_{33}^2)^{\frac{1}{2}}$; effective velocity in a ceramic stack
C	Generic symbol for electrical capacitance and mechanical compliance in the impedance analogy
C_b	Bond compliance
C_c	Low frequency compliance of a ceramic stack
C_o	Electrical capacitance of a ceramic segment
d_{33}	Effective component of the piezoelectric tensor (strain/field at constant stress)
D	Electric flux density
E	Electric field
f	Frequency
$f_o =$	$(f_1 f_2)^{\frac{1}{2}}$; centre frequency
f_1	Cut-off frequency at lower half-power point
f_2	Cut-off frequency at upper half-power point
f_r	Frequency of resonance
F	Complex representation of force
g_{33}	Effective component of the piezoelectric tensor (electric field/stress at constant D)
G	Electrical conductance
i	Instantaneous value of current
I	Complex representation of current
$j =$	$(-1)^{\frac{1}{2}}$
$k =$	$2\pi/\lambda$; wave number

$$k_{33} = d_{33}/(S_{33}^E \cdot \epsilon_{33}^T)^{\frac{1}{2}}$$

k_{eff} Effective electromechanical coupling factor

k_{ij} Coupling factors associated with filter circuits

$K = k_{eff}/(1 - k_{eff}^2)^{\frac{1}{2}}$;   measure of effective coupling

K_o Low frequency value of K

L Generic symbol for electrical inductance and mass in the impedance analogy

L_r Mass of the radiating head

$M = \{C/(C+C_b)\}^{\frac{1}{2}}$;   correction factor for bonding

p Number of segments in a ceramic stack

P Power radiated or absorbed from the supply by a transducer

P_m Maximum power that can be delivered from a given supply (see equation (4.2))

q_a Quality factors associated with filter circuits

Q_m Output or mechanical Q of a transducer

r Terminating resistance of normalized filter circuits

R Generic symbol for electrical and mechanical resistance and in particular radiation resistance

R_g Generator resistance

R_r Radiation resistance

s Laplace transform variable

S_{33}^D Effective component of the elastic compliance tensor at constant D

$S_{33}^E = S_{33}^D/(1-k_{33}^2)$;   effective component of the elastic compliance tensor at constant E

t Time

T Stress

u Instantaneous velocity

v Instantaneous voltage

V		Complex representation of voltage
V_g		Supply voltage
x	=	$2ak$
X		Length in the direction of propagation of longitudinal waves
X_r		Radiation reactance
Y		Generic symbol for admittance
Y		Young's modulus
Z		Generic symbol for electrical and mechanical impedance
Z_o	=	ρAc; mechanical characteristic impedance
Z_r		Radiation impedance
β	=	$(f_2-f_1)/(f_1f_2)^{\frac{1}{2}}$; fractional bandwidth
δ		Dirac delta function
ϵ_{33}^T		Free dielectric constant
λ		Wavelength of longitudinal waves
μ		Function of coupling (see equation (4.40))
ξ		Particle displacement
ρ		Density
ϕ		Electromechanical transformation ratio
χ		Packing factor of a transducer array
ω	=	$2\pi f$; angular frequency
ω_o, ω_r etc.		$2\pi \times$ corresponding frequency (see above)
$\bar{\omega}$		Actual centre frequency of a normalized filter network

CHAPTER I

INTRODUCTION

1.1. Aims and Scope of Study

The objectives of this study are twofold. First
the development of a general technique of analysis applicable
to piezoelectric sonar transducers, based on electrical
equivalent circuits which accurately represent the transducer
in the sonic range. Second, the investigation of the
possibility of extending the bandwidth of piezoelectric
sonar transducers, by a systematic design technique based on
equivalent circuits.

The scope of the study is restricted to the commonly
used extensional type transducers, which employ longitudinal
mode operation of the main constituent mechanical elements.

1.2. Use of Equivalent Circuits

The analysis of complex electromechanical systems,
by means of the direct solution of the intrinsic differential
equations, is fraught with difficulties. The preferred
and well-established method of attack is to formulate the
related 'steady-state' or frequency domain problem in terms
of an analogous electrical circuit. The latter problem is
generally much more tractable on account of the powerful and
well-developed techniques of electrical circuit theory.
The recently developed method of modern systems theory,
employing the state-space formulation, is advantageous in
that it finds the time domain solution directly, while

simultaneously tracing all the variables. At present,
however, its scope is severely limited in comparison with
the equivalent circuit technique. A further advantage of
the equivalent circuit method is that once the basic
analogies are set up, it is usually much easier to form the
equivalent circuit than to derive the intrinsic system
equations. Thus in sonar transducer design and analysis
in general and in this study in particular, the equivalent
circuit method is used. Where required, the time domain
solutions are obtained from the steady state responses by
inverse Fourier transformation.

In the formulation of a circuit representation of a
mechanical system, two alternatives are possible: depending
on whether the impedance analogy or the mobility analogy is
used. The two alternatives, however, are dual networks
and easily interconvertible. The subject of mechanical
analogies is briefly dealt with in section 2.2. In this
study both analogies are employed, depending on suitability
for a particular purpose. For the sake of convenience,
however, equivalent circuits are written in the impedance
analogy, unless specifically stated to the contrary.

Until quite recently, most sonar transducer
studies[1-3] have employed the approximate lumped element
model; a series resonant circuit in parallel with the
electrical capacitance. The elementary theory of transducer
design and operation, including the derivation of this
approximate equivalent circuit, is outlined in section 2.4.

The inadequacies of this representation, however, had been felt as far back as the Second World War, in the light of greater demands on power handling capacity, bandwidth and frequency of operation. Increasing discrepancies between predicted and measured performance has now made imperative the use of more accurate representations, valid throughout the operating frequency range.

The first attempts at updating the simplified equivalent circuit, consisted of corrections for the losses in the ceramic[2], bolt and bond compliances[4] and even for the distributed nature of the ceramic and end mass properties[5]. These corrections have not proved to be of much use as they were still based on the approximate lumped equivalent. Recently, however, a successful analysis routine based on an accurate representation of all transducer components, has been briefly outlined by Becken[6]. The method involves the solution of a complex equivalent circuit, which is only feasible as a result of the development of high speed, digital computers.

Thus, the primary task of this study is the development of accurate equivalent circuits to represent every element of a composite transducer in the full operating frequency range. This is done in Chapter 3, together with the derivation of the geometric limits on the elements to satisfy a prescibed accuracy of representation. These circuits are such that they account for the distributed mass and compliance of both piezoelectric and non-piezoelectric elements, wherever necessary. The effects of the extra compliance introduced by the resin bonds of a ceramic stack

have also been derived, it is believed, for the first time.
For the purposes of design, the lumped element approximations
of the accurate equivalent circuits are derived as well in
Chapter 3.

The success of any analysis technique ultimately
hinges on the accurate circuit representation of 'radiation
loading' which is the reaction of the fluid medium on the
vibrating piston. The accurate representation of the
radiation loading in arrays has been made possible by the
recent work of Morris[28] on the average radiation impedance
of regular plane arrays. Morris' results are scrutinized
in section 3.7 and recast in a form suitable for analysis
and design, as an equivalent constant 'mass' and resistance.

The accuracy of the complete transducer representation
is estimated at within $\pm$ 5% in analysis. For the purposes
of design, however, a margin of 10% error is tolerated to
effect the lumped element reduction. The frequency range
in which the equivalent circuits and the above estimates are
valid is 0-15 kHz, it being assumed that the upper cut off
frequency of any practical transducer is under 15 kHz.

A peculiarity of the accurate equivalent circuits
developed in Chapter 3, is the trigonometric frequency
dependence of individual impedances. Computationally,
however, this is of little consequence and these elements
are no more difficult to handle than the more orthodox
circuit elements.

1.3. Analysis

The technique of analysis employed in this study is based on the accurate equivalent circuit representation outlined above. Since it is found possible to represent all transducer components to within 5% accuracy in the full frequency range of interest, the technique is considerably superior to the approximate methods used formerly. Though a similar representation has been used by Becken[6], it is believed that the intersegment bonding in the ceramic, has not been accounted for in his equivalent circuit.

The impedance analogy equivalent is generally more convenient for the purpose of analysis than the mobility equivalent. In this study the impedance equivalent of the complete transducer is derived from the mobility equivalent which is formulated first. The formulation of the mobility analogue and its transformation to the impedance form, are both relatively simple operations. The direct formulation of the impedance equivalent on the other hand, is a formidable task in the case of complex mechanical systems. Consequently the procedure adopted here is an improvement on current analysis practice (including that of Becken) which employs the latter method.

. Further it has been found possible to cast the impedance analogy representation of any extensional type transducer as a slightly modified ladder network. Since this network could be analysed almost as easily as a ladder network, the resulting circuit analysis problem is

considerably simpler than that encountered by Becken.
This circuit is used to calculate the frequency
characteristics of the transducer.   The derivation of the
complete equivalent circuit and its subsequent analysis is
described in Chapter 5.

The derivations of the transient responses of the
transducer to voltage step and other inputs, is also
considered in Chapter 5.   The step response is derived from
the frequency characteristic by inverse Fourier trans-
formation.   The response to other inputs is then obtained
from the step response by time domain convolution with the
derivative of the input.   The great advantage of this method
is that it is applicable to any system whose frequency
characteristic can be computed or measured.   Further, the
convolution technique is able to handle any input which can
be specified algebraically or numerically, in the time
domain.

Analysis has also been performed with the approximate
lumped element representation of transducers by means of a
simpler method.   This method is briefly outlined in section
5.4.   The scope of the method is restricted to ladder
networks consisting of conventional electrical elements and
formulated in an impedance and frequency normalized form.
Though this method is inferior to the above analysis technique,
it is extremely useful in computing the characteristics of
the normalized filter networks on which design is based.

Transcripts of the analysis routines, which are written in Fortran, are included as Appendices.

1.4. Design Theory

The criteria, on which the design of sonar transducers attempted here is based, are the realization of as large a fractional bandwidth as possible, with reasonably steady values of input impedance and group delay in the paseband. Wide operating bandwidths are needed for the achievement of better 'object resolution' and for more efficient signal processing against background noise and reverberation[1,3]. Since the characteristics of the supply amplifiers are affected by the load, it is also necessary to ensure that the input admittance of the transducer does not fluctuate too widely. The group delay is an important factor in array operation since the directivity of the array is controlled by the relative phase of the electrical inputs.

The subject of transducer design is treated systematically in Chapter 4. The approach adopted there is to formulate a generalized ladder-type equivalent circuit description of possible transducers and to then derive the conditions for broadband operation. The first step in this process is to reduce the transducer essentials to their simplest form. The practical constraints imposed by the transducer essentials and their consequences in terms of optimum performance, are then derived from the generalized circuit. Finally, it is attempted to synthesize realizable

broadband circuits, the performance of which approach the theoretical optimum.

The derivation of realizable broadband circuits is not, however, attempted on an a priori basis of transfer function synthesis. Rather, the store of available filter design data is scanned to pick out those circuits which satisfy the design criteria and which could be built around the transducer essentials. The parameters of the suitable filter circuits are then adjusted within the limiting constraints for optimum performance.

In practice the choice of suitable filter circuits, is severely limited by the practical constraints. It is shown in section 4.1, that both high pass and low pass filter types are excluded. Of available bandpass circuits, only two types are suitable - the 'analogous' or 'canonic' circuits derived from the canonic low pass to band pass transformation, and the coupled resonator bandpass circuits. The circuits could also be based on a variety of different lowpass approximations (such as Butterworth, Chebychev, etc.) and be of two pole or three pole construction. Circuits of order higher than three pole are excluded on account of their complexity.

In section 4.5 the advantages and disadvantages of all these possibilities are investigated and a procedure is evolved to choose the most suitable of them for mechanical realization. It is found that the three pole coupled resonator designs based on equally terminated Butterworth

and low-ripple Chebychev lowpass prototypes, are the most convenient to realize mechanically. The performance characteristics of the Butterworth design are, however, superior to that of the Chebychevs.

It is believed that the procedure described above is an original contribution to the design of piezoelectric sonar transducers. The extraction of transducer designs satisfying prescribed performance criteria from a generalized equivalent circuit description with reference to realizable broadband filter circuits, has not been previously attempted. Furthermore, the systematic design procedure developed, is a considerable improvement on conventional design practice, which is somewhat empirical in nature.

By the procedure outlined above, it is found possible to design transducers possessing bandwidths of the order of 100%. This value is a great improvement on the bandwidths of around 20% realized with conventional designs. The broadband designs are also not much more difficult to construct than the conventional types.

1.5. Experimental Verification of Theory

A 'test' transducer was constructed and tested to verify the equivalent circuit representation assumed in both analysis and design. The design was based on a predominantly mechanical, three pole Butterworth coupled resonator band pass filter. The test design is similar to but not identical to the transducer designed in Chapter 4.

The test transducer was also analysed by means of the analysis technique developed. The experimentally determined

characteristics are presented and compared with the computed results in Chapter 6. The difference between the predicted and measured performance, while not being of unacceptable magnitude (around 10%), is indicative of certain short-comings in the equivalent circuit representation. In section 6.2 it is attempted to locate the cause of this discrepancy. The design improvements inferred from the performance of the test transducer are incorporated in the transducer designed in section 4.6.

CHAPTER 2

PRELIMINARY CONSIDERATIONS

The theory of conventional sonar transducer design
and operation is well treated in the literature[1-3]. In
this chapter, it is proposed to merely outline the salient
features of the subject, to serve as an introduction to the
more rigorous and detailed treatment of subsequent chapters.
The chapter is introduced with a survey of piezoelectric
materials that have been used in sonar transducers and the
criteria which govern the optimum choice. This is followed
by a brief account of the mechanical analogies, on which
the equivalent circuit representations are based. The
elementary theory of composite sonar transducers is
presented in section 2.4 with details of the main
constructional features. This is preceded by the
derivation of the complete equivalent circuit representation
of the commonly employed 'length mode' excitation of a
uniform piezoelectric resonator. Finally the constructional
features of a ceramic stack designed for high power
operation are described.

2.1. Piezoelectric Materials for Sonar Transducers

Though a wide variety of transducer types are
possible, operational sonar equipment has up to now
incorporated either piezoelectric or magnetostrictive
transducer materials. The latter is beyond the purview of

this study.   The former could be divided into two types;
the naturally piezoelectric crystals and polarized ceramic.

Crystal devices have usually employed cut quartz,
Rochelle salt or ammonium dihydrogen phosphate (ADP).   Of
these, ADP was the most widely used until about 1956 when
the operating frequencies were generally in the ultrasonic
range.   Subsequently crystals have been largely displaced
by piezoelectric ceramics, which are more readily adaptable
to sonic range operation.   These are currently employed in
sonar devices as in most other high power applications.
The inferiority of crystals is broadly with respect to their
mechanical strength lower piezoelectric coupling, lower
permittivity and lower resistance to severe ambient
conditions[3].

The ceramics most commonly used are the barium
titanate types and lead zirconate titanate with trace
additives (the PZT-types).   Such ceramic materials are
strongly electrostrictive and exhibit the piezoelectric effect
on polarization.   This is effected by heating the cast
ceramic above the Curie temperature and allowing to cool under
a high electric field when remanent polarization is induced
in the direction of the field.   The properties of the
polarized ceramic are isotropic in directions perpendicular
to that of the remanent polarization.   The driving force or
voltage may be applied parallel to or perpendicular to this
direction, depending on which mode it is desired to excite.

The method of manufacture of the ceramic (casting) makes possible a variety of shapes and sizes. In most high power applications, however, it is customary to use solid cylindrical or tubular construction with axial polarization and excitation. The advantage of this mode (referred to as the longitudinal, length or bar mode with parallel excitation) is that it has the highest practically attainable electromechanical coupling coefficient. The coupling coefficient determines not only the fraction of energy 'coupled' mechanically but also the maximum attainable bandwidth.

Even within the range of available piezoelectric ceramics, a wide variation of properties is obtained. The coupling factor for instance ranges from around 0.4 (for barium titanate types) to 0.7 (for PZT types). For use in sonar transducers, as in all high power applications, the following ceramic properties are highly desirable[3,7].

1. High length mode coupling (see above).

2. Low dielectric loss. This is essential in high power applications to keep the ceramic temperature well below the Curie point. Efficiency is also affected, but this is too small to be of consequence.

3. High Curie temperature to reduce the risk of thermal depolarization by the dielectrically generated heat.

4. High temperature and time stability of the ceramic parameters.

Schofield[2] uses the expression $k^2_{33}/\tan\delta$ as a measure of the suitability of a particular ceramic for sonar

transduction.   Its highest value is obtained with PZT-4

or PXE-4 ceramics.   For these ceramics, the coupling factor

is around 0.7 and tanδ is below 0.02 under normal operating

conditions.   They also possess high Curie temperatures in

the region of 300 - 340 °C.

In spite of the obvious superiority of the PZT-4

types, barium titanate is often used on account of ease of

manufacture, especially when wide bandwidths are not desired.

2.2. Electromechanical Analogies

The use of analogous electrical circuits for the

solution of vibration problems of mechanical systems, is

well established[8-10].   The impedance (or Z) analogy sets

up the correspondence

$$
\begin{array}{lll}
\text{force} & - & \text{voltage} \\
\text{velocity} & - & \text{current} \; .
\end{array}
$$

The more recent mobility (or Z^{-1}) analogy employs

the alternative equivalence of

$$
\begin{array}{lll}
\text{force} & - & \text{current} \\
\text{velocity} & - & \text{voltage} \; .
\end{array}
$$

The consequences of these two analogies, in terms of

mechanical element-electrical element correspondence, follows

directly from the above relations.   The derivation of

mechanical analogies is well treated in the literature[8-10].

The most important of these equivalences are set out

schematically in Figure 2.1.   Here, all elements are

considered in relation to a reference frame, viz., the

'mechanical earth', which is identified with the electrical

earth line in the mobility analogy.   The instantaneous

Schematic representation	Analogous circuit representation		Description and Defining equations
	Mobility Analogue	Impedance Analogue	

Rigid Mass;

$$u_1 = u_2$$

$$F_1 - F_2 = M \frac{du_1}{dt}$$

Series Compliance;

$$F_1 = F_2$$

$$u_1 - u_2 = C_m \frac{dF_1}{dt}$$

Parallel Compliance;

$$u_1 = u_2$$

$$u_1 = C_m \frac{d(F_1 - F_2)}{dt}$$

Constant force mechanical resistance

$$F_1 = F_2$$

$$u_1 - u_2 = R_m F_1 = G_m F_1$$

Constant velocity mecha.ical r sistance

$$u_1 = u_2$$

$$F_1 - F_2 = G\, u_1 - R_m u_1$$

No mecha·ic l analogue of ·nese electri l ements

Figure 2.1- Electrical Analogies of Basic Mechanical Elements

values of force and velocity, F and u respectively,

used in Figure 2.1 could be replaced by the r.m.s. values,

provided the time differentials in the defining equations

were also replaced by a factor $j\omega$, where ω is the angular

frequency.   It is important to note that the correspondence

indicated in the diagram between the directions of 'input

force' and input current, etc., implies the 'compression

positive' rule for stress, which is assumed throughout the

text.   The two terminals of every mechanical element are

marked by the small circles.   The $\curlyvee$ configuration is used

in the schematic representation of mass, because the second

terminal of any rigid mass is the reference earth[10].

The following conclusions from the presentation of

Figure 2.1 are of particular relevance to this study.

1.   Since the impedance equivalent is the dual or

resistance reciprocal of the mobility equivalent in every

case, the two representations are easily inter-convertible.

In this respect it is useful to note that on conversion, a

node is replaced by a mesh and vice versa.

2.   The most striking feature of the mobility anaology

is the preservation of the topological form of the schematic

representation, even as regards mechanical open and short

circuits (which are not shown in the figure).   Since this

greatly facilitates the derivation of equivalent circuits,

the equivalents of complex mechanical systems are always

initially 'written' in the mobility analogy.   The topological

similarity is really a reflection of the intrinsic harmony

of the force-current, velocity-voltage analogy.   Whilst

velocity and voltage are both measured with respect to some

reference, force and current are 'absolute' measures.
The preservation of an easily identifiable reference is in
fact an added advantage of this particular analogy.

3. A short circuit to earth is effected by the attachment
of a very large, rigid mass to the relevant terminal. The
more obvious method of 'connecting to earth' through a very
low compliance is no solution for it then poses the problem
of locating a satisfactory earth, which again has to be a
large rigid mass.

4. An open circuit is realized either by a free terminal
or a highly compliant support.

5. The series capacitance in the mobility analogy and
the parallel inductor in the impedance representation have
no mechanical counterpart. This is a serious limitation
from the standpoint of circuit synthesis employing mechanical
elements.

Though the superiority of the mobility analogy has
been demonstrated in general[11, 12], the impedance analogy
continues to be widely used in the study of piezoelectric
devices. This is partly because the use of the latter
obviates the need for the inclusion of a gyrator, which is
mandatory in the mobility representation of piezoelectric
devices (see section 5.1).

2.3. Derivation of the Equivalent Circuit of a Longitudinally Poled Piezoelectric Bar for Parallel Excitation (after Mason[16] and Redwood[14])

Figure 2.2. depicts the length mode excitation of
a uniform piezoelectric bar of area A and length X. The
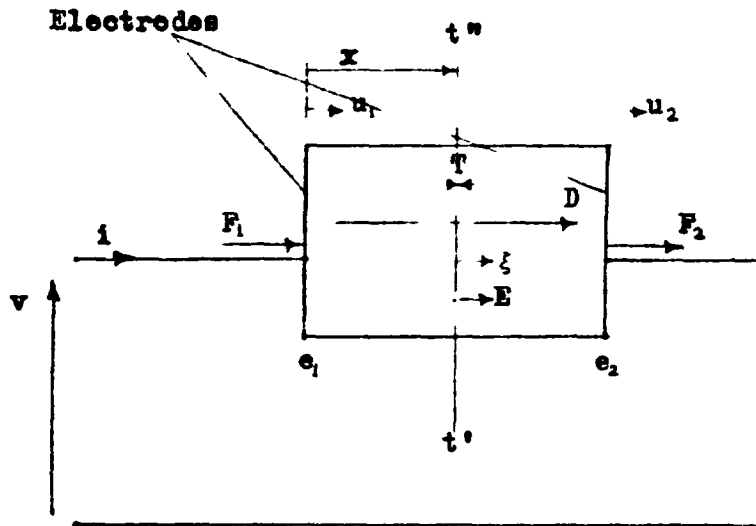exciting voltage v is applied across the electrodes $e_1 e_2$,

Figure 2.2- Parallel Excitation of Longitudinally
Polarized Piezoelectric Bar
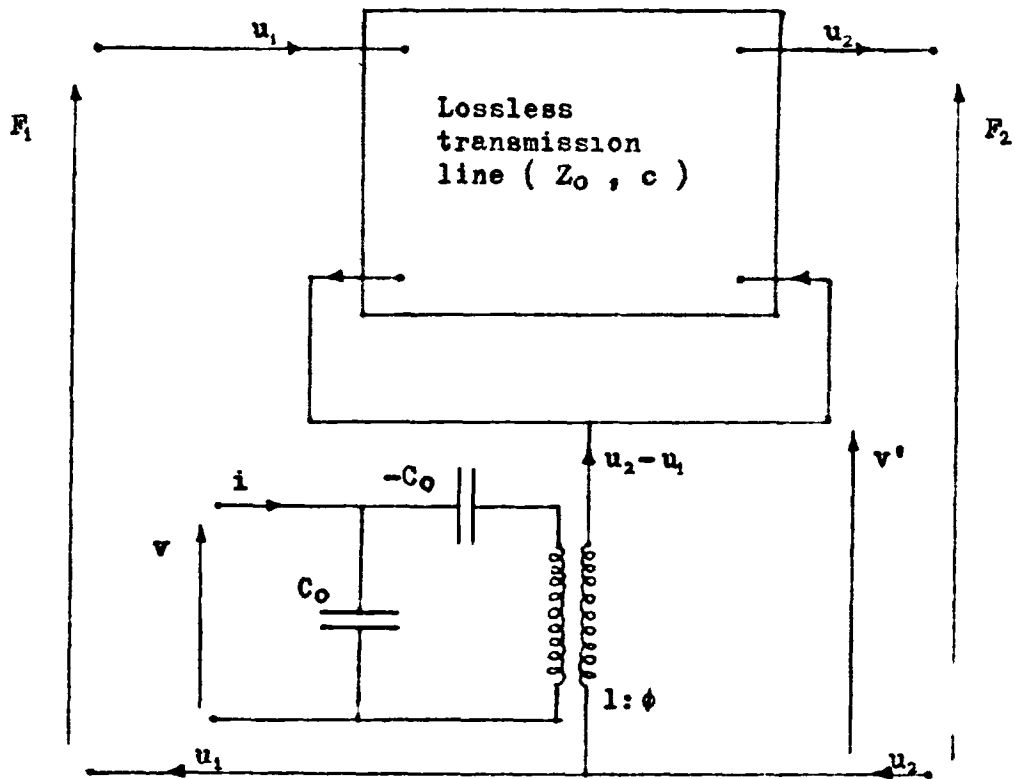
Figure 2.3- Equivalent Circuit of Piezoelectric
Bar of figure 2.2

which are also the mechanical boundaries of the bar. The electric field and the particle displacement at the section t't" are denoted by E and ξ respectively. T is the stress (compression positive) at t't" and D is the flux density throughout the bar. The forces and velocities at the boundaries are indicated in the figure. All variables are functions of position x and time t, except D, i and v which are dependent on t alone.

The piezoelectric equations for pure length mode excitation are shown[3] to be

$$\frac{\partial \xi}{\partial x} = g_{33}D - s_{33}^{D}T \tag{2.1}$$

$$E = \beta_{33}^{T}D - g_{33}T \tag{2.2}$$

where g_{33}, s_{33}^{D} are the relevant components of the piezo-electric tensor (electric field/stress at constant D) and the elastic compliance tensor at constant D respectively. β_{33}^{T} (= $1/\epsilon_{33}^{T}$) is the relevant component of the free dielectric constant. It is also easily demonstrated that

$$\frac{\partial T}{\partial x} = -\rho \partial^{2}\xi/\partial t^{2} \tag{2.3}$$

$$v = \int_{1}^{2} E \, dx \tag{2.4}$$

$$i = A \, dD/dt \tag{2.5}$$

where ρ is the density of the material. Differentiating equation (2.1) with respect to t and substituting u for the particle velocity $\partial \xi/\partial t$

$$\frac{\partial u}{\partial x} = - \frac{\partial}{\partial t}(s_{33}^{D}T - g_{33}D) \quad . \tag{2.6}$$

If T is replaced by F/A (where F is the total compressional force at the plane x) equations (2.3) and (2.6) are readily cast into the form

$$\frac{\partial u}{\partial x} = - S_{33}^D A^{-1}.\partial F'/\partial t \qquad (2.7)$$

$$\frac{\partial F'}{\partial x} = - \rho A.\frac{\partial u}{\partial t} \qquad (2.8)$$

where $F' = F - A.Dg_{33}/S_{33}^D$. $\qquad (2.9)$

Now equations (2.7) and (2.8) are similar to the equations for current and voltage on a lossless transmission line. Therefore the variables u and F' could be represented by the current and voltage on a lossless line of propagation velocity c and propagation constant Z_0 given by

$$c = (\rho S_{33}^D)^{-\frac{1}{2}} \qquad (2.10)$$

$$Z_0 = \rho Ac \qquad . \qquad (2.11)$$

Since the second term of the 'voltage' F' is independent of x, F' could be replaced by F, provided the lower end of the line was biassed to the 'voltage v' above the mechanical earth (see Figure 2.3) where

$$v' = AD.g_{33}/S_{33}^D \qquad . \qquad (2.12)$$

This converts the line into a true impedance analogy representation of the force and particle velocity along the length of the piezoelectric bar. Also, substituting for E in equation (2.4) from equation (2.2) and eliminating T and D (by means of equations (2.1) and (2.5)) it is easily shown that

$$\frac{dv}{dt} = i/C_o - (u_2 - u_1)g_{33}/s^D_{33} \qquad (2.13)$$

where $\qquad C_o = A/\{X(\beta^T_{33} + g^2_{33}/s^D_{33})\}$. $\qquad (2.14)$

The rest of the equivalent circuit is derived from equations (2.12) and (2.13) to yield the complete representation of Figure 2.3 where

$$\phi = C_o g_{33}/s^D_{33} \qquad (2.15)$$

is the conversion ratio of the electromechanical transformer.

A more detailed derivation of the equivalent circuit is given by Redwood[14] and Martin[17].

2.4. Elementary Theory of Conventional Composite Transducers

The simplest method of piezoelectric sound generation is the excitation of a single ceramic bar (such as depicted in Figure 2.2) at its fundamental resonance. In practice, the ceramic block is mass loaded at the ends, in the manner illustrated by the prototype of Figure 2.4. The advantages of this arrangement are as follows:

1. The natural resonant frequency is lowered by the extra mass. It is thus possible to use shorter blocks of ceramic, which considerably reduce the manufacturing problems.

2. The ceramic is fully utilized unlike in the elementary resonator where only the central portion is active. Consequently the dielectric and mechanical dissipation is lower. The dynamic or effective coupling is also much higher and almost equal to the static value.
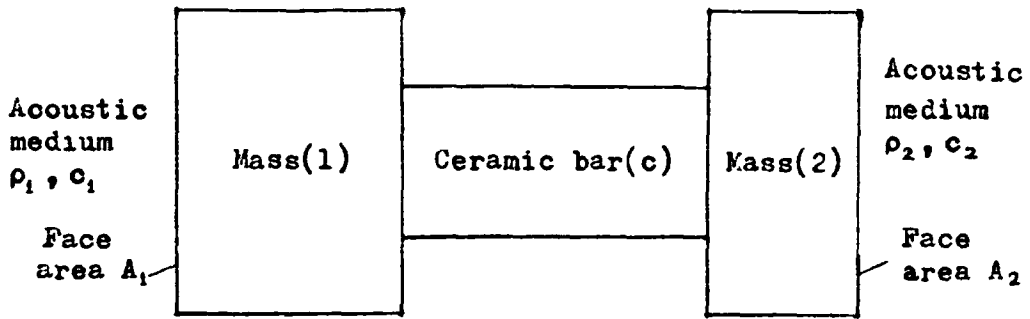
Figure 2.4- Diagram of Basic Composite Transducer
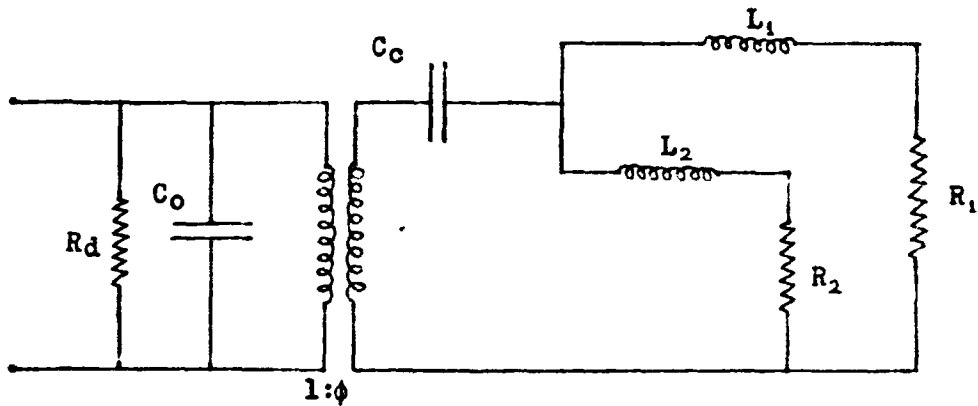
Figure 2.5- Equivalent Circuit of Basic Composite
Transducer
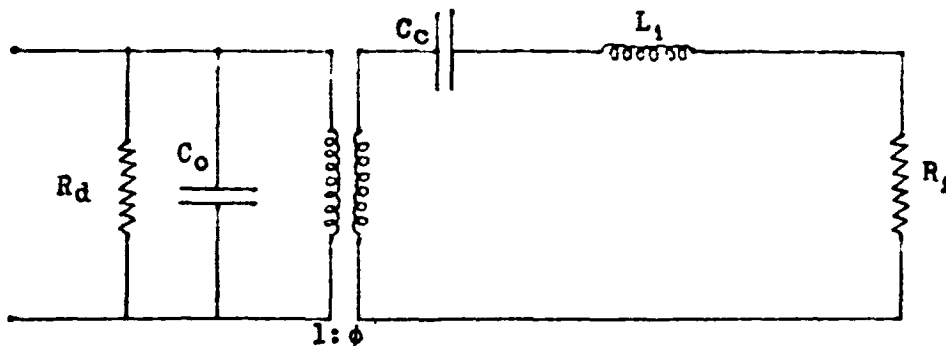
Figure 2.6- Simplified Equivalent Circuit of
Composite Transducer

3.   Since the radiating area is increased, a better
impedance match to a fluid medium such as water, is
possible.

4.   Heat dissipation problems are considerably reduced.

The (Z-analogy) lumped equivalent circuit of this
composite transducer, is given in Figure 2.5 (see section 3.3
for derivation).   The correspondence between the mechanical
elements and the circuit representation is indicated by the
suffices in the latter which correspond to the parenthesised
symbols of the former.   The two masses are represented by
L_1, L_2 and the ceramic compliance by C_c.   The radiation
load on either side is accounted for by R_1 and R_2.   In the
elementary theory of transducers, it is customary to neglect
the mass of the ceramic and assume plane wave radiation from
the two faces A_1, A_2 whence

$$R_1 = \rho_1 c_1 A_1, \qquad R_2 = \rho_2 c_2 A_2 \qquad . \qquad (2.16)$$

Here ρ, c refer to the density and velocity of propagation
of the fluid media.   The values of the electrical
capacitance C_o, the electromechanical transformation ratio
ϕ and the ceramic compliance C_c in terms of the basic ceramic
parameters, is given in section 3.2.   The dielectric loss
is accounted for by the resistance R_d.

In practical sonar transducers, one side (say 1) is
exposed to the fluid medium in which it is desired to transmit
sound.   The other (2), is commonly 'air backed'.   The mass
L_1 is then referred to as the radiating mass and L_2 as the
countermass.   Since the countermass is usually about an

order of magnitude greater than the radiating mass, the branch containing L_2, R_2 may be deleted from the circuit without incurring significant loss of accuracy in the vicinity of the resonance of C_c and L_1. The resulting circuit, that of Figure 2.6, is the one most commonly used in elementary analyses of composite transducers[2,3]. The most relevant results of such analyses are summarized below.

1. The operating (or centre) frequency of the transducer is given by

$$\omega_r^2 = 1/L_1 C_c \quad . \tag{2.17}$$

The approximate representation of Figure 2.6 is valid up to around ω_r, provided L_1 is an order of magnitude greater than the ceramic mass.

2. The mechanical or output Q is defined as

$$Q_m = \omega_r L_1/R_1 \quad . \tag{2.18}$$

For conventional designs Q_m is typically in the range 3-8.

3. If E is the electric field in the erami , it can be shown[3] that the p wer P_r per unit volume of the ceramic delivered to the mechanical side of the circuit is given by

$$P_r = \omega_r E^2 k_{eff}^2 \epsilon_{33}^T Q_m \quad . \tag{2.19}$$

Here k_{eff} is the effective coupling factor (see below).

4. The dielectric loss per unit volume of ceramic is

$$P_d = \omega E^2 \epsilon_{33}^T \tan\delta \tag{2.20}$$

where $\tan\delta = 1/\omega C_o R_d$.

5. The effective coupling of the transducer can be defined[2] as

$$k^2_{eff} = \phi^2 C_c / (C_o + \phi^2 C_c) \quad . \qquad (2.21)$$

The effective coupling (which is close to k_{33}) is around 0.4 for barium titanate and around 0.7 for PZT type ceramics.

In this study the factor K, defined by

$$K^2 = k^2_{eff} / (1 - k^2_{eff}) \qquad (2.22)$$

is found to be a more convenient measure of coupling. The corresponding K values for barium titanate and PZT-ceramic are 0.436 and 1.0 respectively. In practice the coupling is reduced somewhat below these values by bonds, etc., (see Chapter 3).

6. The most important consideration from the standpoint of this study is the maximum bandwidth obtainable from the conventional design. In ordinary operation the electrical capacitance C_o is 'tuned out' at ω_r by a shunt or series inductance L_o and the transducer is fed through a resistance R_o. The characteristics of such arrangements has been studied by Thurston[13], who concludes that the effects of the shunt and series coil are nearly the same. He estimates the maximum 3-dB power bandwidth to be about K. In section 4.3 (two pole design) and Appendix I it is shown that a half-power bandwidth of $\sqrt{2}$ K is possible. The shortcoming of both of these derivations, however, is the assumption that K
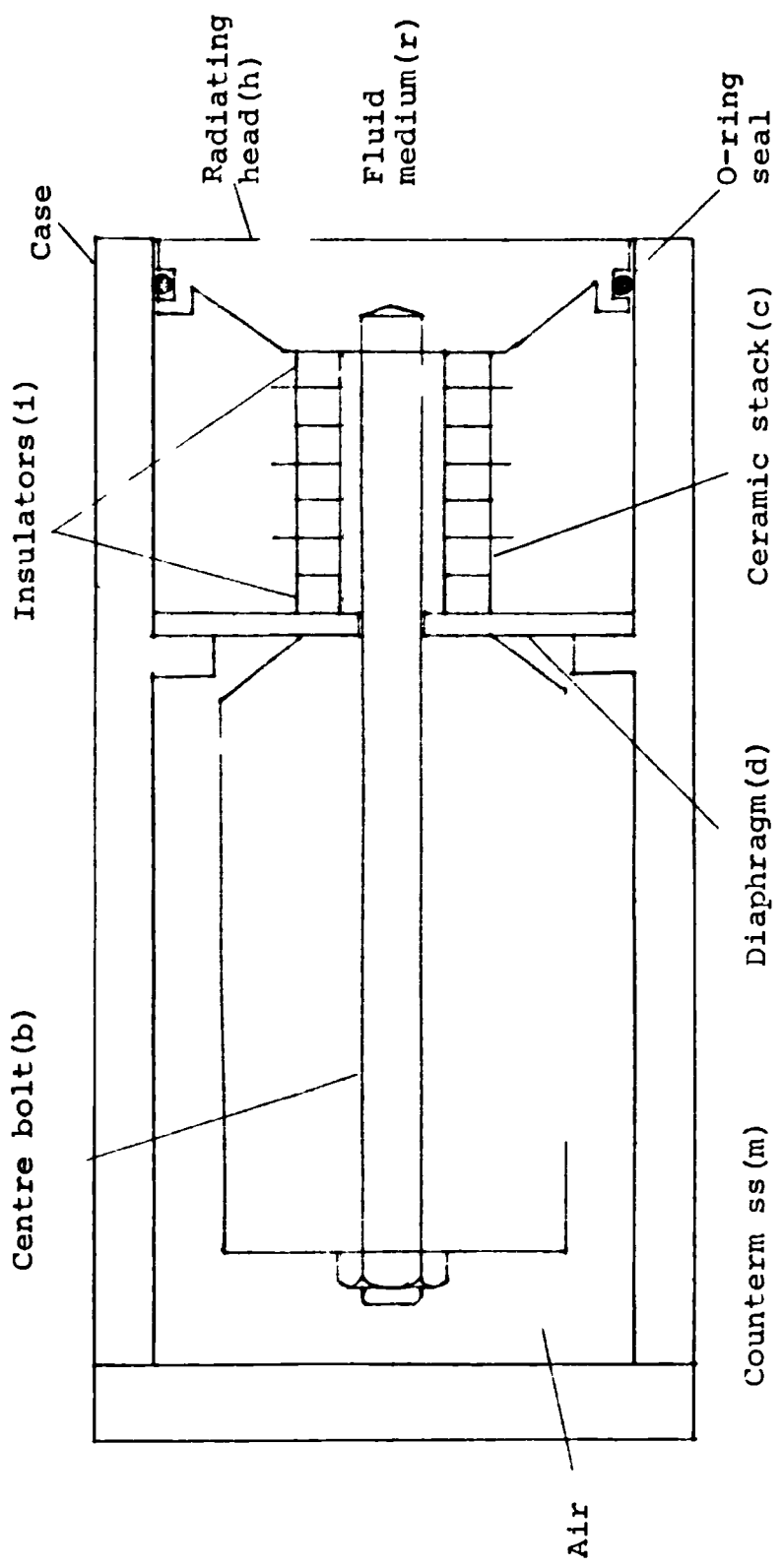
Figure 2.7- S etch of Conventional 10 kHz Trans uc r (Full size)

is the sole limiting criterion. In practice, the low
values of Q_m required to achieve the above bandwidth,
cannot be realized.

In Appendix I, however, the fractional bandwidth
of a shunt tuned transducer (with negligible R_d) is derived
as a function of the Q-factors as well as the coupling.
It is there shown that though a maximum bandwidth of $\sqrt{2}$ K
is theoretically possible, it can in practice only be
achieved with barium titanate transducers. For barium
titanate with a 'k_{eff}' around 0.35, the maximum realizable
bandwidth is 50%. The bandwidths of the commonly used
sonar transducers, however, are generally around 20%.

In acoustic terms, the elevation of L_2 well above
L_1 creates a node near the countermass end of the ceramic.
On account of this, composite transducers are usually
supported near the ceramic-countermass interface, or at some
point on the countermass. The support is commonly a highly
compliant diaphragm which effectively isolates the transducer
from the case. A typical sonar transducer incorporating
the chief constructional features is depicted in Figure 2.7.

The transducing section is realized as a stack of
ceramic rings, bonded together and insulated from the rest of
the transducer. The reasons for and details of stacking
are discussed in the next section. The centre bolt, which
maintains the bias stress on the ceramic, also serves to hold
the assembly together. The bias stress is such that the
ceramic is never in tension under ordinary operating
conditions. The presence of the bonds, the bolt and the
insulators however reduce the effective coupling.

Electroded faces

Direction of stress and strain

Cemented joints

P — direction of polarisation

E — direction of electric field
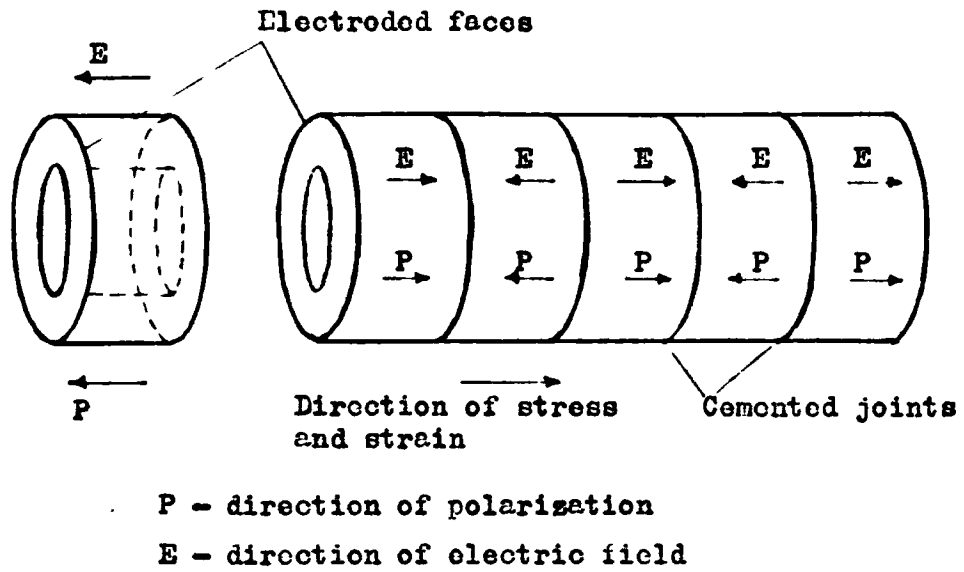
Figure 2.8- Length Mode Operation of Ceramic Stack with Parallel Excitation

The radiating head and the diaphragm are usually constructed out of beryllium copper whereas the countermass and the bolt are of steel.

2.5. Construction of the Ceramic Stack

The main constructional features of a conventional type sonar transducer were described in the previous section. The tubular shape of the ceramic section is dictated by the need to accommodate a centre bolt. The reason for the adoption of a segmented construction of a ceramic stack in high power applications is briefly as follows.

The power handled by a ceramic transducer is proportional to the ceramic volume and the square of the exciting field (see equation 2.19). Since the lateral dimensions of the ceramic are limited by the requirements of length mode operation (see section 3.5), the power is maximised by making the ceramic as long as possible and by using the highest practicable field. Both of these conditions for high power operation are simultaneously satisfied without entailing very high voltages by the segmented arrangement depicted in Figure 2.8.

The complete bar is made up of p identical short segments with individual electrodes. The directions of polarization and excitation alternate along the stack (as indicated). Mechanically, the result is as if the bar were continuous, with uniform polarization and excitation throughout. Electrically, however, two advantages accrue. The required voltage for the same output power is reduced by p. Further if p is even the two end electrodes, which are in mechanical contact with the rest of the transducer, can

be kept at the potential of the low side of the supply.
The impedance seen at the electrical terminals is reduced by
a factor p^2. The sole disadvantage of this arrangement is
the necessity of bonding the segments together to obtain good
mechanical contact.

The process of construction of the stack is as
follows. The individual segments are cast in moulds and
then ground down to the required length specifications as the
surfaces of contact must be finished to a high degree of
precision. Before polarization, the conducting surfaces are
sputtered or painted on. The segments are bonded together
by thin layers of resin cement which commonly incorporates a
sheet of wire cloth. The wire cloth ensures good electrical
contact and the formation of a mechanically efficient joint.
The resin is allowed to set under compressive stress.

Since a high field is necessary to induce the
required remanent polarization, the dielectric strength of
the ceramic imposes a limit on the length of bar that could
be effectively polarized. This limit is of the order of a
few inches. In practical high power stack construction,
however, it is unusual to employ segments longer than a
centimetre on account of operating voltage restrictions.

The power handling capacity of a ceramic stack is
usually governed by the following considerations[3,7].

1. The dynamic strength and the level of mechanical
    depolarization.

2. The dielectric dissipation which should be small enough
    to ensure no appreciable thermal dipolarization.

3. The electric field should be small enough to preclude electric depolarization.

The practical limits of high intensity operation are usually supplied with the ceramic specifications.

CHAPTER 3

EQUIVALENT CIRCUITS

This Chapter is primarily concerned with the following aspects of equivalent circuit representation of piezoelectric transducer elements:

1. The representation of the mechanical and electro-mechanical (ceramic) elements, so as to allow for the distributed mass and compliance of practical transducer components. This representation, which for convenience is referred to as the 'accurate' formulation, is the one used in analysis.

2. The reduction of the accurate formulation of solid elements into conventional type mechanical circuit components, such as pure masses and compliances. This reduction, which is necessary for transducer design, is referred to as the 'approximate' formulation.

3. The derivation of the geometric limits on the elements within which each of the above formulations is justified, vis-a-vis the operating frequency range.

4. The representation of the radiation loading on a transducer in a regular array, as a combination of analogous circuit elements, in the frequency range of interest.

The equivalent circuits of this Chapter are based on the analogies described in section 2.2. For convenience, the impedance analogy is used throughout. Since the detailed studies of equivalent circuits presented here are not essential to transducer design theory, the Chapter may be omitted on a first reading.

The accurate and approximate representations of plain mechanical and ceramic elements is considered in sections 3.1 - 3.3. The effect of the inter-segment bonding on the equivalent circuit of the ceramic stack is treated next in section 3.4. The elements considered in these sections are all assumed to be of uniform cross-section. The circuit representation of such an element, in either analogy, is a uniform transmission line (see section 2.3). The transmission line analogy with its spatially distributed parameters is necessary for the study of the propagation of transient signals (see Redwood[14]). For the purposes of this study, however, it is more convenient to use the T or Π representations of a line at steady sinusoidal frequencies. This reduction, while entailing no loss of accuracy in the steady state, casts the equivalent circuit in the form of lumped impedances, thus rendering it amenable to the techniques of circuit analysis.

The line analogy itself is based on the assumption of pure longitudinal mode propagation in all the solid elements. In section 3.5 it is found that the lateral dimensions of practical transducer components are such that this condition is closely approximated to. Practical transducers are currently designed with centre frequencies of around 5 or 10 kHz. The corresponding upper cut-off frequencies are usually no more than 7.5 and 15 kHz respectively. Thus these values are used in estimating the validity of the approximations effected in this study. Further, it is assumed that spurious resonances fall outside the passband.

The chapter is concluded with the derivation of the equivalent circuit representation of the radiation impedance

of piston sources, radiating singly and in arrays.

Though the accurate equivalent circuits of solid elements can be derived to a high degree of precision (1 - 3% error), the radiation load in arrays is only determinate to within $\pm$ 5%.   Further, the parameters of ordinary ceramic materials are prone to drift by as much as $\pm$ 5%.   Thus the individual elements of the accurate formulation are no more accurate than $\pm$5%.   For the purposes of design, however, a greater margin of error ($\pm$ 10% off the low frequency value) is tolerated in the approximate formulation.

3.1. Mechanical Elements

The transmission line model of longitudinal wave propagation on a bar of uniform cross-section, is indicated in Figure 3.1 (for derivation, see sections 2.2.and 2.3 and Skudrzyk[15]).   There F and u represent the force and particle velocity on the bar.   If Z_o, c are the characteristic impedance and velocity of propagation on the line

$$Z_o = \rho A c$$

and $$c^2 = Y/\rho$$

(3.1)

where ρ, Y, A are the density, Young's modulus and area of cross-section of the bar.   At steady sinusoidal frequencies, the line model could be replaced by the T or Π equivalents of Figure 3.2 where ω is the angular frequency, k (= ω/c), the wave-number and X the length of the bar.

When kX is small compared to unity, the following approximations can be effected

$$\sin kX \simeq 2 \tan kX/2 \simeq kX \qquad .$$

(3.2)

a. Uniform cross-section bar   **b. Transmission line model**
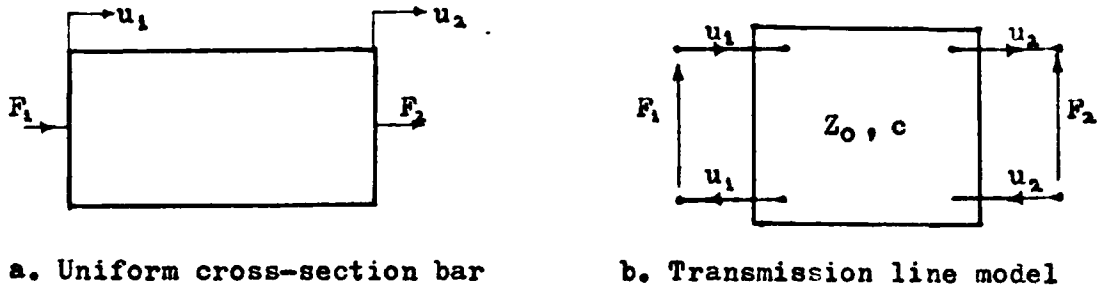
Figure 3.1- Longitudinal Wave Propagation on a Uniform
Cross-section Bar

a. T-equivalent   **b. Π -equivalent**
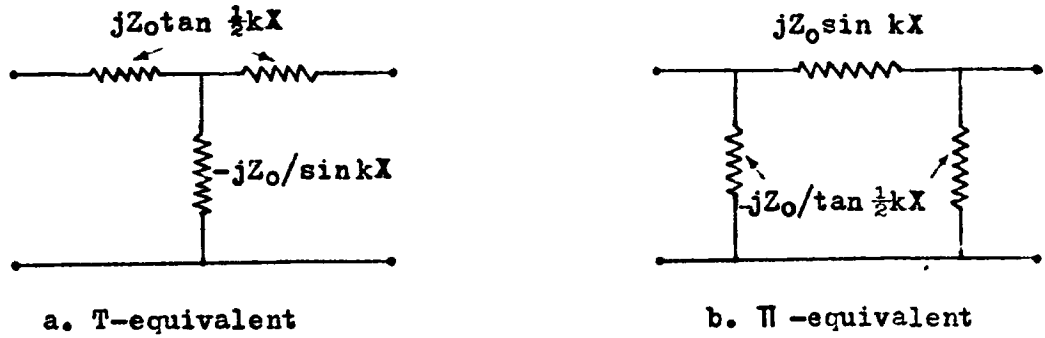
Figure 3.2- Steady State Representation of Uniform
Mechanical Line

a. T-equivalent   **b. Π -equivalent**
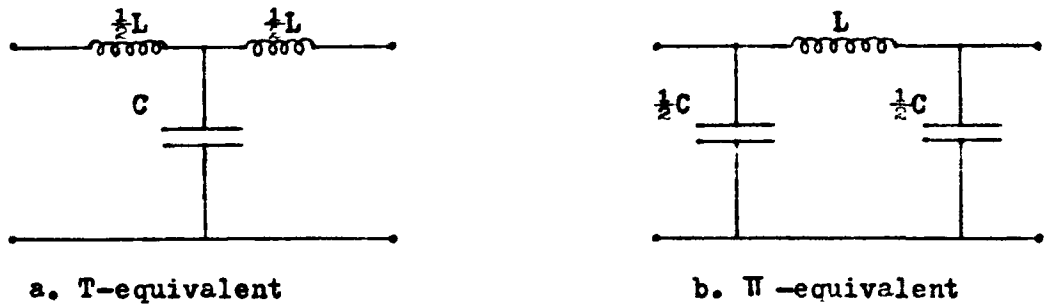
Figure 3.3- LC Reduction of the Uniform Mechanical Line
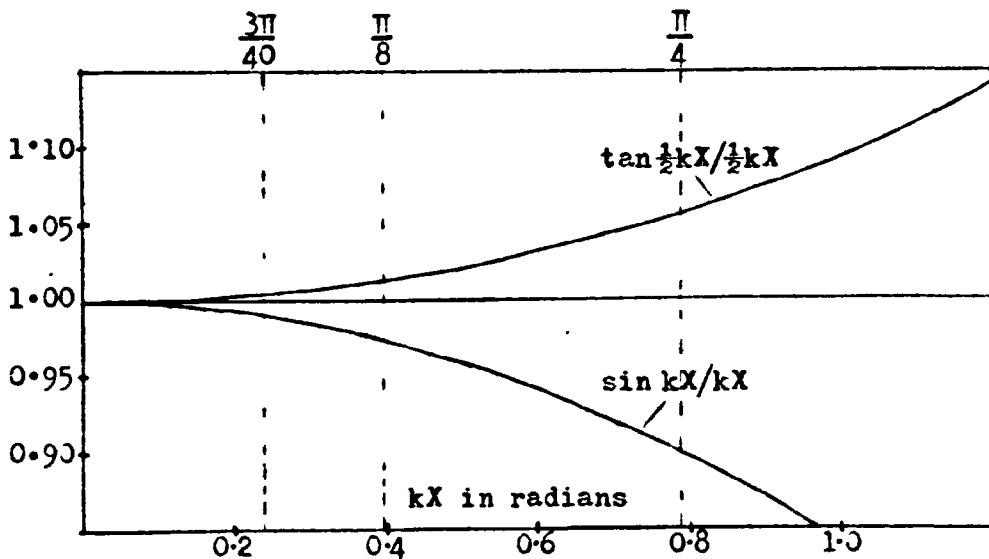
Figure 3.4- Behaviour of the Characteristic Functions of
a Mechanical Line

This reduces the steady-state equivalents to the simpler form of Figure 3.3, where

$$L = \rho A X$$
$$C = X/YA$$

(3.3)

Here C and L are the effective compliance and mass of the bar at low frequencies. If C is small compared to the mass L, then the bar behaves as a pure mass and if L is small compared to C, as a pure compliance; reducing to the 'ideal' elements considered in section 2.2. The condition for approximately ideal behaviour, in either case

$$f_2 << 1/2\pi(LC)^{\frac{1}{2}}$$

or

$$\omega_2 X/c << 1$$

(3.4)

is the same as the condition for the LC reduction of the line. Here f_2 is the upper cut-off frequency. A more explicit limit of applicability of the reduction can be derived from a plot of the functions sin kX/kX and tan(kX/2)/(kX/2) against kX (Figure 3.4).

It is observed that both functions are accurate to within $\pm$ 2.5% of the low frequency values for kX $\leq$ $\pi/8$. For kX $\leq$ $\pi/4$, however, the maximum deviation is increased to $\pm$ 10%. Thus the former limit is adopted in analysis and the latter in design. These limits imply the following restrictions on the length of bar.

Maximum length of bar (in cm) to satisfy the ideal element reduction up to 7.5 kHz

	$\pm$ 2.5% accuracy	$\pm$ 10% accuracy
Steel	4.3	8.7
Beryllium Copper	3.3	6.5
Aluminium	4.2	8.4

If the upper cut-off frequency is 15 kHz (instead of 7.5) the values are halved. These restrictions on the length of mechanical elements are generally quite easy to satisfy in practical designs. In analysis, however, if the 2.5% limit is not satisfied the accurate formulation of Figure 3.2 must be used.

The limits on the lateral dimensions, necessary to satisfy the longitudinal wave approximation, are considered in section 3.5.

3.2. Equivalent Circuit of a Tubular Ceramic Segment

The equivalent circuit representation of the longitudinal mode excitation of a uniform piezoelectric bar with parallel field, has been derived in section 2.3. This circuit was first derived by Mason[16] in its frequency domain formulation and subsequently by Redwood[14] in the form presented in Figure 2.3. Martin[17] has extended the representation to include lateral effects and losses in commonly used ceramic tubes. Martin's formulation is particularly important as the limits of pure longitudinal mode operation can be derived from it (see section 3.5 on 'Lateral Effects and Losses'). In the immediately foregoing treatment, however, it is assumed that lateral effects and losses are negligible.

Under steady sinusoidal excitation, the equivalent circuit of a uniform ceramic bar (such as depicted in Figure 2.8) is easily reducible from the form of Figure 2.3 to that of Figure 3.5 where
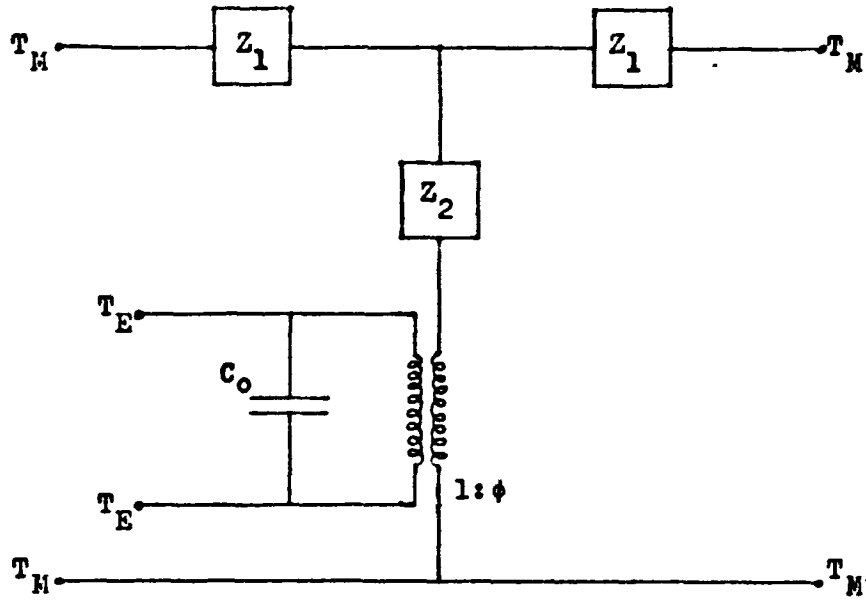
Figure 3.5- Steady State Equivalent of a Single
Ceramic Segment
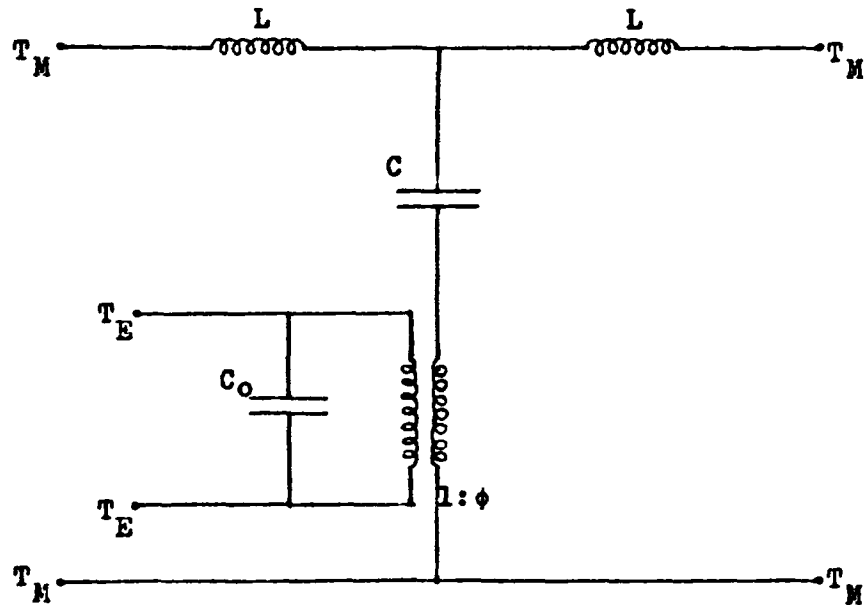
Figure 3.6- Equivalent Circuit of Ceramic Segment
for $kX << 1$

$$Z_1 = j\rho A c \tan kX/2$$

$$Z_2 = -j\rho A c/\sin kX + j\phi^2/\omega C_o$$

$$k = \omega/c$$

$$c = (\rho s_{33}^D)^{-\frac{1}{2}}$$

$$\phi = A d_{33}/s_{33}^E X$$

$$C_o = (1 - k_{33}^2)\varepsilon_{33}^T A/X$$

<div align="right">(3.5)</div>

Here in addition to the symbols defined in section 2.3, d_{33} is the relevant component of the piezoelectric tensor (strain/field at constant stress) and k_{33}, the longitudinal coupling factor defined in equation (3.8). A and X are the area of cross-section and length of the ceramic segment. C_o is the electrical capacitance and ϕ the electromechanical transformation ratio. In Figure 3.5 (and subsequent diagrams) the mechanical terminals are marked T_M and the electrical terminals T_E.

In the absence of an electrical input the equivalent circuit reduces to that of a purely mechanical line (compare with Figure 3.1). Thus, as in the case of a purely mechanical line, the complete equivalent of figure 3.5 may be approximated by that of Figure 3.6, for values of kX << 1 where

$$C = s_{33}^E X/A$$

$$L = \rho A X/2$$

<div align="right">(3.6)</div>

In practice X never exceeds 1 cm and the upper frequency limit is 15 kHz. The value of kX corresponding

to these two limiting values for lead zirconate titanate
type ceramics is $3\pi/40$. From the graphs of Figure 3.4 it is
clear that the error incurred by the use of the approximate
value is less than 1% for both L and C at the greatest value
of kX. The approximation is even better for barium
titanate. The above practical limit on kX is very important
as many of the approximations effected in this Chapter are
based on it. Restated in terms of angular frequency it
becomes

$$\omega X/c \leq 0.2355 \qquad\qquad (3.7)$$

The two impedances Z_1 (and L in the low frequency
approximation) represent the effective mass of the ceramic.
Similarly Z_2 (or C) is the effective ceramic compliance.
For small values of kX the two terms of Z_2 can be algebraically
combined to yield the nett compliance C. Comparing these
circuits with the equivalent circuit of Figure 3.1 it is
clear that the term $j\phi^2/\omega C_o$ increases the effective compliance
of the ceramic. This term accounts for the field generated
piezoelectrically from the strain in the material,which is a
form of 'back E.M.F.'. It is in fact absent in those cases
where the direction of motion is perpendicular to the
applied field. In the earlier publications it has been
customary to include this term in the equivalent circuit as
a negative capacitor - C_o on the electrical side. This
alternative is somewhat more convenient when considering the
effects of incident mechanical transients on a transducer.
In most cases, however, the formulation adopted here, of
including it in the mechanical compliance, is preferable.

One of the most important parameters of a piezo-electric transducer, is its energy coupling factor which is a measure of the fraction of total energy that is coupled into the mechanical side. The static, or low frequency coupling[3], for the particular mode considered, is given by

$$k_{33}^2 = d_{33}^2/\epsilon_{33}^T \cdot s_{33}^E \quad . \tag{3.8}$$

This value also represents the upper limit on dynamic or effective coupling[3], under other operating conditions. A consideration of coupling in the fundamental terms of energy is not however of direct relevance in a study of transducers from their equivalent circuits. Mason[16] has shown that the effective coupling factor can be expressed as a function of the ratio C/C_o. Thus with reference to Figure 3.6 which is applicable at low frequencies, it is observed that

$$1/(1 + C_o/C\phi^2) = k_{33}^2 \quad . \tag{3.9}$$

Extending this relation to the general case of Figure 3.5 the effective coupling factor k_{eff} could be defined as follows (after Schofield[2])

$$k_{eff}^2 = 1/(1 + j\omega C_o Z_2/\phi^2) \quad . \tag{3.10}$$

It is clear from the form Z_2 that the effective coupling at higher values of kX is less than the static coupling value of k_{33}. Since high coupling is of prime importance in the design of sonar transducers it is desirable to work in the range of frequency for which kX << 1. A further advantage from the point of view of broadband transducer design is

that the effective values of mass and compliance are
constant in this range.

The coupling factor as defined above is not a
convenient measure to use when considering the effect of
bonds on the coupling and the dependence of the maximum
bandwidth on the coupling.   In such cases a simple function
of the effective coupling given by

$$K^2 = k^2_{eff}/(1 - k^2_{eff}) = \phi^2/j\omega C_o Z_2 \qquad (3.11)$$

proves to be more useful.   The reciprocal relationship is

$$k^2_{eff} = K^2/(1 + K^2) \qquad . \qquad (3.12)$$

Since a one-to-one relationship exists between the two
variables (only positive values of both being admissible)
K is just as good a measure of the coupling.   As such the
term 'coupling factor' will be used to refer to K as well.

If K_o is the value of K at low frequencies (when
kX << 1)

$$K_o^2 = C\phi^2/C_o = k^2_{33}/(1 - k^2_{33}) \qquad . \qquad (3.13)$$

K_o is referred to as the low frequency coupling factor.

3.3.   Equivalent Circuit of the Ceramic Stack
   (after Martin[19])

The equivalent circuit of a single tubular segment of
the stack of Figure 2.8 has been studied in the previous
section.   If p such segments are bonded together as
described in section 2.5, the equivalent circuit of the
composite electromechanical system, neglecting the bonding,
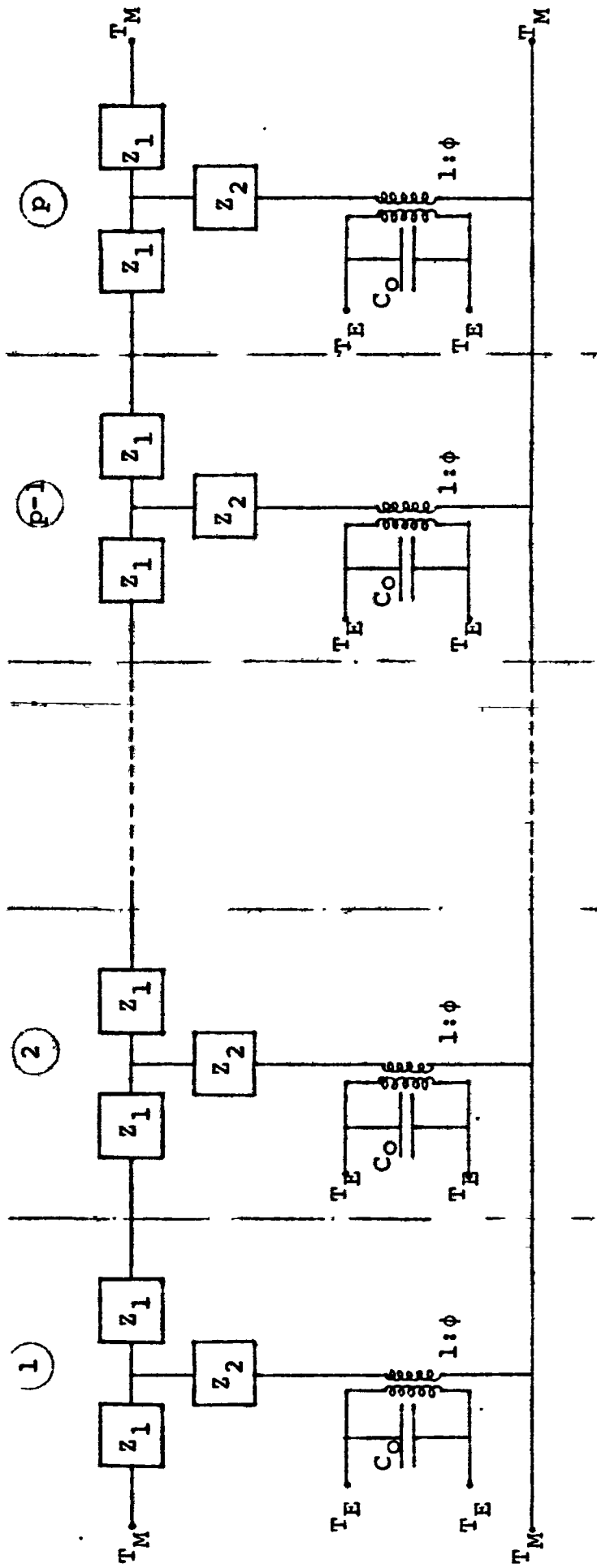
Figure 3.7 - Equivalent Circuit of a Ceramic Stack of p Segments

is that of Figure 3.7.   Martin[18,19] has shown that when
the electrical terminals are connected in parallel this
circuit is reducible to the relatively simple form of
Figure 3.8.   The rationale of this contraction is as follows.

Since the electrical terminals are connected in parallel
the electrical capacitances C_o add up to the aggregate value
of pC_o.   Further, as the primaries of the electromechanical
transformers are now in parallel the potential differences
across the secondaries must be equal.   The secondaries are,
however, commoned on one side.   Therefore the other sides
of the secondaries are at a common potential as well and are
thus effectively connected together.   The mechanical side
of the circuit now consists of p identical T-sections
connected in cascade.   Thus if Z_o is the characteristic
impedance and γ the propagation constant of each section,
the cascaded mechanical system as a whole is represented
exactly by a single T section of characteristic impedance
Z_o and propagation constant $p\gamma$.   This leads directly to the
contracted circuit of Figure 3.8. Z_o and γ for a
symmetrical T-section having Z_1 in the series arms and Z_2
in the parallel arm, are

$$Z_o = [Z_1 Z_2 (2 + Z_1/Z_2)]^{\frac{1}{2}}$$

$$\gamma = 2 \; \text{arcsinh}(Z_1/2Z_2)^{\frac{1}{2}} \quad .$$

$$(3.14)$$

Therefore it follows that the impedances of the contracted
equivalent circuit of Figure 3.8 are

$$Z_{1p} = Z_o \; \tanh \; p\gamma/2$$

$$Z_{2p} = Z_o/\sinh \; p\gamma$$

$$(3.15)$$
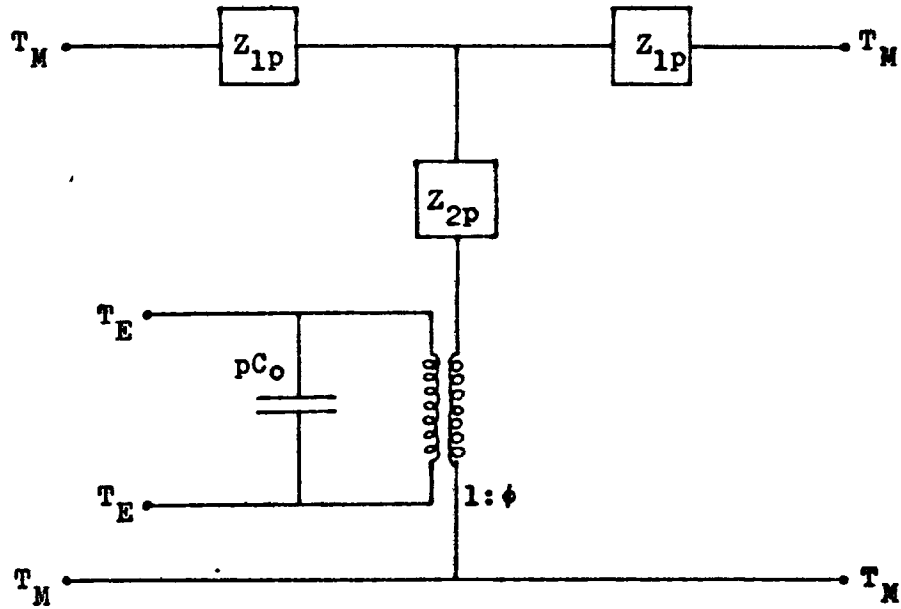
Figure 3.8- Contracted Form of the Equivalent
Circuit of a Ceramic Stack
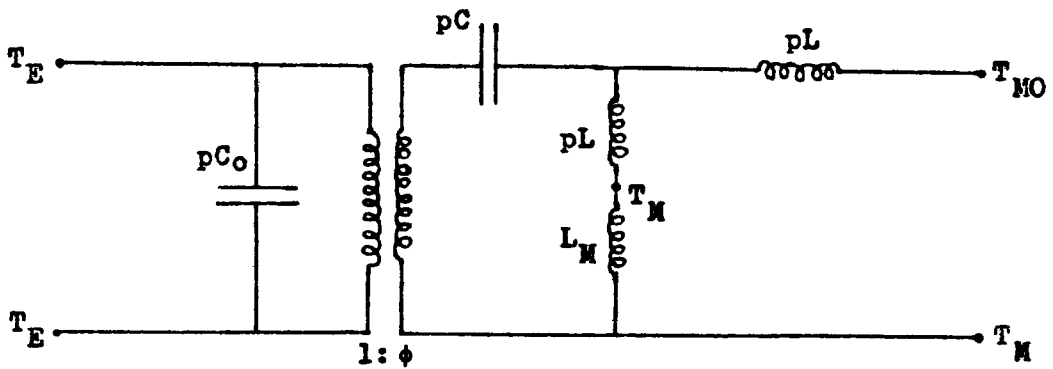
Figur 3.9- LC Reduction of the Equivalent Circuit
of a Stack Bonded to a Countermass L_M

These equations, when used in conjunction with equations (3.6) for a single segment, determine the contracted form of the equivalent circuit as precisely as that of a single segment. It was shown in section 3.2 that the elements of the circuit of a single segment are determinate to an accuracy of 1% by the approximate LC equivalent of Figure 3.6. The use of the LC approximation, rather than the exact equivalent of Figure 3.5, is found to greatly simplify the explicit mathematical formulation of Z_{1p}, Z_{2p}. Since the loss of accuracy suffered by this procedure is inconsequential the LC formulation is used in the derivation of Z_o and γ which now become

$$Z_o^2 = (2 - \omega^2 LC)L/C \qquad (3.16)$$

$$\gamma = 2 \operatorname{arcsinh}(-\omega^2 LC/2)^{\frac{1}{2}}$$

Substituting for L, C in terms of the ceramic constants and the stack geometry (from equations (3.6)) these equations reduce to

$$Z_o = (1 - \delta^2)^{\frac{1}{2}} \rho A c_e \qquad (3.17)$$

$$\gamma = 2j \arcsin \delta$$

where $\quad \delta^2 = \omega^2 LC/2 = (\omega X/2c_e)^2 \qquad (3.18)$

and $\quad c_e = (1 - k_{33}^2)^{\frac{1}{2}} c$

In section 3.2 (equation 3.7) it was shown that for practical designs the condition $\omega X/c \leq 0.2355$ was operative in the frequency range of interest. Combining this condition with a value of 0.7 for k_{33} (which is typical for lead zirconate titanate type ceramics) it follows that

$$\delta \leq 0.118 \quad . \tag{3.19}$$

Therefore the errors incurred in the estimation of Z_o, γ by the approximations

$$(1 - \delta^2)^{\frac{1}{2}} = 1$$

$$\arcsin \delta = \delta \tag{3.20}$$

applied to equations (3.17) are fractional parts of 1% at the highest frequency of operation. Since the errors are less at lower frequencies, the above approximations are completely justified in relation to the predetermined margin of tolerable error. Thus equations (3.17) simplify to

$$Z_o = \rho A c_e$$

$$\gamma = j\omega X/c_e \tag{3.21}$$

which, on substitution in equations (3.15), yield

$$Z_{1p} = j\rho A c_e \tan(\omega pX/2c_e)$$

$$Z_{2p} = \rho A c_e / j \sin(\omega pX/c_e) \tag{3.22}$$

The form of these equations is similar to that of the exact equation of a single segment as is to be expected. Thus it is possible to identify pX as the effective length and c_e as the effective longitudinal velocity with respect to the ceramic stack. While pX is in fact the actual length of the stack the effective velocity c_e is between 70-70% of the actual longitudinal velocity c (for lead zirconate titanate ceramics).

Subject to a correction for bonding, the accuracy of the above formulation of the equivalent circuit of a ceramic stack is both necessary and sufficient to satisfy the

requirements of transducer analysis. It will be shown in the foregoing section that the correction for bonding leaves the mathematical form of the equivalent circuit elements intact and merely introduces a modification of the parameters C_o, ϕ, Z_o and γ. The trigonometric nature of the expressions for Z_{1p}, Z_{2p} are no more difficult to program for the purposes of analysis than are the conventional impedance functions $j\omega L$ and $1/j\omega C$. Synthesis, however, in terms of these functions, is clearly impossible if available circuit synthesis data is to be utilized. Thus it becomes necessary to invoke the low frequency approximations of equations (3.2) again, to reduce Z_{1p}, Z_{2p} to LC form as well. The result is naturally similar to the LC reduction of a single segment. The LC reduction of the stack which is depicted in Figure 3.9 is drawn inclusive of a large rigid mass L_M to which, it is assumed, one end of the stack is firmly bonded. The mass itself is assumed to be held by supports of negligible stiffness.

The reason for anchoring the stack to a large mass (usually called the countermass) is clear from the diagram. If L_M is large enough the 'current' through that branch is negligibly small. In real terms this means that the 'countermass side' of the stack is kept effectively stationary thus ensuring that mechanical power transfer takes place through the other side. In terms of topology the result is a network having one electrical port and one mechanical port (the other mechanical port being effectively open circuited). Thus the equivalent circuit of a stack is reduced to its simplest form of a capacitance coupler pair pC_o, pC separated by the ideal transformer $1:\phi$. The magnitude of these capacitors

are controllable by means of the geometric parameters X, A but their ratio is constant at K^2 (see equation (3.13)). The presence of the mass pL (before the output terminal T_{MO}) is of little consequence from the standpoint of synthesis because in any transducer circuit the mechanical output would be via a mass (the radiating mass in simple transducers) which is generally larger than pL and to which pL conveniently adds.

In practice it is difficult to make L_M large enough though its anchoring (to the case) by means of high compliance supports, presents no special problems.

For the purposes of synthesis it has already been decided to tolerate a deviation of 10% on the low frequency value. From Figure 3.14 this is equivalent to

$$\omega pX/c_e \leq \pi/4 \qquad . \qquad (3.23)$$

For lead zirconate titanate ceramics, this limit implies a maximum stack length of 2.5 cm for an upper cut-off frequency of 15 kHz. If the upper cut-off frequency is 7.5 kHz, as is often the case, the stack length could be as high as 5 cm. The corresponding limits for barium titanate are 3.6 and 7.2 cm. These limits are unfortunately quite restrictive and constitute a serious obstacle to the design of wide-band transducers.

Since the fractional deviation of compliance is proportional to ω^2, the maximum error can be reduced by half if the design value is satisfied at 2.23 times the lower cut off frequency. From equation (3.11) it is seen that this implies working at an effective coupling K of 97.2% of the

low frequency value K_o. The further reduction of K, by the elevation of the tolerated deviation, is not very desirable as the coupling is reduced by the bonding as well.

The nett result of the above restrictions on stack length is to impose a limit on the power handling capacity of broadband transducers.

3.4. Effect of Bonds on the Equivalent Circuit of a Ceramic Stack

A major shortcoming of Martin's formulation of the equivalent circuit of ceramic stacks is the scant attention paid to the intersegement bonding. Martin states that current bonding techniques '... permit the assembly of ... segmented systems, with small effects due to the cement joints'. This is certainly not the experience of the practice on which this study is based. In fact, it is extremely unlikely that efficient joints could be set up in any sonar transducer stack, such that their effects are negligible. In view of this it is essential to develop a theory for the effects of bonding on the contracted equivalent circuit if this is to be preserved as a reasonably precise representation of the ceramic stack.

The chief effect of the bonding is to introduce extra compliance between the ceramic segments. The bond compliance C_b is typically about 10% of the segment compliance C, for a ¼ cm segment. An exact representation of the bonds would, of course, allow for the finite though small mass of the bonds (1% of the segment mass) and the losses in the joints. It is unlikely, however, that these would significantly improve the correction for bonding which, by
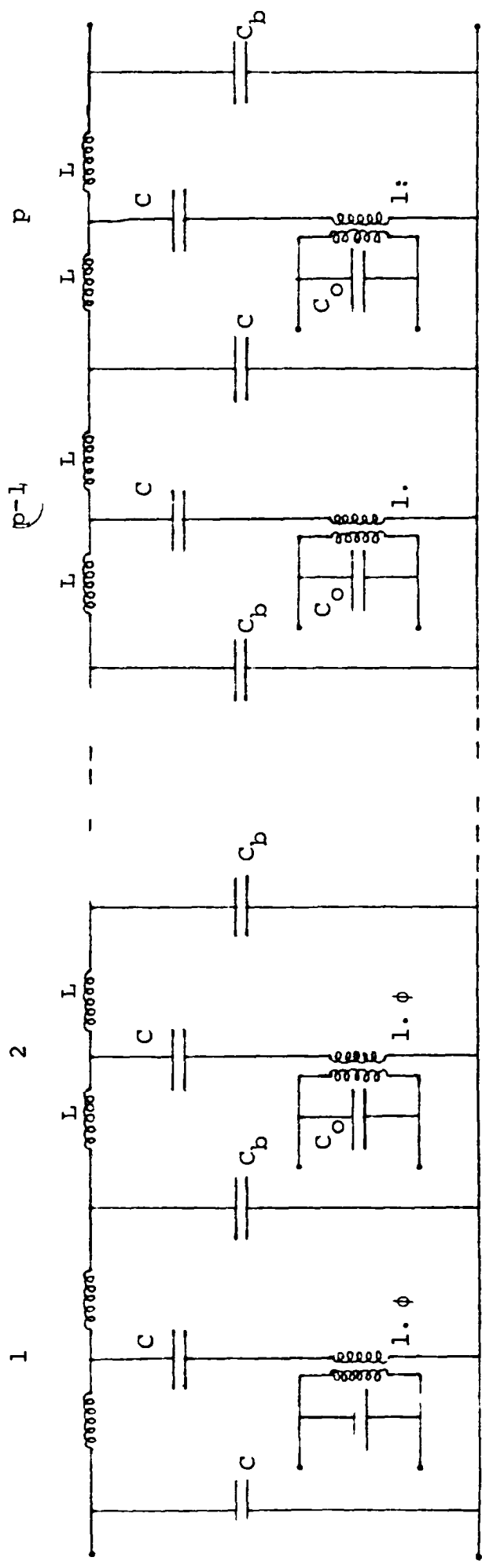
Figur 3.1 - Equivalent Circuit of a Ceramic Stack of p Segments, Inclusive of Bondin

itself, is a second order effect. As such, in the foregoing theory, bonds are represented by pure and constant compliances C_b.

The equivalent circuit of Figure 3.7 incorporating the LC approximation of Z_1, Z_2 and modified to include the bonding, is re-drawn in Figure 3.10. As it stands this equivalent circuit is not amenable to reduction into a compact form. Consider however the T-section of Figure 3.11 which is extracted from Figure 3.10 and which consists of a bond compliance with its adjacent elements. This network is very easily transformed into the Π-section of Figure 3.12 where

$$L' = (1 - \omega^2 LC_b/2)L$$

$$\text{and} \quad C_b' = C_b/(1 - \omega^2 LC_b/2) \quad .$$

(3.24)

Involving the parameter δ, defined in equation (3.18), these equations become

$$L' = (1 - \delta^2 . C_b/C)L$$

$$C_b' = C_b/(1 - \delta^2 C_r/C)$$

(3.25)

Combining the upper limit on δ^2 (from equation (3.19)) with a value of 0.1 for C_b/C, it is clear that the approximation

$$L' = L, \qquad C_b' = C_b$$

(3.26)

is correct to within 0.14% in the frequency range of interest. The assumed value of 0.1 for C_b/C is, in fact, an upper limit on this particular ratio, as it is unusual to design segments shorter than $\frac{1}{2}$ cm. Further the approximation does not depend on the elements L, C being
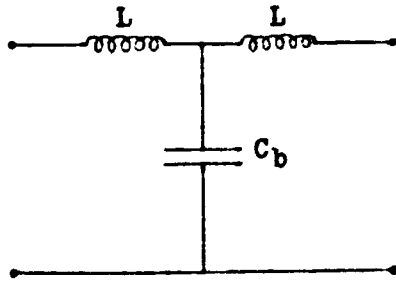
Figure 3.11

Figure 3.12

a.

b.
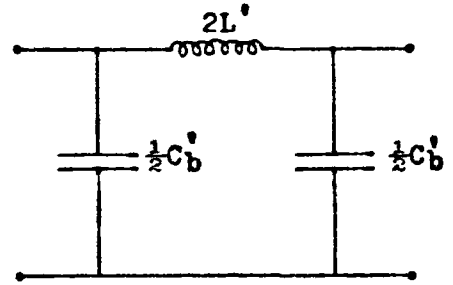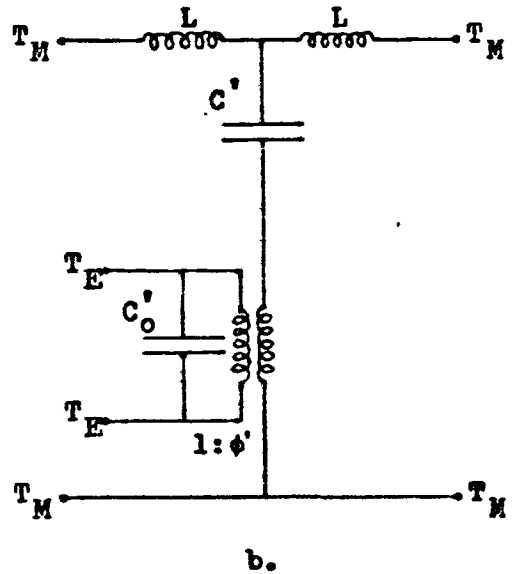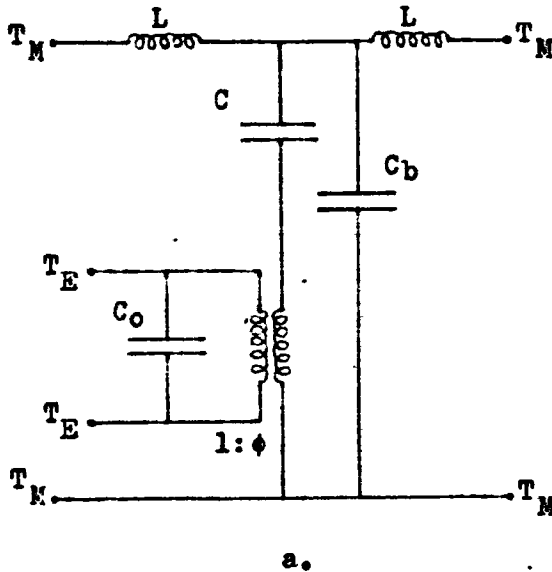
Figure 3.13- Equivalent Circuit of a Single Segment,
Inclusive of Bonding
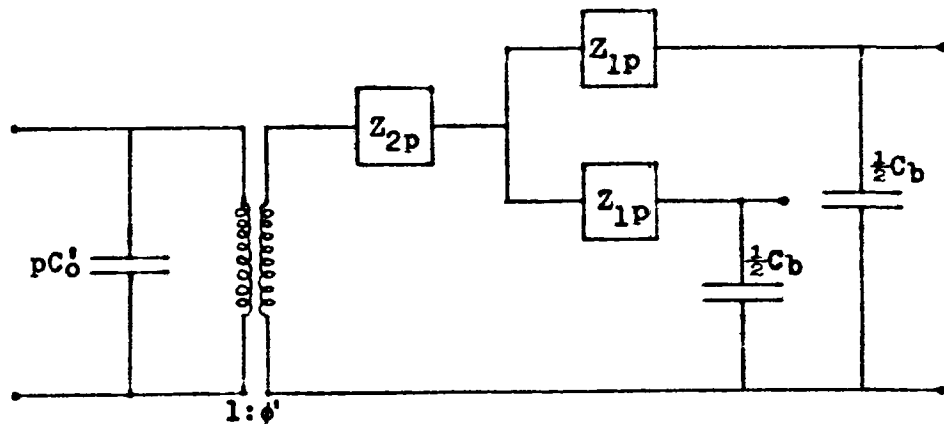
Figure 3.14- Contracted Form of the Equivalent Circuit
of a Ceramic Stack, Inclusive of Bonding

constant, provided they do not fall far below their low frequency values. It is in fact easily demonstrated that provided the segment length does not exceed 1 cm, the above approximation is valid up to about 15 kHz.

The importance of the above transformation is that it shifts the bonds such that they appear in parallel across the segment compliance C and the secondary of the electro-mechanical transformer. Inserting the equivalent Π-network of Figure 3.12, in place of the T-extract of Figure 3.11, the equivalent circuit of a single segment of the stack is now transformed into that of Figure 3.13a. This circuit itself can be simplified into that of Figure 3.13b, where

$$M^2 = C/(C + C_b)$$
$$\phi' = M^2 \phi$$
$$C_o' = C_o + M^2 \phi^2 C_b \qquad (3.27)$$
$$C' = C + C_b .$$

The circuit of Figure 3.13b, however, is of the same form as the original equivalent circuit of a ceramic segment (Figure 3.6). Thus the composite equivalent circuit, consisting of p such sections is suitable for the application of Martin's contraction, as described in section 3.3. Since the only difference between Figures 3.6 and 3.13b is that ϕ, C_o, C in the former are replaced by ϕ', C_o', C' in the latter, the result follows by direct substitution. The resulting contracted equivalent which now includes the bonding, is depicted in Figure 3.14 where

$$Z_{1p} = j\rho Ac_e M \; \tan(\omega pX/2c_e M)$$
$$Z_{2p} = \rho Ac_e M/j \; \sin(\omega pX/c_e M) \qquad (3.28)$$

Comparing this result with equations (3.22) of section 3.3, it is clear that the bonds reduce the effective characteristic impedance Z_o by a factor M and increase the effective length in the ratio of $1/M$. Further the electrical capacitance is increased and the electromechanical transformation ratio ϕ is reduced by M^2. The two residual compliances $C_b/2$ of Figure 3.14 are small enough to be neglected. In actual analysis, however, they are conveniently incorporated in the compliances of the insulating blocks which usually flank a ceramic stack.

If K' is the effective coupling inclusive of the effects of bonding, it follows from equation (3.11) that

$$(K')^2 = (\phi')^2 / j \omega C_o' Z_{2p} \quad . \tag{3.29}$$

It is also very easily shown, by direct substitution, from equations (3.27) that the low frequency coupling K_o' is reduced from K_o (defined by equation (3.13)) to

$$(K_o')^2 = (K_o)^2 / (1 + C_b/C + K_o^2 C_b/C) \quad . \tag{3.30}$$

In the derivation of the broadband filter circuit on which the design of the broadband transducer is based, the above reduction of coupling has to be accounted for as well as the depreciation resulting from the dependence of K' on frequency.

In a typical design incorporating $\frac{1}{2}$ cm ceramic segments, the presence of the intersegment bonds was found to have the following effect:

$$
\begin{aligned}
C'/C &= 1.10 & \phi'/\phi &= 0.91 \\
C_o'/C_o &= 1.065 & K_o'/K_o &= 0.925 \quad .
\end{aligned}
\tag{3.31}
$$

It is important to note that the modifications caused by bonding, being a second order correction, has negligible effect on the criterion of equation (3.8). It also does not affect the validity of the approximations of equations (3.20) and Figure 3.9. Thus the LC reduction of a ceramic stack inclusive of the effects of bonds is obtained simply by the replacement of C_o, ϕ, C in Figure 3.9 by C_o', ϕ', C' respectively.

3.5. Lateral Effects and Losses

The equivalent circuit representation of longitudinal waves on a uniform cross-section bar (derived in section 3.1) is valid provided the lateral dimensions are much smaller than the wavelength λ. Otherwise the lateral motion may be accounted for by a corrected value of the velocity c. From the graph of the exact velocity correction for lateral inertia against a/λ for a circular bar of radius a (Skudrzyk[15]), it is observed that if $a \leq \lambda/8$ the error incurred by the use of the uncorrected value is less than 3%. For an upper frequency limit of 7.5 kHz this implies a maximum bar diameter of 17 cm for steel and aluminium and 12 cms for beryllium copper. At 15 kHz the maximum values are reduced by half. The lateral dimensions of practical transducer elements generally fall within these limits.

In the case of piezoelectric ceramic, however, the corresponding limits are derived from Martin's solution. Martin's solution[17] of the vibrations of longitudinally polarized ceramic tubes accounts for lateral motion as well as losses. Further, he has cast the correction for lateral motion as functional modifications of the basic ceramic

parameters governed by the variable f/f_r. Here f_r is the
frequency of first radial resonance of the tube. It is
observed from Martin's results that the ceramic parameters
are accurate to within 1% of their low frequency values
(for both barium titanate and lead zirconate titanate) if

$$f/f_r \leq 0.34 \qquad . \qquad (3.32)$$

The dependence of f_r on the inner and outer radii
(r_1 and r_2 respectively) of the ceramic tube, culled from
experimental estimations[20,21], is given approximately by

$$f_r = c/\pi(r_1 + r_2) \qquad (3.33)$$

in the range $0.2 \leq r_1/r_2 \leq 0.5$. Here c is the longitudinal
velocity in the ceramic. The upper bound on (r_1+r_2) thus
becomes

$$(r_1 + r_2) \leq 0.34 \ c/\pi f_2 \qquad (3.34)$$

where f_2 is the upper frequency limit. Since the inner
radius r_1 of a ceramic stack is generally under 0.75 cm,
the outer radius is restricted to 6.3 cm for barium titanate
and 5 cm for lead zirconate titanate for an f_2 of 7.5 kHz.
If, however, f_2 is 15 kHz the respective bounds are reduced
to 2.8 cm and 2.2 cm. These limits are very easily
satisfied in practice.

In the synthesis of electrical filter networks it is
customary to treat elements possessing Q-factors greater than
50 as lossless. The resulting errors in the filter
characteristics are found to be negligible. The mechanical
elements, including the mass and compliance of the ceramic

stack, satisfy this criterion as their Qs are generally above 100. The effective Q of the electrical capacitance element C_o, however, is usually lower on account of dielectric loss (see section 2.4). It is also a function of the drive level and the frequency. In practice it is customary by the proper choice of ceramic (see section 2.1) and by limitation of the drive level, to ensure that the effective Q is above 50. This condition is satisfied if $\tan\delta \leq 0.02$.

3.6. Radiation Impedance of a Single Piston Source

In the study of the performance of sonar transducers it is usual to represent the reaction of the fluid medium on the radiating face (or piston face) as a complex impedance Z_r^{22}. The radiating face is generally plane and circular in shape as this simplifies construction and minimizes the lateral dimensions for a given face area. Sonar transducers are commonly operated in regular packed arrays and the impedance characteristics of arrays are accordingly dealt with in the next section. A brief account of the character-istics of the individual elements of arrays (viz. single, circular piston sources) is however a necessary pre-requisite to the study of arrays. Further, since transducers are usually tested out as single sources, it is necessary to explicitly formulate the impedance of such sources.

Under steady operating conditions, if F is the r.m.s. reaction force on the face of a rigid piston and V is the r.m.s. velocity of the face, the radiation impedance Z_r is defined as

$$Z_r = R_r + jX_r = F/V \quad . \tag{3.35}$$

The variables F, V are in general complex and a function of frequency f and piston radius a for a given medium. R_r and X_r are the radiation resistance and reactance respectively. The quantity X_r/ω is usually referred to as the 'equivalent mass' of the fluid medium for a particular frequency ω, by analogy with mechanical mass in the impedance analogy. The general method of handling radiation in an equivalent circuit is to represent Z_r which, by virtue of its definition, is an impedance in the impedance analogy, as ordinary circuit elements. Thus, in the first instance, Z_r is represented by a resistance R_r and an inductance X_r/ω, in series. In the mobility analogy the radiation load becomes a conductance R_r and a capacitance X_r/ω in parallel. The complexity of analysis is hardly affected at all by the frequency dependence of R_r and X_r/ω provided this dependence is explicitly determined. In the synthesis of broadband transducers, however, it is essential to work in a frequency range for which R_r and X_r/ω are substantially constant. Sometimes, even when X_r/ω is not constant, it is possible to swamp its variation by a large enough head mass with which it appears in series in the equivalent circuit. Since the design of broadband transducers is based on electrical filter circuits the output variable, with respect to which the broadbanding is effected, is the output power. In either analogy the output power is given by

$$P = |F|^2/R_r = R_r|V|^2 \qquad . \qquad (3.36)$$

The determination of the radiation impedance of underwater sound sources is based on acoustic radiation

theory rather than direct experiment. The derivation is simplest for the case of a plane piston source in an infinite rigid baffle and is consequently well treated in the literature[22,23]. The result which is given below is commonly formulated as a function of the compound variable x, which is defined in terms of k and the piston radius a as

$$x = 2ak \qquad . \qquad (3.37)$$

The use of the double subscript for impedance becomes meaningful in the context of array interactions. In this section the coincident double subscript merely indicates that it is the self-impedance (or resistance, or reactance) which is being considered. Thus if

$$Z_{11} = R_{11}(x) + jX_{11}(x) \qquad (3.38)$$

and $\qquad Z_o = \rho cA \qquad (3.39)$

where A is the piston area and ρ, c are the density and velocity of sound in the fluid medium, the explicit formulation of impedance cast in a form that facilitates computation is

$$R_{11} = \sum_{n=1}^{\infty} R_n \ , \qquad X_{11} = \sum_{n=1}^{\infty} X_n \qquad (3.40)$$

where

$$R_n = -\{x^2/(4n^2+4n)\}R_{n-1}, \qquad R_1 = Z_o x^2/8$$

$$X_n = -\{x^2/(4n^2-1)\}X_{n-1}, \qquad X_1 = 4Z_o x/3\pi \qquad .$$

These functions are displayed graphically in Figure 3.15 where the epithet 'baffled' means 'infinitely
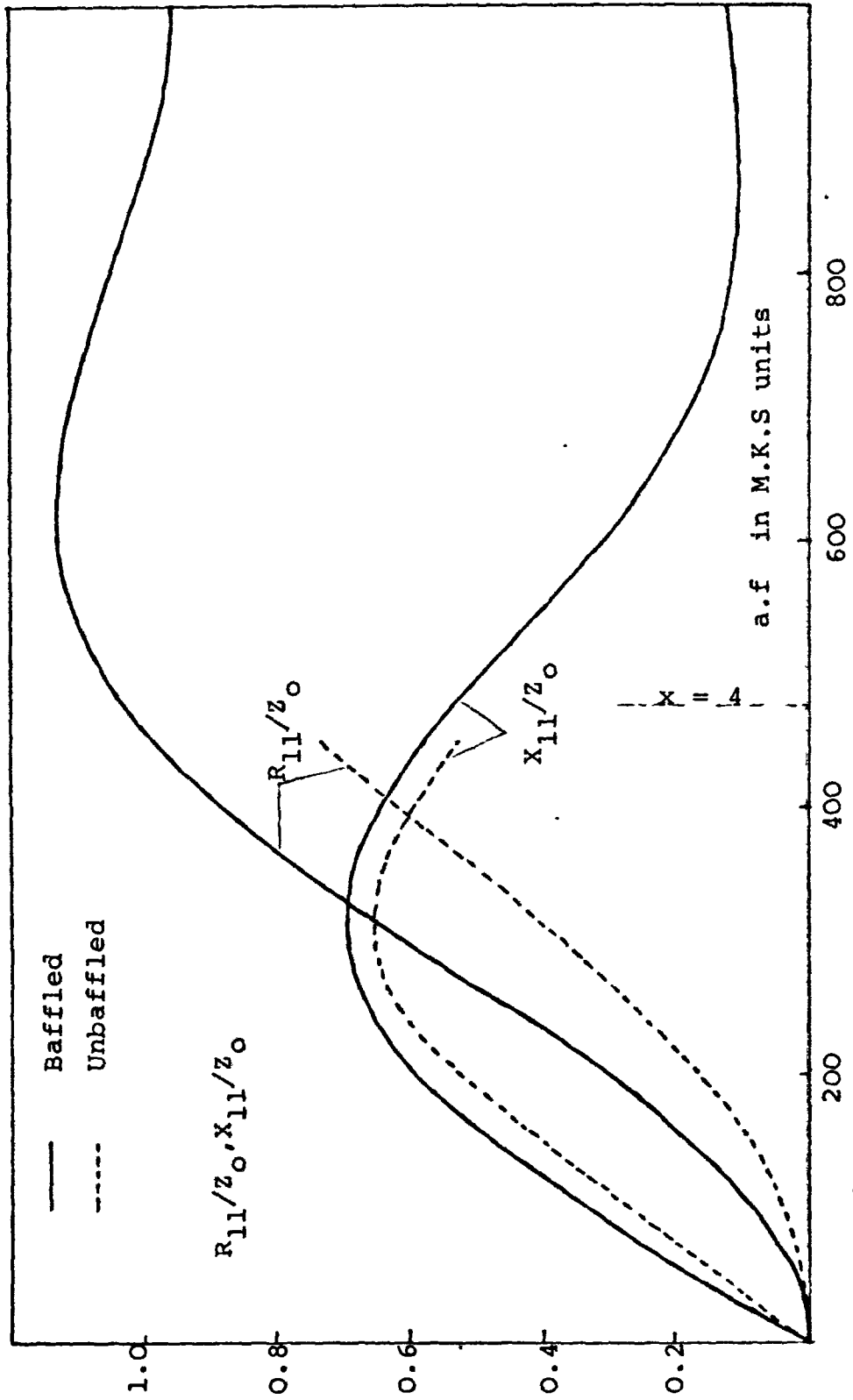
Figure 3.15- Radiation Impedance of a Single Piston Source as a Function of a.f

baffled'. The functions are plotted against the compound variable a.f, which is simply related to the variable x by

$$a.f = x.c/4\pi \quad . \quad\quad (3.41)$$

The above functions can be approximated to simple algebraic expressions[22], in the regions $x > 4$ and $x < 2$. The low frequency approximation ($x < 2$) is applicable when the piston behaves as a simple source and is not of much interest in sonar transducer design. The high frequency approximation ($x > 4$) is

$$R_{11}/Z_o = 1.0, \quad\quad X_{11}/Z_o = 4/\pi x \quad . \quad\quad (3.42)$$

In this region the radiation resistance is constant at Z_o while the reactance is negligibly small (see Figure 3.15). It is in fact possible to cast X_{11} as a negative capacitance for greater precision in a circuit representation, but for output Qs greater than 2, its effect is inconsequential. Thus the high frequency region is ideally suited, circuit-wise, for broadband operation. The lower cut-off frequency f_1 (for sea water) is then set at

$$a \ f_1 = 478 \quad . \quad\quad (3.43)$$

Thus for an f_1 of 4.78 kHz which implies that f_2 is in the region of 15 kHz, the piston radius a has to be greater than 10 cms. In practice it is not possible to construct suitable pistons of diameter 10 cms (or over), which do not flex in the region 5-15 kHz. Thus the design of broadband transducers to operate in isolation in a large rigid baffle is not a practical proposition. The above approximation is not even useful from the standpoint of

analysis as the exact expressions are not much more difficult to program. In the analysis programs the values of R_{11}, X_{11} are calculated at each individual frequency from the series expressions of equations (3.40) the summation being carried out up to 100 terms.

The effect of finite baffles on the radiation impedance of single piston sources has been studied in some detail by Crane[24]. His calculations indicate that a baffle radius of 3-5 times the piston radius is adequate to approximate to infinite baffle performance, except in the lower reaches of frequency. The computational technique adopted by Crane is not described here on account of its extreme complexity. His results for unbaffled piston sources are, however, included in Figure 3.15 as this is of relevance in the testing of transducers. In the analysis program the radiation impedance of an unbaffled projector is obtained by writing Crane's values, numerically, into the program. Intermediate values are approximated to by linear interpolation.

It is important to observe that even though the radiation impedance is resistive and constant for $x > 4$ the radiation pattern is 'closer' to that of a simple source up to $x \backsim 6$[22]. A 'beam' type pattern is not in fact approached until $x \backsim 24$. Thus in the case of transducer arrays which are operated near $x \backsim 2$, acoustic interaction effects are strong.

3.7. Average Radiation Impedance of Piston Sources in Regular Plane Arrays

In order to radiate large quantities of energy in highly directive patterns which are also electronically

steerable, it is customary to group many individual trans-
ducer elements into regular arrays of diverse configuration.
The effective impedance seen by the jth element of a
regular array of n elements is given by[25]

$$Z_j = \sum_{i=1}^{n} Z_{ij} V_i / V_j \tag{3.44}$$

where V_i is the velocity (phasor) of the ith element.
Z_{ij} is the mutual impedance between the ith and jth elements.
The self-impedance of the jth element is included as Z_{jj}.
Z_{ij} is a function of the array geometry and the frequency.
Thus the effective impedance of any individual element is
dependent on frequency, its position in the array and the
drive levels. The variation of Z_j through a regular plane
array has been studied by Freedman[26]. He has also
formulated certain approximations to Z_{ij} which are valid in
particular ranges of 'a.k'.

The design of individual elements of an array is
beyond the scope of this study. The procedure adopted here
is to develop a single design based on a value which is the
arithmetic mean of the effective impedances of all the
elements of a plane regular array.

The estimation of average radiation impedance of
regular arrays was first attempted by Toulis[27]. His results
however are valid only in very limited ranges of frequency.
The technique adopted by Morris[28] is to determine the
average value of Z_j from equation (3.44), assuming equal
piston velocities. The calculation is based on Freedman's
approximations for Z_{ij}. Morris' results which are used in
this study for the design of array elements are given below.

Thus, if R_r and X_r are the average radiation resistance and reactance of the elements of a regular plane array of transducers, in a large baffle, then

$$R_r = R_{11} + R_{11} \cdot D_1/N_1$$

$$X_r = X_{11} + R_{11} \cdot D_2/N_1$$

where (3.45)

$$N_1 = 1.0 - 0.0411 \ a.k + 0.138 \ (a.k)^2$$

$$N_2 = 1.0 - 0.0090 \ a.k + 0.118 \ (a.k)^2 \ .$$

R_{11}, X_{11} and a have the same meaning as in section 3.6 and D_1, D_2 are functions of the piston spacing and packing configuration only. Morris has shown that if A_a is the area of array associated with each element, then D_1, D_2 are functions of A_a/λ^2 only, whatever the packing configuration (square or triangular). Thus if χ (= A/A_a) is the packing factor, D_1, D_2 are functions of $A/\lambda^2\chi$. It follows that the computation of average impedance for a square packed array would yield results of general applicability to any regular packed array of the same piston radius and packing factor. The computation is most convenient for a square packed array. For a regular square N × N array of inter-element spacing 'd', the formulae for D_1, D_2 as given by Morris are

$$D_1 = (1/N^2) \sum_{i=1}^{N} \sum_{j=1}^{N} \sum_{\ell=1}^{N} \sum_{m=1}^{N} \sin\theta(i,j,\ell,m)/\theta(i,j,\ell,m)$$

(3.46)

$$D_2 = (1/N^2) \sum_{i=1}^{N} \sum_{j=1}^{N} \sum_{\ell=1}^{N} \sum_{m=1}^{N} \cos\theta(i,j,\ell,m)/\theta(i,j,\ell,m)$$

$$\theta(i,j,\ell,m) = kd\{(i-j)^2 + (\ell-m)^2\}^{\frac{1}{2}}$$

where the terms for which $i = j$ and $\ell = m$ are excluded from the summations. The above formulae are programmable as they stand but the computing time associated with the calculation could be reduced in the ratio of 250:1 by exploiting the symmetry of the array. Thus equations (3.46) could be reduced to

$$D_1 = (1/N^2) \sum_{i=1}^{(N-1)} \sum_{j=0}^{i} \mu_{ij} \sin \delta_{ij}/\delta_{ij}$$

$$D_2 = (1/N^2) \sum_{i=1}^{N-1} \sum_{j=0}^{i} \mu_{ij} \cos \delta_{ij}/\delta_{ij}$$

$$\delta_{ij} = dk(i^2 + j^2)^{\frac{1}{2}}$$

$$\mu_{ij} = 4\phi(N-i)(N-j)$$

(3.47)

where $\phi = 1$ when $i = j$ or $j = 0$

and $\phi = 2$ when $i \neq j$ and $j \neq 0$.

The packing factor for a square packed array is defined by the d/a ratio according to the formula

$$\chi = \pi a^2/d^2 .$$

(3.48)

Thus a d/a ratio of 2.5 corresponds to a packing factor of 0.5025. A computer program for the determination of the average radiation impedance of regular arrays, according to the above formulae, is included in Appendix II.

Plots of the average radiation impedance of 10 × 10 and 15 × 15 square arrays of packing factor 0.5025, against a.f, are depicted in Figure 3.16. The average impedance values are calculated from equations (3.40),(3.45) and (3.47).
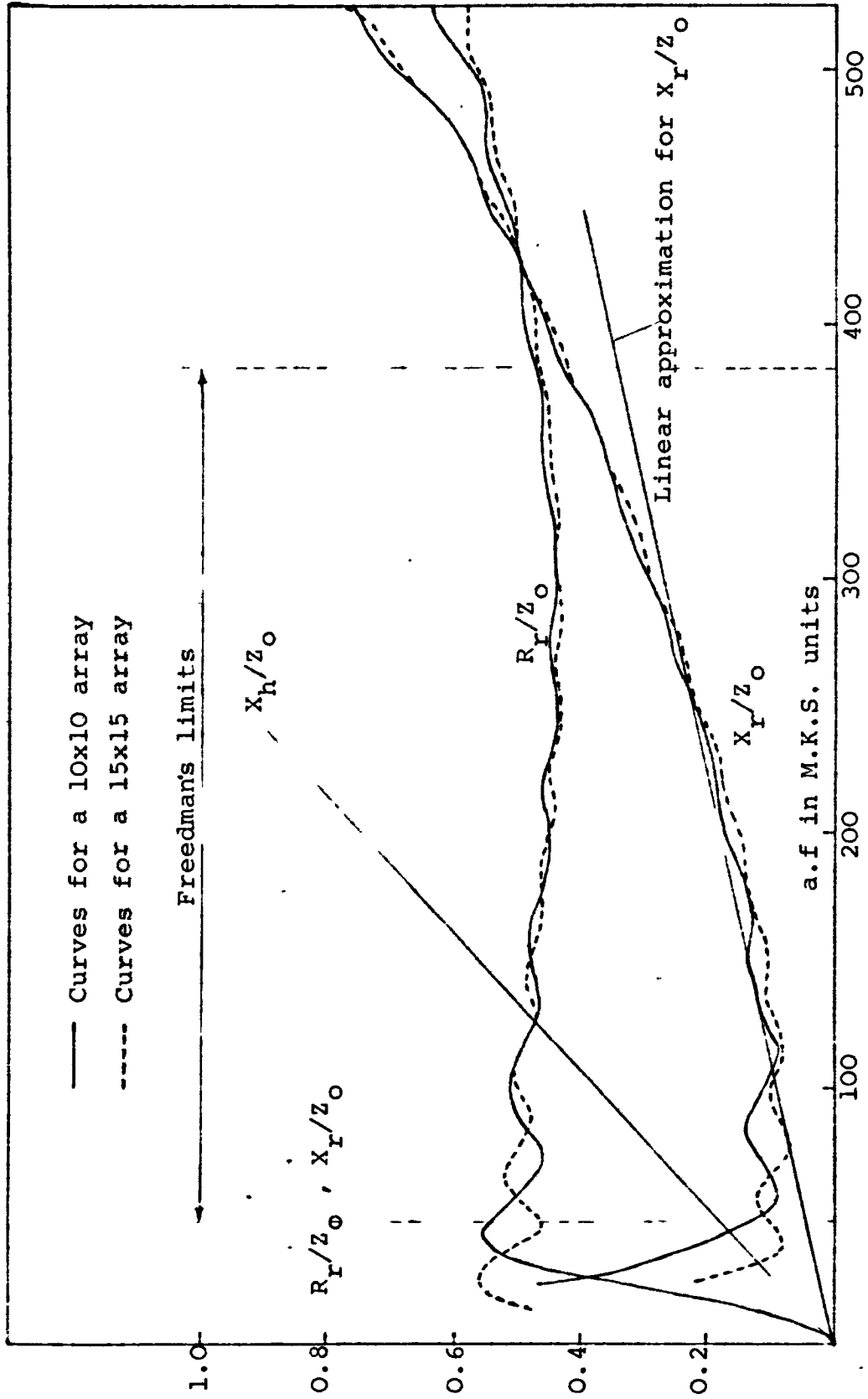
Figure 3.16- Average Radiation Impedance as a Function of a.f for 10x10 and 15x15 Regular Plane Arrays of Packing Factor 0.5025

In these equations for a fixed value of d/a, it is observed that the variables a and f are everywhere combined. Thus a plot of average radiation impedance against the compound variable a.f is sufficient to disclose all the necessary information pertaining to its dependence on both a and f. Further the actual extent of the array (N) appears to have little influence on the average radiation impedance except at low values of a.f when the wavelength is of the order of the lateral dimensions of the array (N.d). The packing factor can hardly be considered as an independent parameter as it is usually kept close to its highest practically realizable value of 0.5 for square arrays. However, for the sake of completeness, impedance curves for d/a ratios of 2.5 and 3.0 are compared in Figure 3.17.

The most important consideration with regard to the estimation of average radiation impedance is the validity limits of the theory. Since Morris' derivation of average impedance is based on Freedman's 'second approximation' it is necessary to consider the range of applicability of the latter. Freedman has compared the results of his approximations for mutual radiation impedance with tables of exact data. He places no restrictions on the permissible values of d.k, but concludes that his 'second approximation' is valid throughout the range

$$0.2 \leq a.k \leq 1.6 \qquad (3.49)$$

but not beyond the upper bound. He does not define an explicit lower limit. If 'average radiation impedance', as calculated above, is to be freed of any dependence on the extent of the array, however, it is necessary to establish a

$R_r/Z_o, X_r/Z_o$

Curves for a packing factor of 0.5025

Curves for a packing factor of 0.3490

R_r/Z_o

X_r/Z_o

a.f in M.K.S. units
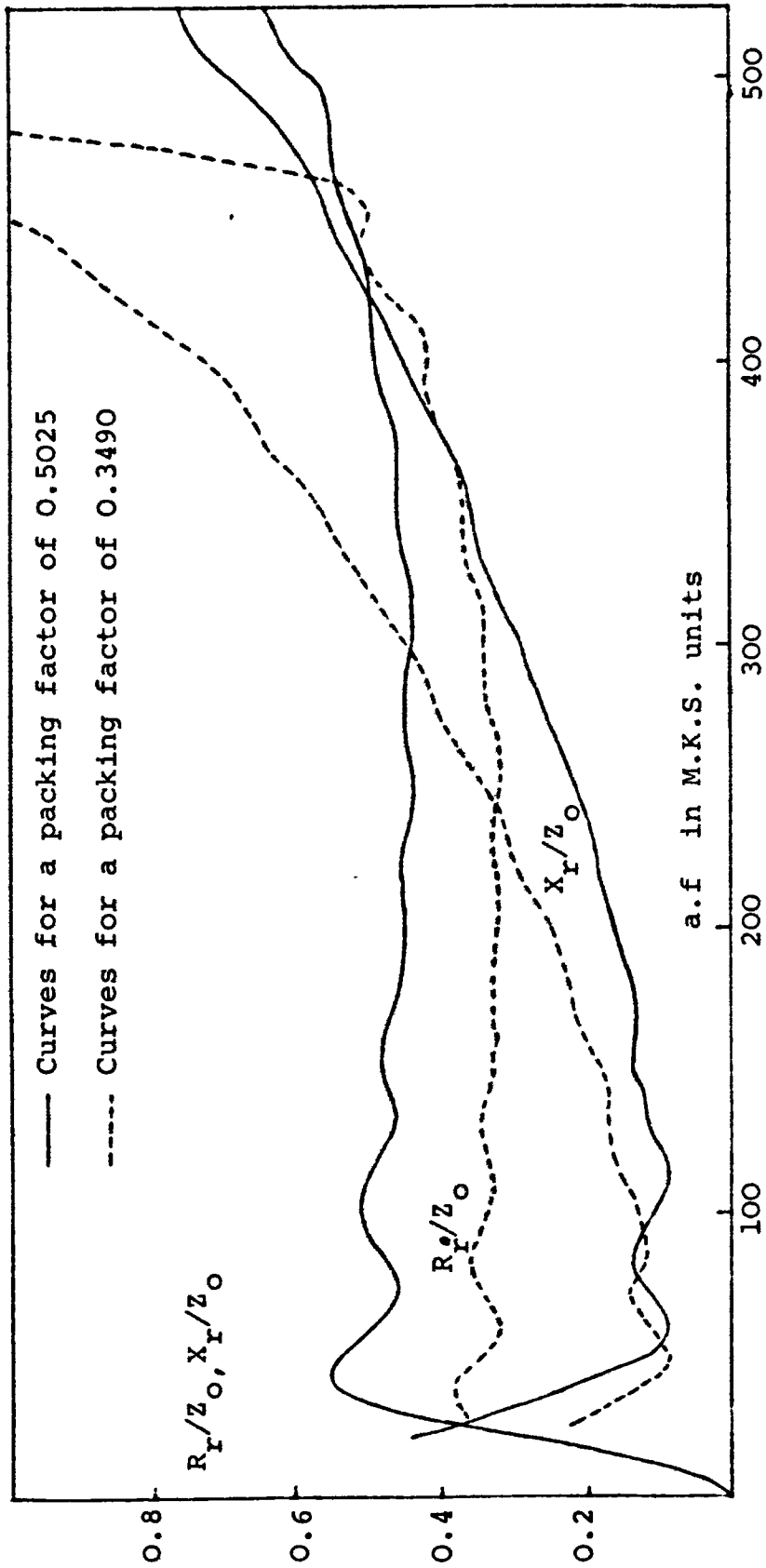
Figure 3.17- Average Radiation Impedance of a 10x10 Square Array as Function of a.f for Two Values of Packing Factor

lower bound beyond which the concept of average impedance
ceases to be meaningful. For square arrays of extent
greater than M × M, the lower limit could be set at

$$af \geq 500/M \quad . \quad (3.50)$$

This limit is inferred empirically from Figure 3.16 on the
basis that the least array length is determined by the
greatest value of wavelength (for a d/a of 2.5). If it is
assumed that practical arrays are not less than 10 × 10,
the above inequality reduces to

$$af \geq 50 \quad (3.51)$$

which is practically the same as the lower bound of (3.49).
Thus the limits expressed in (3.49) are adopted as the
validity limits of the average impedance derivation.
Expressed in terms of af they are

$$50 \leq af \leq 382 \quad . \quad (3.52)$$

Since Freedman is primarily concerned with the applicability
of his 'second approximation' to every single element of
the array, the upper bound may well be more stringent than is
warrantable in an estimation of average impedance for the
whole array. An examination of Figure 3.16, however,
reveals that it is only within these bounds that the
radiation resistance and reactance exhibit the degree of
'linearity' which is necessary for the design of broadband
transducers. Thus the applicability of the formulation
outside these limits is not of primary interest within the
purview of this study.

The frequency range available within these bounds
expressed as a ratio of upper to lower frequency is 7.64.

This range is more than adequate for the design of all conceivable broadband devices (see section 4.5). In fact the lower limit is placed somewhat higher (at around 100) in practical designs to ensure reasonable 'linearity'.

It is interesting to observe that the Freedman upper limit is closely equivalent to

$$2a \leq \lambda/2 \qquad . \qquad (3.53)$$

The linear approximations for R_r and X_r derived from the graphs of Figure 3.16 are

$$R_r = 0.475 \ Z_o$$
$$X_r = a.f \ Z_o/1125 \qquad . \qquad (3.54)$$

The fractional variation of R_r about the mean value is less than $\pm$ 5.4% throughout the Freedman range. This level of constancy is excellent for the incorporation of R_r as the terminating resistance of a broadband filter circuit (see section 4.5).

In any transducer, X_r appears in series with the reactance of the head mass X_h. A plot of a typical value of X_h (for an output Q of around 2) is included in Figure 3.16. It is clear from the figure that the adoption of the linear approximation for X_r (also depicted in Figure 3.16) results in a maximum drift of the sum $(X_h + X_r)$ of around $\pm$ 5% in the a.f range 100 to 400. This variation has negligible effect on the transducer characteristics. The only undesirable effect of this variation is the imposition of a lower limit on the output Q.

Thus it is possible to represent the average radiation impedance of an array by a constant resistance and an

'equivalent mass' in series, in a frequency range adequate for the design of a broadband transducer. The synthesis of a broadband transducer for array operation is based on the approximations of 3.54, which are assumed to hold in the range

$$100 \leq af \leq 400 \quad . \tag{3.55}$$

If f_o is the centre frequency of a transducer operating in th's range, it is p s ible to separate the total output Q into two components Q_h and Q_r which are defined as

$$Q_h = (X_h/R_r) \quad \text{at } f = f_o \tag{3.56}$$

$$Q_r = (X_r/R_r) \quad \text{at } f = f_o \quad . \tag{3.57}$$

Using the approximations of equations (2.54), Q_r reduces to

$$Q_r = af_o/535 \quad . \tag{3.58}$$

Q_h is, of course, adjusted such that the sum works out to the desired output Q. If af_o is fixed at 200, Q_r becomes 0.3744. If af_o is raised to 225, Q_r rises to 0.421. The increase is not too significant if the total Q is not less than 1.6, the lower limit adopted in practice. The design value of af_o must be fixed as high as possible to facilitate mechanical realization of the filter circuit.

CHAPTER 4

DESISN OF PIEZOELECTRIC SONAR
TRANSDUCERS

In this Chapter a technique is developed for the
design of broadband piezoelectric sonar transducers. The
technique is based on the formulation (in section 4.1) of a
generalized equivalent circuit incorporating the essential
components of any extensional type transducer. This
generalized circuit is then used to elicit particular
configurations which operate as broadband filters.

The theory of the optimum filter circuits
realizable within the framework of the generalized
formulation is developed in sections 4.3 and 4.4. In
section 4.5 the most suitable of these circuits is chosen
on the basis of performance and mechanical realizability.
The detailed design of a broadband transducer based on the
optimum choice is presented in section 4.6. The computed
characteristics of the designed transducer are also included
in section 4.6.

The transducer design discussed in section 4.6 is
somewhat different from the test design discussed in
Chapter 6. The former was developed some time after the
construction and testing of the latter and, in fact,
incorporates certain design improvements derived from the
measurements on the test transducer.

4.1. Generalized Equivalent Circuit of a Piezoelectric
Sonar Transducer

In section 3.3 it was shown that the 'transducing
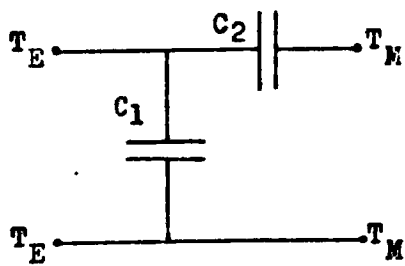
Figure 4.1- Transducing
Section
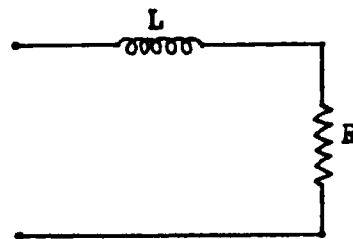
Figure 4.2- Radiating
Section
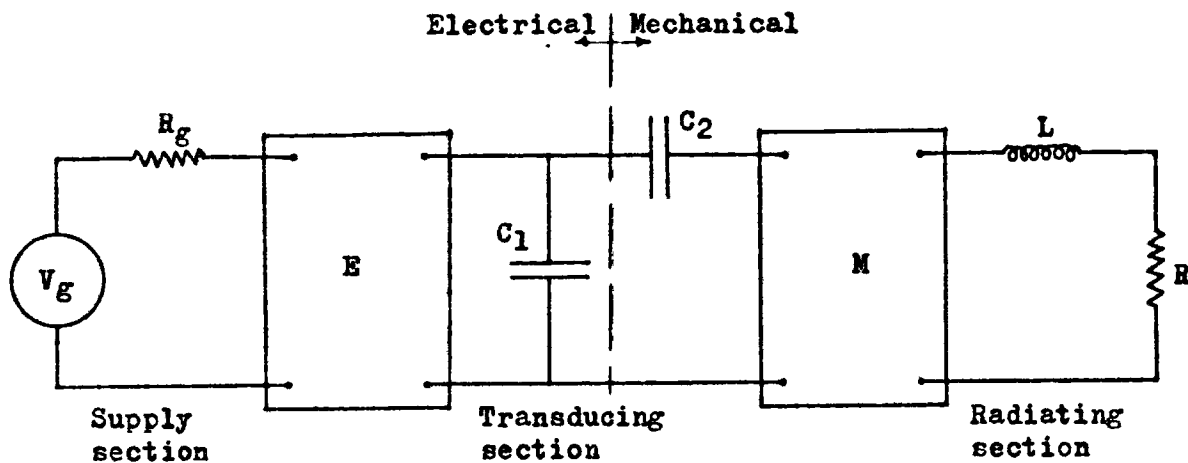
Figure 4.3- Generalized Equivalent Circuit of a Piezoelectric
Sonar Transducer
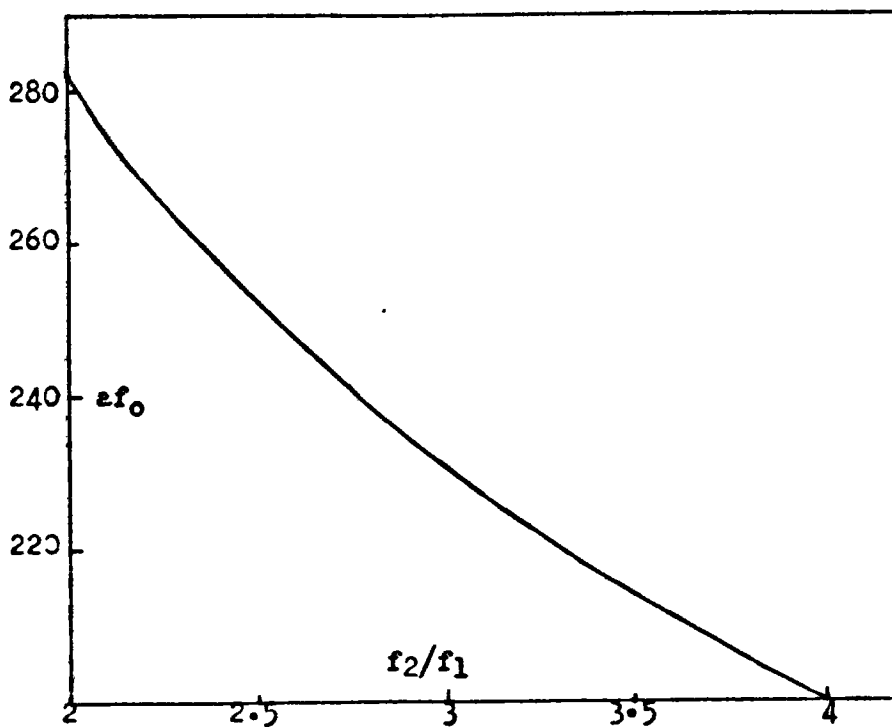
Figure 4.4- Optimum Value of $a.f_o$ as a Function
of f_2/f_1

section' of a piezoelectric sonar transducer could be represented, for the purposes of design, by a capacitance coupler pair, separated by the ideal electromechanical transformer. If the transformer is excluded by referring the circuit to the electrical side, the network of Figure 4.1 results. Here

$$C_2/C_1 = K^2 \qquad (4.1)$$

where K is a measure of the effective coupling (see section 3.2) and C_1, C_2 are dependent on the parameters of the ceramic stack. T_M, T_E represent the mechanical and electrical terminals, respectively.

In section 3.7 it was found possible to represent the radiating head and the radiation load in an array, as a series L-R combination. It was shown that if the radiating head mass was included with the radiation reactance in the equivalent mass L both L and R (the radiation resistance) were substantially constant in a particular range of frequency. Thus if the transducer passband was chosen to fall within this frequency range the 'radiating section' can be represented by the circuit of Figure 4.2.

The transducing and radiating sections are integral parts of any extensional piezoelectric transducer with the circuits of Figures 4.1 and 4.2 being their most succinct expression. Together with the supply they constitute the essential ingredients of such a transducer. Between the transducing and radiating sections, however, it is possible to introduce extra-mechanical elements. Similarly electrical elements could be interposed between the transducing section and the supply. Consequently any practical

transducer could be represented by the generalized circuit
of Figure 4.3 where the networks E and M represent the
optional electrical and mechanical elements. The supply
is assumed to be a constant voltage source of constant
internal resistance R_g.

The generalized equivalent circuit of Figure 4.3
is clearly a ladder network with constant source and load
resistances. Also if the elements of M are chosen subject
to the restrictions discussed in sections 3.1 and 3.5, the
circuit components are conventional LC type series and
parallel elements. Thus the problem of design for broadband
operation could be solved by choosing the elements of E, M
and the component values such that the resulting circuit
is a ladder type filter with a broad passband.

This method of transducer design is adopted in this
study, as a large store of circuit synthesis data for
ladder networks is already available[30-32]. Further, since
modern filter synthesis is executed on the basis of matched
impedance and constant group delay operation in the passband,
the other design criteria are automatically satisfied.

It is immediately obvious, however, that on account
of the presence in the circuit of C_1 and C_2 which are of the
same order of magnitude, both high pass and lowpass networks
are excluded. The choice of available bandpass circuits is
also severely curtailed by the need to satisfy the mechanical
realizability conditions for the elements of M. In particular
parallel inductors are excluded as they possess no mechanical
counterpart (see section 2.2). The electrical elements too
must be neither cumbersome nor too costly to realize.

Consequently only two types of bandpass filter circuits[32] are found to be realizable within the framework of the generalized circuit. These are the canonic (or analogous) bandpass designs and the coupled resonator designs. Both bandpass designs are derived from the same low pass configurations. The canonic bandpass circuits are obtained by the exact lowpass to bandpass transformation. The coupled resonator circuits are narrow band approximations of the corresponding canonic designs.

The derivation of the two types of bandpass circuits and the tailoring of the circuit parameters for realizability and optimum performance is dealt with in sections 4.3 and 4.4. As a necessary prelude to this, however, the practical and theoretical consequences of the generalized representation of Figure 4.3 are discussed in section 4.2.

Since filter design is more convenient with normalized circuits the generalized circuit is impedance scaled to the level of the radiation resistance R and frequency scaled to the chosen centre (angular) frequency ω_o. This is done by multiplying the resistances in the circuit by $1/R$, the inductances by ω_o/R and the capacitances by $R\omega_o$. Consequently the terminating resistance in the normalized circuit and the centre (angular) frequency are both reduced to unity.

4.2. Properties of the Generalized Equivalent Circuit

The maximum power P_m that could be drawn from the supply (of Figure 4.3) is given by

$$P_m = |V_g|^2/4R_g \qquad . \qquad (4.2)$$

If P is the radiated power and V is the 'voltage' across R

$$P = |V|^2/R \quad . \tag{4.3}$$

Clearly P is always less than P_m. If V_m is the value of V corresponding to $P = P_m$, $|V|$ is also always less than $|V_m|$. The passband of the generalized transducer circuit is defined as the region of frequencies for which

$$P \leq P_m/2 \tag{4.4}$$

or $\quad |V/V_m| \geq 0.7071 \quad . \tag{4.5}$

Most transducers are designed such that their P or V characteristic has the standard bandpass shape depicted in Figure 4.9. Thus if f_1, f_2 are the lower and upper cut-off frequencies, corresponding to the half-power points (or the 3dB points on the $|V/V_m|$ characteristic) the centre frequency f_o and the fractional bandw'dth β are given by

$$f_o^2 = f_1 f_2 \tag{4.6}$$

$$\beta = (f_2 - f_1)/f_o \tag{4.7}$$

If $P = P_m$ at $f = f_o$ the maximum bandwidth β_{max} that could be obtained from the generalized circuit of Figure 4.3 is governed primarily by the effective coupling of the transducing section. Baerwald[29] has shown that, if equation (4.1) is the sole constraint on the generalized circuit, β_{max} is given by

$$\beta_{max} = 2K \quad . \tag{4.8}$$

This limit is also equivalent to

$$(f_2/f_1)_{max} = (K + \sqrt{K^2+1})^2 \quad . \tag{4.9}$$

If finite mid band loss is tolerated (i.e., if $P < P_m$ at $f = f_o$), the maximum bandwidth could be even higher.

In practice, however, equation (4.1) is not the sole constraint on the generalized circuit. The output or mechanical quality factor Q_m is another. In relation to the generalized representation Q_m is defined as

$$Q_m = \omega_o L/R \quad . \tag{4.10}$$

For a given circuit configuration, the bandwidth is dependent on Q_m as well as K though less sensitively on the former. The dependence is explicitly derived for the case of the conventional (2 pole, canonic) transducer, in Appendix I. On account of the need to design for pistons that do not flex (or 'flap') in the passband, the practically realizable values of Q_m are limited to

$$Q_m \geq 1.6 \quad . \tag{4.11}$$

A lower value of Q_m is also undesirable from the point of view of the radiation impedance approximation (see section 3.7).

It has been shown in Chapter 3 that the representation assumed in the generalized equivalent circuit holds to within $\pm$ 10% of the true value up to the upper limit of frequency provided the derived geometric limits are adhered to. The upper limit of frequency is 7.5 or 15 kHz depending on the centre frequency chosen. In the case of the radiating section in particular the representation is justified provided $Q_m \geq 1.6$ and a.f (where a is the piston radius) lies in the range
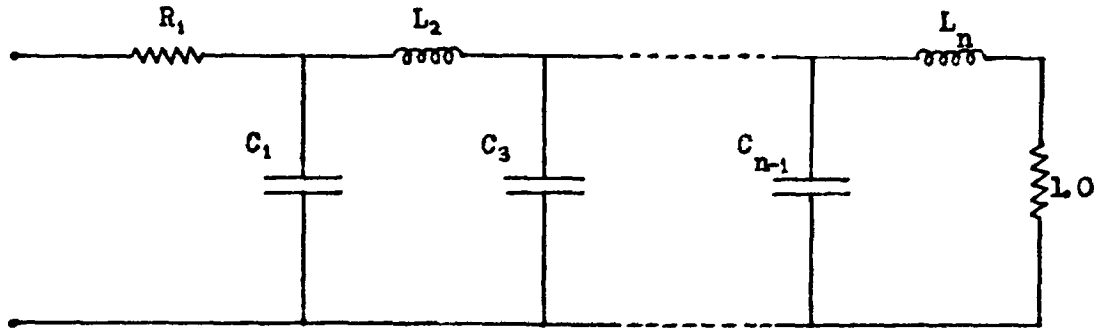
Figure 4.5- Normalized n-pole Lowpass Filter Circuit
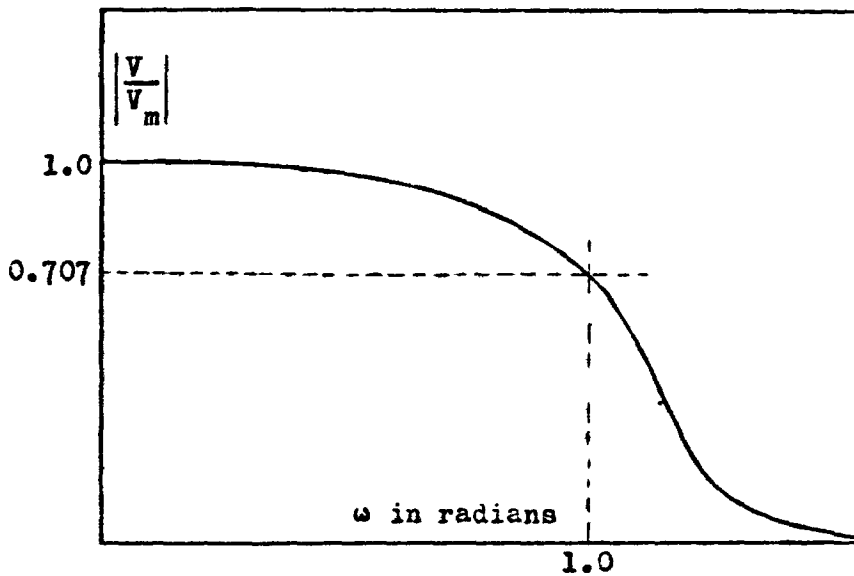
Figure 4.6- Amplitude Response of a Lowpass Filter
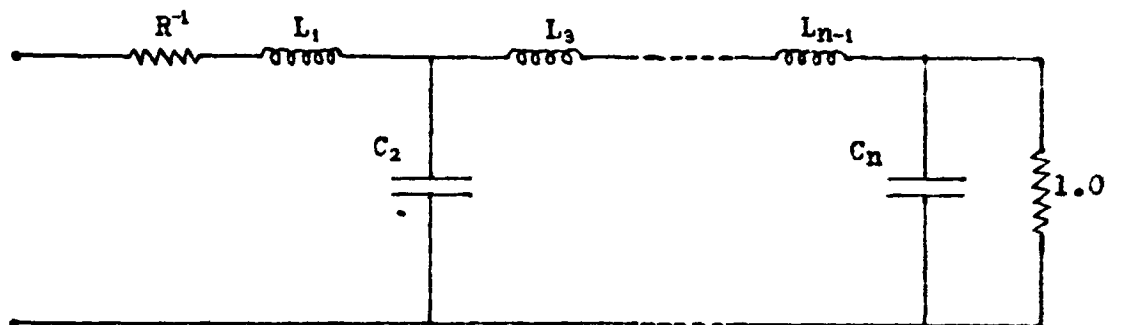
Figure 4.7- Dual Network of a n-pole Lowpass Filter

$$100 \leq af \leq 400 \quad . \tag{4.12}$$

Thus the chosen centre frequency and piston radius must be such that $af_1 - af_2$ falls within this range. Since f_2/f_1 for realizable broadband circuits rarely exceeds 3.5, the frequency span available within this range (4:1) is more than adequate. The centre frequency implicit in equation (4.12) ($af_0 = 200$) is used when comparing the mechanical realizability of alternative broadband circuits. In actual transducer designs, however, the highest possible value of af_0 is employed as this facilitates realizability. The optimum value of af_0 which does not violate the restrictions of equation (4.12), is plotted against f_2/f_1 in Figure 4.4. The nett result is that there is little independent control over a and f_0. For the circuits considered in this study af_0 lies within the range

$$200 \leq af_0 \leq 250 \quad . \tag{4.13}$$

4.3. Canonic Bandpass Circuits
Low-pass Prototype

The general n-pole lowpass prototype from which the bandpass designs are derived is given in Figure 4.5. This circuit is impedance and frequency normalized such that the terminating resistance is unity and the 3-dB cut-off frequency is at $\omega = 1.0$. The amplitude characteristic of the filter $|V/V_m|$ (as defined in section 4.2) is depicted in Figure 4.6. The shape of the characteristic and the actual values of the elements $C_1 - L_n$ depend on the specific lowpass filter used (such as a Butterworth 3-pole, Chebychev 2-pole, etc.). An equally terminated Butterworth 3-pole filter would, for instance, have

$$R_1 = C_1 = C_3 = 1.0, \qquad L_2 = 2.0 \qquad\qquad (4.14)$$

and the frequency characteristic would be 'maximally flat'. The dual network of the n-pole lowpass prototype is that of Figure 4.7 where

$$L_1 = C_1, \quad C_2 = L_2, \quad \ldots, \quad L_n = C_n \quad . \qquad\qquad (4.15)$$

Since the dual network has the same frequency characteristic as the original it could be used as an alternative lowpass prototype when necessary.

The normalized k (coupling) and q factors defined with respect to the normalized lowpass filter of Figure 4.5 are as follows (see Zverev[32] for details)

$$k_{12} = (C_1 L_2)^{-\frac{1}{2}} , \qquad k_{23} = (L_2 C_3)^{-\frac{1}{2}} , \text{ etc.} \qquad (4.16)$$

$$q_1 = R_1 C_1, \qquad q_n = L_n \qquad . \qquad\qquad (4.17)$$

The k and q factors constitute an alternative description of a lowpass filter instead of the element-wise specifications of Figures 4.5 and 4.7. In the case of circuit of Figure 4.7 the k and q values are

$$k'_{12} = (L_1 C_2)^{-\frac{1}{2}}, \qquad k'_{23} = (C_2 L_3)^{-\frac{1}{2}} \text{ etc.} \qquad (4.18)$$

$$q_1' = R_1 L_1 \quad , \qquad q_n' = C_n \qquad . \qquad\qquad (4.19)$$

From equations (4.15) it is clear that the k and q values are the same for either network. Thus the normalized k and q description of a filter is more general than the element-wise description.

Derivation of the canonic bandpass circuit from the lowpass prototype

The canonic bandpass circuit is derived from the
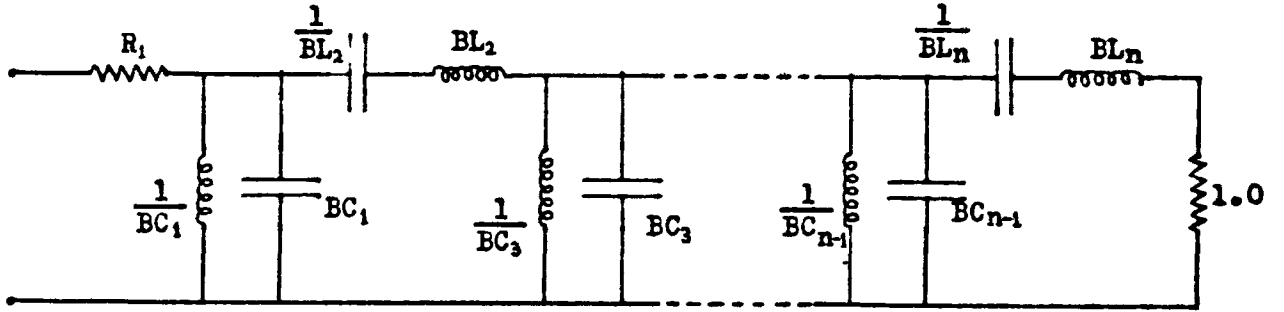
Figure 4.8- Normalized n-pole Canonic Bandpass Filter Circuit
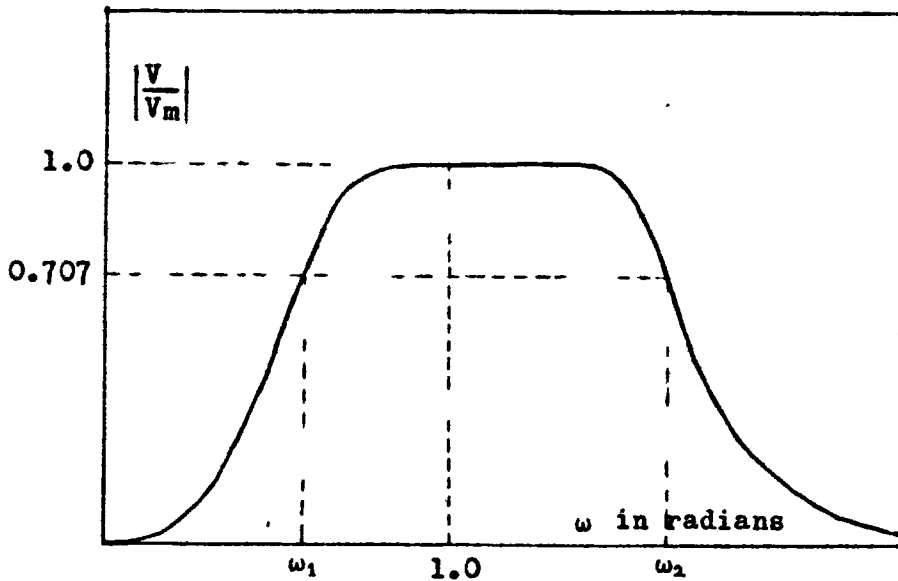
Figure 4.9- Frequency Characteristic of Canonic Bandpass
Filter
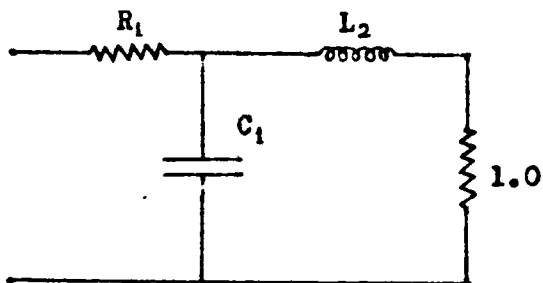
Figure 4.10- Two Pole Lowpass
Prototype
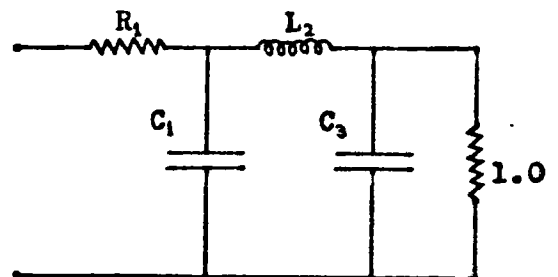
Figure 4.11- Three Pole
Lowpass Prototype

lowpass prototype by the application of the s-plane transformation

$$s_n = \frac{1}{\beta}(s/\omega_0 + \omega_0/s) \qquad (4.20)$$

to every reactive element of the latter circuit. In the above transformation β is the fractional bandwidth and ω_0 the centre frequency of the desired bandpass filter. If B is the inverse of β and ω_0 is fixed at unity (for a frequency normalized bandpass circuit) the above transformation reduces to

$$S_n = B(S + 1/S) \qquad . \qquad (4.21)$$

Thus a series impedance $s_n L$ in the lowpass circuit is transformed into $sL' + 1/sC'$ where

$$L' = BL \quad \text{and} \quad C' = 1/BL \qquad . \qquad (4.22)$$

Similarly a shunt admittance $s_n C$ is transformed into $sC'' + 1/sL''$ where

$$C'' = BC \quad \text{and} \quad L'' = 1/BC \qquad . \qquad (4.23)$$

Applying this transformation to the lowpass filter of Figure 4.5 the impedance and frequency normalized canonic bandpass filter of Figure 4.8 is obtained. The amplitude response $|V/V_m|$ of this filter is depicted in Figure 4.9. It is very easily shown (from equation (4.21)) that the 3-dB points ω_1, ω_2 are such that

$$\omega_2 - \omega_1 = 1/B \qquad (4.24)$$

and $\qquad \omega_1 \omega_2 = 1 \qquad .$

Since the lowpass to bandpass transformation is exact, the characteristic possesses geometric symmetry about $\omega = 1.0$.

If the lowpass prototype of Figure 4.7 had been used instead, the resulting bandpass circuit would have 'begun' with a series LC pair and terminated with a parallel LC pair.

The bandpass circuit of Figure 4.8 can clearly be fitted into the generalized transducer circuit of Figure 4.3. The transducing section must however be realized in the end capacitor pair BC_{n-1}, $1/BL_n$ for otherwise an unrealizable shunt inductor would appear on the mechanical side of the circuit. The conditions for mechanical realization are

$$BL_n = Q_m \qquad \qquad (4.25)$$

and $\qquad 1/(B^2 L_n C_{n-1}) = K^2 \qquad . \qquad (4.26)$

These equations are derived from equations (4.1) and (4.10). Using equations (4.16) and (4.17) the above relations simplify to

$$Bq_n = Q_m \qquad \qquad (4.27)$$

and $\qquad B = k_{n-1,n}/K \qquad . \qquad (4.28)$

It is observed that a particular choice of K in equation (4.28) alone explicitly defines all the element values of the bandpass circuit. For the resulting circuit to be practically realizable, however, B and q_n must be such that the condition of equation (4.11) is satisfied. Further since the fractional bandwidth is 1/B, the maximum bandwidth is obtained for the least value of circuit coupling $k_{n-1,n}$ and the maximum value of piezoelectric coupling K. Thus it is advantageous to use lowpass prototypes with low values of $k_{n-1,n}$.

$$B = k_{12}/K \quad \text{Electrical Mechanical}$$
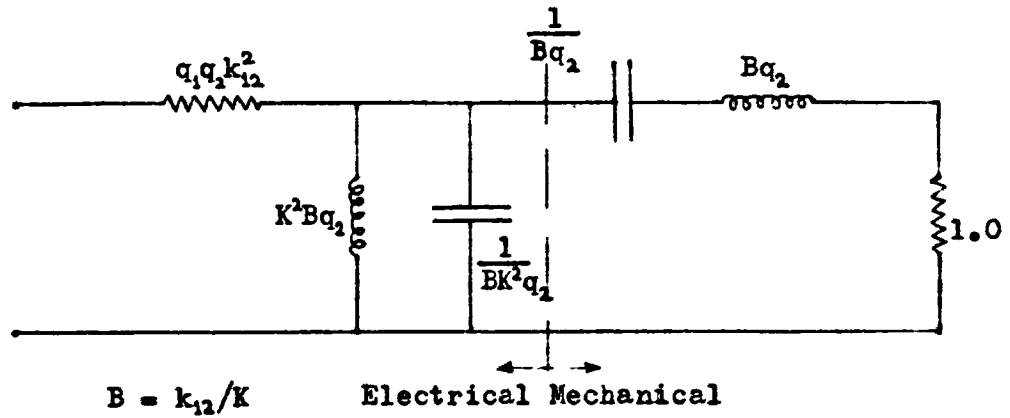
Figure 4.12- Normalized 2-pole Canonic Bandpass Circuit

$$B = k_{23}/K \quad \text{Electrical Mechanical}$$
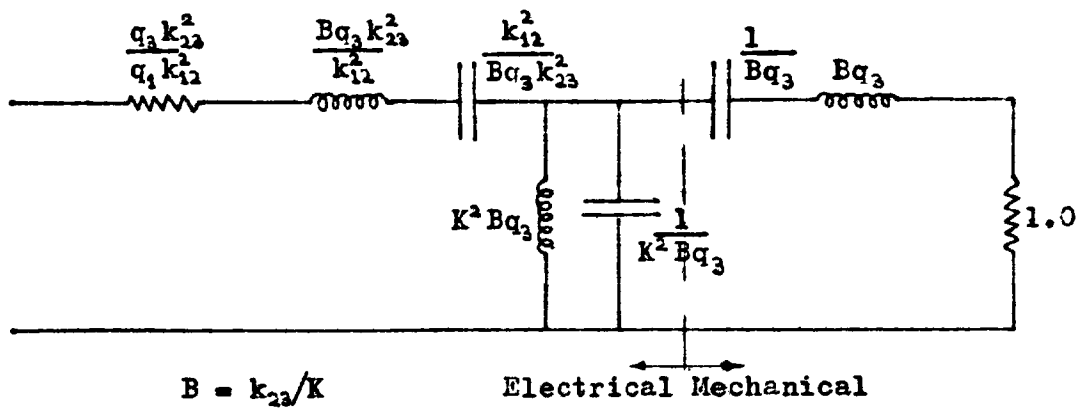
Figure 4.13- Normalized 3-pole Canonic Bandpass Circuit
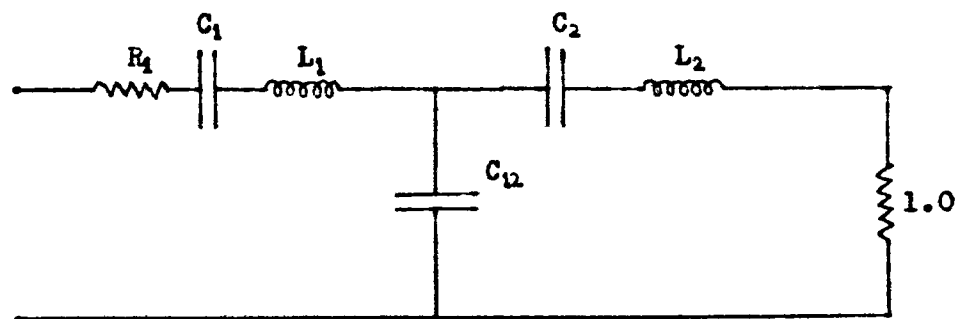
Figure 4.14- Two-pole Coupled Resonator Bandpass Circuit
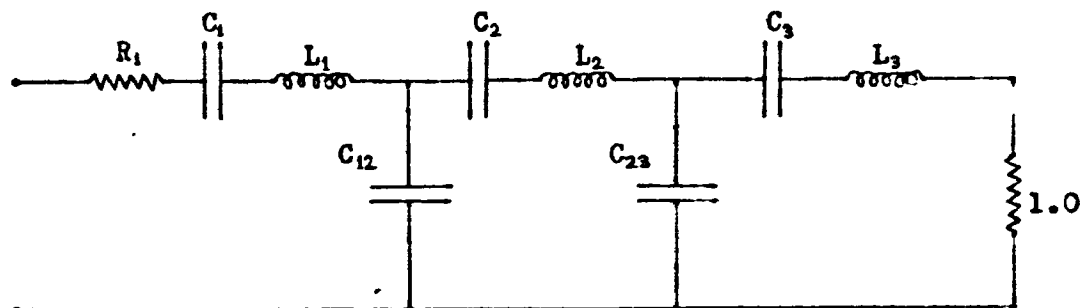
Figure 4.15- Three-pole Coupled Resonator Bandpass Circuit

In practice it is not feasible to realize bandpass circuits of order higher than 3-pole. Further a perusal of the k, q tables[32] for standard lowpass filters reveals that no significant reduction of $k_{n-1,n}$ is obtained for higher order filters.

Specific bandpass designs derived from the 2-pole and 3-pole lowpass prototypes of Figures 4.10 and 4.11 are given in Figures 4.12 and 4.13. The element values of these circuits are given in terms of the k, q values and B and K, as this is the most convenient form.

4.4. Coupled Resonator Bandpass Circuits

The canonic lowpass to bandpass transformation, though theoretically correct, is not always justified in practice. An alternative circuit is available in the coupled resonator approximation of a canonic bandpass design. The coupled resonator bandpass circuits are generally less sensitive to variations of the element values. They are also more convenient to realize mechanically. Since they are only an approximation to the exact canonic designs, the formulations are theoretically valid[32], only within a narrow frequency band (20% of the centre frequency). As a result of actual analysis, however, it has been established that passbands up to 120% could be obtained from Butterworth type standard coupled resonator designs without serious deterioration of characteristics. The transformation does not hold satisfactorily for filter types other than Butterworth and low ripple Chebychev equally terminated designs at such large bandwidths.

The theory of coupled resonator bandpass filter design is well treated in the literature[31,32]. The rules for the derivation of the relevant filter circuits from the normalized k and q values are given below.

Couplied resonator bandpass circuits consist of basic L-C resonator pairs 'coupled' together by reactive elements and terminated at either end in a pure resistance. The L-C resonator elements may be in parallel in the nodal circuit designs or in series in the mesh circuit designs. The coupling elements could be capacitative, inductive or mutual inductive. For realization as piezoelectric sonar transducers, however, only series resonator pairs coupled by shunt capacitors are suitable. The circuit diagrams of such coupled resonator filters based on 2-pole and 3-pole lowpass prototypes are given in Figures 4.14 and 4.15. As in the case of the canonic designs higher order circuits are not considered on account of the complexity of the resulting circuits and because improved performance cannot be obtained from them.

Clearly both circuits are realizable within the framework of the generalized transducer circuit. In the case of the 3-pole design, however, the transducing section could be incorporated in the pair C_{12}, C_2 or the pair C_{23}, C_3. If the former course is chosen the broadband transducer would consist of one electrical resonator and two mechanical resonators and vice-versa if the latter alternative is adopted.

The mesh circuit designs of Figures 4.14 and 4.15 must satisfy the following requirements for operation as bandpass filters[32].

1. The value of the coupling capacitance C_{ij} between the ith and jth meshes must be such that

$$C_{ij} = (C'_i C'_j)^{\frac{1}{2}} B/k_{ij} \qquad (4.29)$$

where C'_i, C'_j are the total series capacitances of the ith and jth meshes respectively and k_{ij} is the appropriate value of normalized circuit coupling.

2. Each mesh must resonate at the centre frequency with the other meshes open circuited. For the frequency normalized circuits considered in this section

$$C'_i L_i = 1 \qquad (4.30)$$

for each mesh where L_i is the appropriate mesh inductance.

3. The input and output Q factors must be Bq_1 and Bq_n respectively. Thus

$$L_1/R_1 = Bq_1, \qquad L_n = Bq_n \qquad . \qquad (4.31)$$

In addition to the above requirements for operation as a bandpass filter, two extra constraints are introduced by the need to realize the circuit as a sonar transducer (see section 4.1). The first of these (equat'on (4.1)) could be expressed in the context of the mesh circuits of Figures 4.14 and 4.15 as

$$C_j = K^2 C_{ij} \qquad . \qquad (4.32)$$

The second which is a lower limit on the realizable Q_m (equation (4.11)) is not formulated here as an explicit algebraic constraint. The significance of this constraint in relation to realizable bandpass circuits is further discussed in section 4.5.

In the foregoing formulation of the above relations for 2-pole and 3-pole designs the variables C'_i, C'_j are replaced by L_i^{-1}, L_j^{-1} from equation (4.30) for convenience.

Two-pole coupled resonator bandpass design

The circuit of Figure 4.14 would behave as a bandpass filter suitable for realization as a piezoelectric sonar transducer provided the following equations were satisfied.

$$C_{12}^{-1} = (L_1 L_2)^{\frac{1}{2}} k_{12} / B \qquad (4.33)$$

$$L_1 = C_1^{-1} + C_{12}^{-1} \qquad (4.34)$$

$$L_2 = C_2^{-1} + C_{12}^{-1} \qquad (4.35)$$

$$L_1 = R_1 B q_1 \qquad (4.36)$$

$$L_2 = B q_2 \qquad (4.37)$$

$$C_2 = K^2 C_{12} \qquad (4.38)$$

The factors k_{12}, q_1, q_2 depend on the specific lowpass prototype chosen and K is the effective piezoelectric coupling. In spite of the extra constraint introduced by the piezoelectric coupling, the seven parameters of the filter circuit, inclusive of B, are related by only six equations. This is a consequence of the flexibility of coupled resonator designs. As a result it is possible to tailor the parameters for an optimum value of B. Since maximum bandwidth is desired the required optimum is the least value of B. The minimization of B is effected as follows.

Eliminating C_2 between equations (4.38) and (4.25)

$$L_2 = \mu C_{12}^{-1} \qquad (4.39)$$
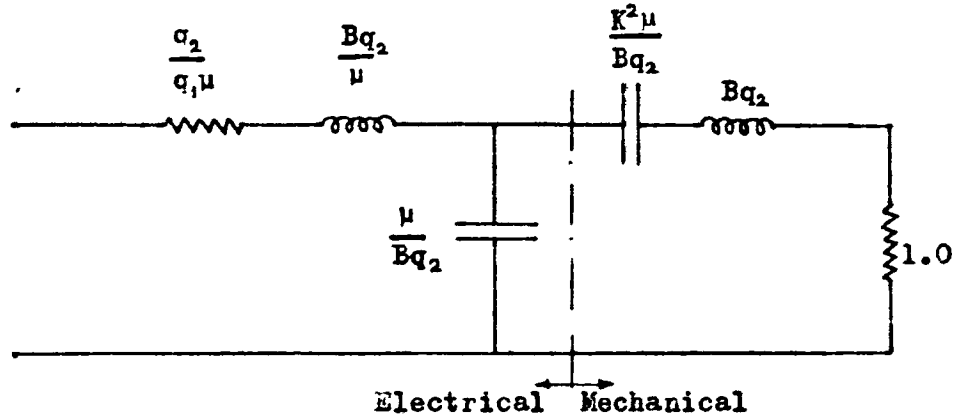
Figure 4.16- Optimum Design of 2-pole Coupled
Resonator Circuit
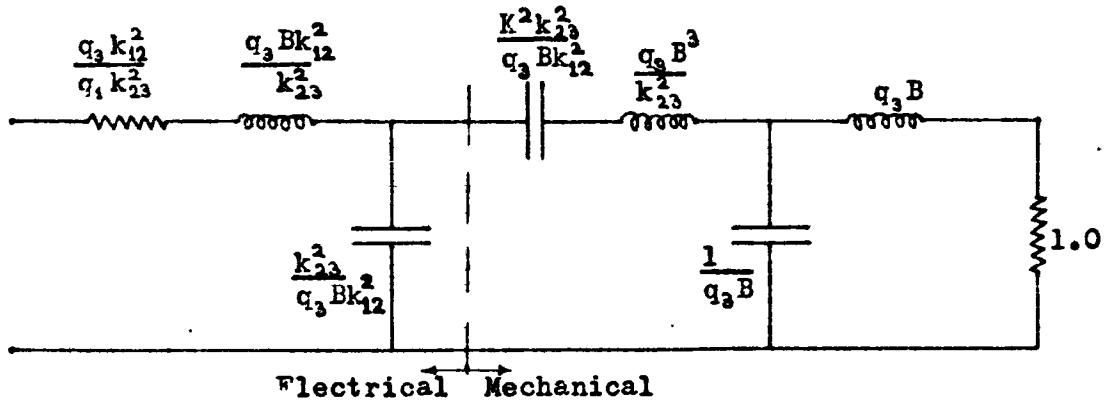
Figure 4.17- Optimum Design of Predominantly Mechanical
3-pole Coupled Resonator Circuit
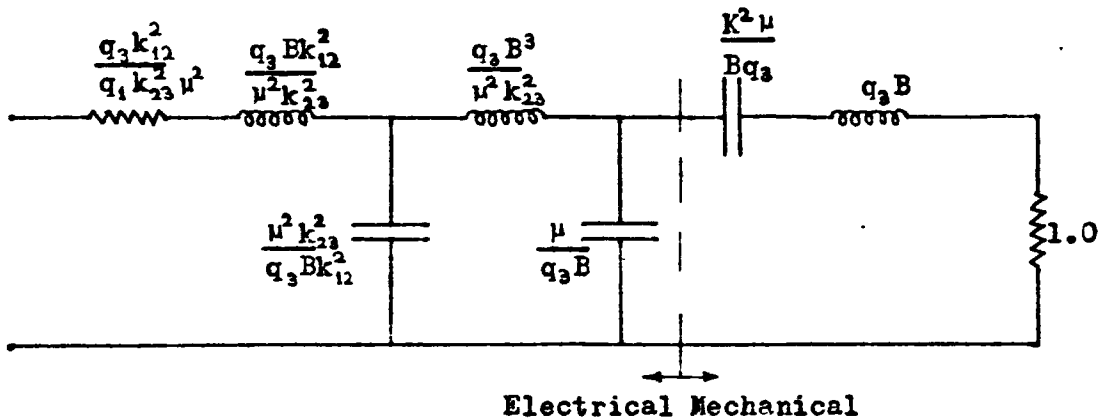
Figure 4.18- Optimum Design of Predominantly Electrical
3-pole Coupled Resonator Circuit

where $\qquad \mu = (K^2+1)/K^2$ $\qquad$. $\qquad$ (4.40)

Substituting for C_{12} from equation (4.33) in equations (4.34) and (4.39) and eliminating L_2, it is easily shown that

$$B^2 = \mu k_{12}^2/(1 - L_1^{-1}C_1^{-1}) \qquad . \qquad (4.41)$$

Thus the least value of B is obtained for the greatest value of $L_1 C_1$. C_1 can, however, be made effectively infinite by eliminating it altogether from the circuit when the above expression reduces to

$$B = \mu^{\frac{1}{2}} k_{12} \qquad . \qquad (4.42)$$

The reduction also determines the element values explicitly as it eliminates one variable from the original set. The resultant optimum circuit design is given in Figure 4.16.

Three-pole coupled resonator bandpass design

$\qquad$ The constraining equations for the 3-pole coupled resonator circuit of Figure 4.15 are given below. The design is based on the 3-pole lowpass prototype which is defined by the values q_1, q_2, k_{12} and k_{23}.

$$C_{12}^{-1} = (L_1 L_2)^{\frac{1}{2}} k_{12}/B \qquad (4.43)$$

$$C_{23}^{-1} = (L_2 L_3)^{\frac{1}{2}} k_{23}/B \qquad (4.44)$$

$$L_1 = C_1^{-1} + C_{12}^{-1} \qquad (4.45)$$

$$L_2 = C_{12}^{-1} + C_2^{-1} + C_{23}^{-1} \qquad (4.46)$$

$$L_3 = C_{23}^{-1} + C_3^{-1} \qquad (4.47)$$

$$L_1 = R_1 B q_1 \qquad\qquad (4.48)$$

$$L_3 = B q_3 \qquad . \qquad\qquad (4.49)$$

The specific formulation of the 'piezoelectric coupling' equation depends on the position of the transducer coupler. Assuming this is realized in C_{12}, C_2 for a 'predominantly mechanical' circuit

$$C_2 = K^2 C_{12} \qquad . \qquad\qquad (4.50)$$

In this case ten variables are constrained by eight equations. The derivation of the least value of B is similar to that for the case of the 2-pole filter.

Using equation (4.50), equation (4.46) can be restated as

$$L_2 = \mu C_{12}^{-1} + C_{23}^{-1} \qquad\qquad (4.51)$$

where μ was defined in equation (4.40). Substituting for C_{12} and C_{23} from equations (4.43) and (4.44), equations (4.45), (4.51) and (4.47) become

$$1 = L_1^{-1} C_1^{-1} + (L_2/L_1)^{\frac{1}{2}} k_{12}/B \qquad\qquad (4.52)$$

$$1 = \mu (L_1/L_2)^{\frac{1}{2}} k_{12}/B + (L_3/L_2)^{\frac{1}{2}} k_{23}/B \qquad\qquad (4.53)$$

$$1 = L_3^{-1} C_3^{-1} + (L_2/L_3)^{\frac{1}{2}} k_{23}/B \qquad . \qquad\qquad (4.54)$$

Eliminating (L_1/L_2) and (L_3/L_2) between the above equations it can be shown that

$$B^2 = \mu k_{12}^2/(1 - L_1^{-1} C_1^{-1}) + k_{23}^2/(1 - L_3^{-1} C_3^{-1}) \qquad . \qquad (4.55)$$

As before the least value of B is obtained when $C_1 = C_3 = \infty$ when

$$B = (\mu k_{12}^2 + k_{23}^2)^{\frac{1}{2}} \quad . \qquad (4.56)$$

The corresponding 'predominantly mechanical' optimum design is given in Figure 4.17.

If, however, the transducing section is realized in the pair C_{23}, C_3 equation (4.50) is changed into

$$C_3 = K^2 C_{12} \quad . \qquad (4.57)$$

In this case it is easily demonstrated that the optimum value of

$$B = (k_{12}^2 + \mu k_{23}^2)^{\frac{1}{2}} \qquad (4.58)$$

is obtained when $C_1 = C_2 = \infty$. The corresponding 'predominantly electrical' optimum design is given in Figure 4.18.

A great advantage of the optimum designs is the elimination of all but one of the series capacitances from the general circuit which considerably reduce realization problems. The derivation of such optimum designs is possible for 4-pole coupled resonator circuits as well. The resulting bandwidth, however, is not greater than that for 3-pole designs though the cut-off is sharper.

The bandwidth and centre frequency of the derived optimum circuits is found (on analysis) to deviate considerably from that predicted by the theory. The bandwidth is around 35% in excess of the predicted value for 2-pole designs and around 60% higher for 3-pole circuits. The centre frequency is depressed to around $\omega_o = 0.78$, from

the nominal value of $\omega_O = 1.0$. Thus in using coupled resonator designs the effective centre frequency $(\bar{\omega})$ and bandwidth (β) must be measured from the computed characteristics. The reasons for this discrepancy, which is not present in the exact canonic designs, have been given at the beginning of this section.

Further, the variable B can no longer be regarded as the inverse of the bandwidth β. Thus, in the case of the three coupled resonator optimum designs, B must be taken to be defined by equations (4.42), (4.56) and (4.58). It is also worth noting that though equations (4.56) and (4.58) define values of B greater than that given by equation (4.42) the computed bandwidths of the 2-pole and 3-pole circuits are about the same.

As in the case of the canonic designs, it is observed that the output Q of the three coupled resonator designs is Bq_n (though B is no longer equal to β^{-1}). Bq_n must, however, be such that equation (4.11) is satisfied.

4.5. Properties of the Alternative Broadband Circuits

In sections 4.3 and 4.4 two canonic and three coupled resonator bandpass circuits were developed for realization as broadband piezoelectric sonar transducers. Further, any of these circuits could be based on a number of alternative sets of k and q values. Thus it is necessary to devise some means of choosing the most suitable of these circuits for mechanical realization.

Before considering mechanical realizability, however, it is convenient to eliminate the filter circuits whose computed characteristics are unsuitable. For this purpose

the circuits considered were analysed by means of the technique developed for normalized ladder-type filter networks. This technique is described in section 4.4.

It is found on analysis that the coupled resonator designs are satisfactory only for equally terminated Butterworth and low-ripple Chebychev prototypes. The canonic bandpass circuits are not subject to this restriction. Even in the case of the canonic circuits, however, only equally terminated designs are considered as these are much less sensitive to variations. Also for any given circuit the Butterworth design is the least sensitive of all. Thus with respect to this criterion alone it is the most suitable.

Of the two types of bandpass filter,the coupled resonator circuits are less sensitive to variations of the element values than the canonic designs[32]. It is also found that the 3-pole coupled resonator designs are better in this respect than the 2-pole designs.

With equally terminated Butterworth and low ripple Chebychev bandpass filters it is further possible to modify the circuit by arbitrarily reducing the terminating resistance without altering the other element values. It is found on analysis that this modification has little effect on the bandwidth or the shape of the characteristic provided the reduction is not much more than 50%. This result could also be justified theoretically. It does, however, introduce a uniform mismatch loss of 0.5 dB for a reduction from 1.0 to 0.5. While the loss sustained is tolerable the circuit is modified in such a fashion that its mechanical realization is greatly facilitated. In fact, without this particular

artifice it is not possible to develop any realizable
3-pole broadband transducer circuits.

A comparison of the five broadband circuits reveals
that all except the predominantly mechanical 3-pole coupled
resonator design have identical mechanical configurations.
The mechanical circuit in these cases is a single mechanical
resonator consisting of the ceramic compliance, the
radiating head mass and the radiation resistance is series
(compare with Figure 4.3). This configuration is simply
realizable in the conventional transducer design illustrated
in Figure 2.7 and described in sections 2.4 and 3.3.
Further, it is clear that both 2-pole designs are particular
cases of the conventional design incorporating one mechanical
resonator and one electrical resonator. The 3-pole
canonic circuit and the predominantly electrical 3-pole
coupled resonator circuit are thus seen as electrical
extensions of the 2-pole designs.

In the case of the predominantly mechanical 3-pole
coupled resonator design alone, extra mechanical elements are
present in the circuit. The mechanical form of this circuit
is simply obtained by comparison with the equivalent circuits
of the single mechanical resonator designs. Thus, from
Figure 4.17 and section 2.2 it is clear that the extra
elements consist of a single series mass-compliance pair
introduced between the ceramic compliance and the radiating
head mass. The rest of the mechanical construction is
similar to that of the conventional design. The electrical
part of the circuit consists of the electrical capacitance
of the ceramic and a series inductor. Thus this circuit is

a mechanical extension of the conventional 2-pole design incorporating two mechanical resonators and one electrical resonator. A diagram of a transducer design based on this circuit is given in Figure 4.22.

The five circuits derived in sections 4.3 and 4.4 are of course only the normalized versions of realizable circuits. The 'un-normalized' or real element values corresponding to a radiation resistance of R and a centre frequency ω_o are obtained by multiplying the resistances, inductances and capacitances in the normalized circuit by the factors F_r, F_ℓ and F_c respectively, where

$$F_r = R/r \qquad (4.59)$$

$$F_\ell = R\bar{\omega}/r\omega_o \qquad (4.60)$$

$$F_c = r\bar{\omega}/\omega_o R \quad . \qquad (4.61)$$

Here $\bar{\omega}$ is the effective centre frequency (as defined in section 4.4) and r the terminating resistance value (reduced if necessary from 1.0) of the normalized circuit. Though $\bar{\omega}$ is 1.0 in the canonic circuits, in the coupled-resonator circuits it is generally around 0.77.

From equations (3.54) and (3.39) it can be shown that if a is the piston radius

$$R = 2.3 \times 10^6 . a^2 \quad . \qquad (4.62)$$

Substituting for R in the above equations

$$F_r = (2.3 \times 10^6 / r) a^2 \qquad (4.63)$$

$$F_\ell = (0.366 \times 10^6 \, \bar{\omega}/r) a^3 / af_o \qquad (4.64)$$

$$F_c = (r\bar{\omega}/14.44 \times 10^6) / a(af_o) \quad . \qquad (4.65)$$

Since af_o as fixed for a particular circuit it follows that

$$F_r \propto a^2, \qquad F_\ell \propto a^3 \quad \text{and} \quad F_c \propto a^{-1} \quad . \qquad (4.66)$$

But the absolute value of the resistances in a particular transducer design is determined by F_r. Similarly F_ℓ and F_c determine the absolute values of the masses and the compliances. Consequently the transducer scales precisely, that is, if the centre frequency is increased in a certain ratio, all the geometric dimensions must be reduced in the same ratio. Thus a particular (normalized) broadband circuit which is mechanically realizable at 5 kHz is also realizable at any other frequency. For convenience, the realizability of alternative c'rcuits is compared at 5 kHz.

An example of the deta'led design procedure of a sonar transducer is given in section 4.6. Before the execution of such a procedure, the most suitable circuit for a particular value of effective coupling K, is chosen in the following manner.

In practice it is found that of all the mechanical components the ceramic compliance and the radiating head are the most difficult to realize. A radiating head approximating to 'rigid p'ston' conditions is realizable provided Q_m is greater than 1.6. A value of Q_m greater than 2.0 is, however, much more desirable.

The compliance of the ceramic stack is approximately given by

$$C_2 = s_{33}^E \, pX'/A \qquad (4.67)$$

where pX' is the total length of the stack and A its area of cross section. The maximum value of pX' for a PZT-ceramic transducer (at ω_o = 5 kHz) is around 5.0 cm (see section 3.3). If flexing of the stack is to be avoided and a reasonable quantity of power handled, the area A must not be less than about 5 cm^2. These two limits result in the ceramic compliance C_2 being limited to

$$C_2 \leq 1500 \times 10^{-12} \text{ m/Nw} \qquad (4.68)$$

for a 5 kHz transducer in PZT. The corresponding limit for barium titanate is around

$$C_2 \leq 1400 \times 10^{-12} \text{ m/Nw} \qquad . \qquad (4.69)$$

These limits on C_2 are of course somewhat arbitrary but adequate as a guide to design.

The values of C_2 and Q_m required by a number of alternative broadband circuits are compared in the following table. For the purposes of this comparison it is assumed that K = 0.845, f_o = 5 kHz and a = 4 cm (i.e., af_o = 200). If C_2^n is the ceramic compliance and L^n the 'output inductor' in the respective normalized filter circuits, C_2 and Q_m are given by

$$C_2 = F_c C_2^n = r\bar{\omega} C_2^n / 1.156 \times 10^8 \qquad (4.70)$$

and $\qquad Q_m = \bar{\omega} L^n / r \qquad . \qquad (4.71)$

The values of $\bar{\omega}$, f_2/f_1 and β are obtained from the computed characteristics of the relevant filter circuit. For convenience, the 'predominantly electrical' and 'predominantly mechanical' 3-pole coupled resonator designs are abbreviated to CR3-E and CR3-M respectively. The

canonic 2-pole, 3-pole and coupled resonator 2-pole are similarly denoted by C2, C3 and CR3. The value of r is chosen arbitrarily, as explained earlier in this section.

Comparison of the Realizability of Alternative
Designs for K = 0.845

Description of Circuit	r	$\bar{\omega}$	f_2/f_1	β %	C_2^n	L^n	Q_m	C_2 in 10^{-12} m/Nw
CR2 Butterworth	1.0	0.76	3.24	125	1.105	1.550	1.180	7270
C2 Butterworth	1.0	1.00	3.12	120	.845	1.180	1.180	7300
C3 Butterworth	1.0	1.00	3.12	120	1.195	.837	.837	10340
C3 Chebychev (0.5 dB ripple)	1.0	1.00	3.42	131	.700	1.430	1.430	6060
C3 Legendre	1.0	1.00	3.82	145	.666	1.500	1.500	5760
CR3-E Butterworth	1.0	.72	3.25	125	1.315	1.303	0.940	8210
CR3-M Butterworth	1.0	.77	3.05	117	.548	1.303	1.004	3640
CR3-M Butterworth	0.5	.77	3.05	117	.548	1.303	2.008	1820
CR3-M Chebychev (0.01 dB ripple)	0.5	.77	3.06	118	.481	1.485	2.280	1598
CR3-M Chebychev (0.1 dB ripple)	0.5	.77	3.06	118	.409	1.750	2.690	1356

It is clear from the table that the 2-pole designs are quite unrealizable. In fact C_2 is so much in excess of the upper limit, that it is not even necessary to try alternative

designs such as Chebychev etc. Clearly r has to be around 0.25 before 2-pole designs in PZT begin to be realizable.

The 3-pole canonic designs are just as unsuitable for mechanical realization, on account of excessive values of C_2. In canonic designs, however, it is possible to use 'unequally terminated' prototypes with non-symmetrical k and q values. Though it is possible to reduce C_2 by this means the resulting values are still unrealizable. These designs are not included in the table.

The same as true of the predominantly electrical CR3-E circuit.

The predominantly mechanical CR3-M circuits alone possess values of C_2 and Q_m which fall within or closely approach the realizability limits. Even these circuits however are realizable only when r is reduced to 0.5. It is further observed that mechanical 'realizability' improves as the ripple tolerance is increased from zero (Butterworth) to 0.01 dB and 0.1 dB. Thus the Chebychev designs could be regarded as modifications of the Butterworth circuit for improved realizability at the expense of ripple in the passband.

On analysis, however, it is found that the ripple amplitude is magnified by the lowpass to coupled resonator bandpass transformation. Consequently the 0.1 dB ripple Chebychev design has to be rejected on account of large variations in the passband.

Thus the only acceptable, mechanically realizable designs, are the CR3-M Butterworth and 0.01 dB ripple Chebychev, with r = 0.5. Fortunately these designs are also

the least sensitive to variations of the element values.

In both cases Q_m is greater than 2 but C_2 is somewhat beyond the design limit. In an actual design, however, af_o is generally higher than the value of 200 used in the above comparisons. Since $F_c \propto 1/af_o$ (equation (4.65)), C_2 is, as a result, reduced to fall below the limit of equation (4.68). Since the realization of C_2 is the critical factor in the realizability of a particular circuit it is essential to make af_o as large as possible. The optimum value of af_o for a particular f_2/f_1 is given by the graph of Figure 4.4.

It is observed that the highest value of bandwidth β is obtained for the C3 Legendre design (145%). The maximum possible bandwidth for a K of 0.845, as predicted by Baerwald (equation (4.8)) is 169%. Thus the realizable CR3-M Butterworth and Chebychev circuits harness only 70% of the 'potential' bandwidth for this value of K.

4.6. Transducer Design in Lead Zirconate Titanate Type Ceramic

In section 4.5 it was shown that the CR3-M Butterworth or low-ripple Chebychev circuits were the most suitable for realization as broadband transducer designs in PZT-type ceramics. It was also shown that the mechanical form of this circuit is a simple modification of the conventional trans-ducer design. The derivation of the detailed mechanical design from the normalized bandpass filter circuit is as follows. The symbols and formulae used in this section are defined or derived in Chapter 3 and section 4.5.

Choice of circuit and centre frequency

It is assumed that the active section is to be constructed of a PZT-type ceramic (AM 525), possessed of the

following properties:

$$k_{33} = 0.69$$

$$d_{33} = 2.96 \times 10^{-12} \ m/V$$

$$s_{33}^E = 16.2 \times 10^{-12} \ m^2/Nw$$

$$= 7670 \ kg/m^3$$

$$\epsilon_{33}^T = 11410 \times 10^{-12} \ F/m$$

From which it is easily shown that

$$c_e = 2835 \ m/s$$

and $\qquad K_o{}^2 = .9075$.

It is found by experiment that the value of a gauze-resin bond between alternate ceramic segments could be expressed as

$$C_b = 0.000442 \ s_{33}^E/A$$

where A is the bond (and ceramic) area of cross-section. Assuming a ceramic segment thickness of 0.5 cm the effective value of low-frequency coupling $K_o{}'$ inclusive of the effect of bonds is found (from equation (3.30)) to be given by

$$K_o{}' = 0.881 \ .$$

The effective coupling at operating frequencies drops off from the above value according to equation (3.29). Thus a value of coupling lower than $K_o{}'$ has to be used as the working value. The working value of effective coupling, which is chosen by a trial-and-error process, is taken in this instance to be

$$K = 0.845.$$
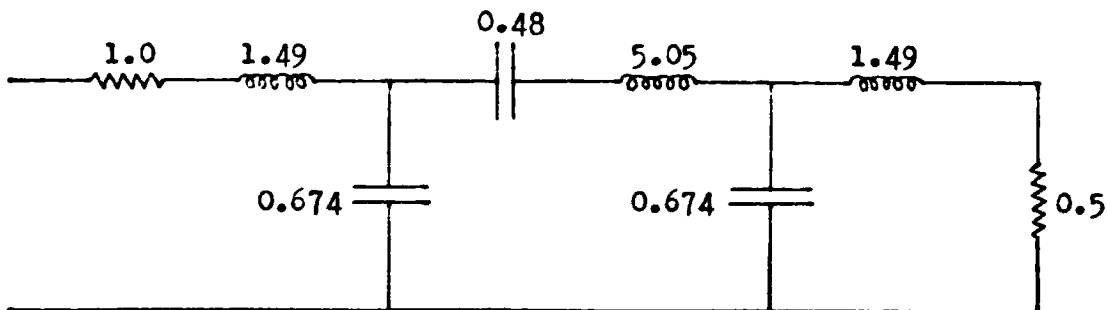
All inductors in henries
All capacitors in farads
All resistors in ohms

Figure 4.19- Normalized Circuit of Designed
Transducer

Electrical | Mechanical
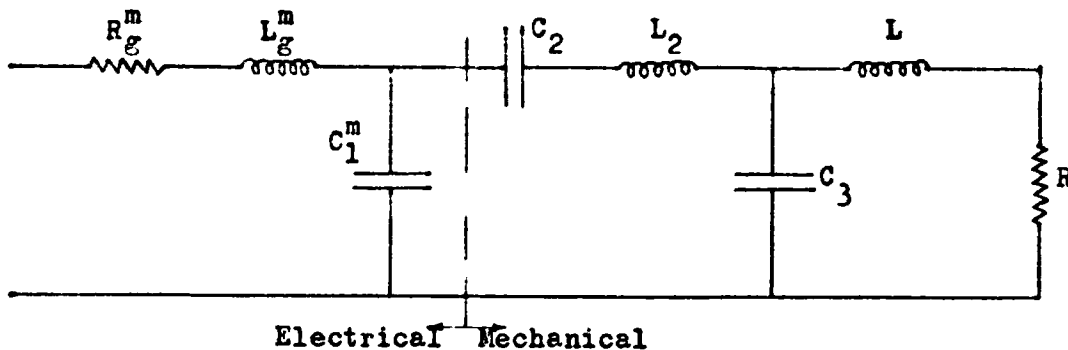
Figure 4.20- Equivalent Circuit of Designed Transducer
Referred to the Mechanical side

$1: \phi'$
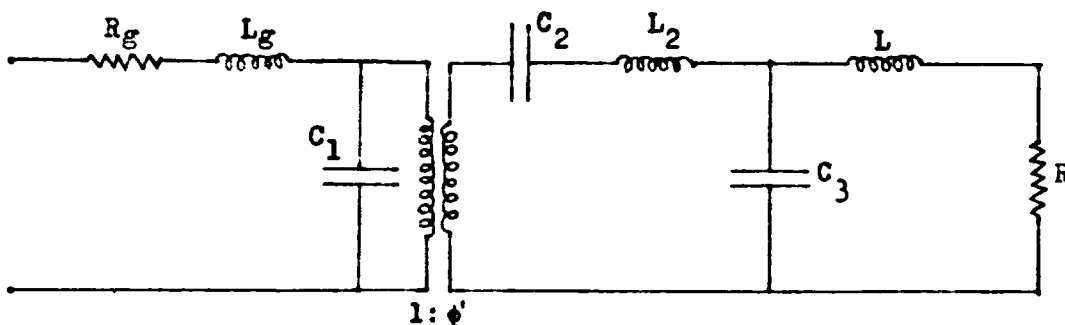
Figure 4. 21- Equivlent Circuit of Designed Transducer
with Electromechanical Transformer

For this value of coupling the 0.01 dB ripple
Chebychev version of the CR3-M circuit of Figure 4.17 works
out to that of Figure 4.19.   The terminating resistance r
is reduced to 0.5 for the reasons given in section 4.5.
Though the Butterworth design is less sensitive than this
Chebychev, the latter is chosen as it is easier t realize
mechanically.   The derived bandpass circuit is based on
the following k and q values:

$$k_{12} = k_{23} = 0.6818$$

$$q_1 = q_2 = 1.1811 .$$

It is decided to centre the transducer at 4.015
kHz.   Since f_2/f_1 for this circuit is 3.06 (see table
section 4.5), the optimum value of af_o (from Figure 4.4) is
229.   This results in a piston radius 'a' of 5.71 cm and
cut-off frequencies of

$$f_1 = 2.3 \text{ kHz} \quad \text{and} \quad f_2 = 7.0 \text{ kHz} .$$

The appropriate scaling factors are found from equations
(4.63) - (4.65) to be

$$F_r = 14980$$
$$F_\ell = 0.457$$
$$F_c = 2033 \times 10^{-12} .$$

The scaling of the normalized circuit by these factors
yields the actual mechanical circuit to be realized (Figure
4.20).   The numerical values of the elements are as follows:

$$R = R_g^m/2 = 7490 \text{ Nw.s/m}$$

$$L = L_g^m = 0.6785 \text{ kg}$$
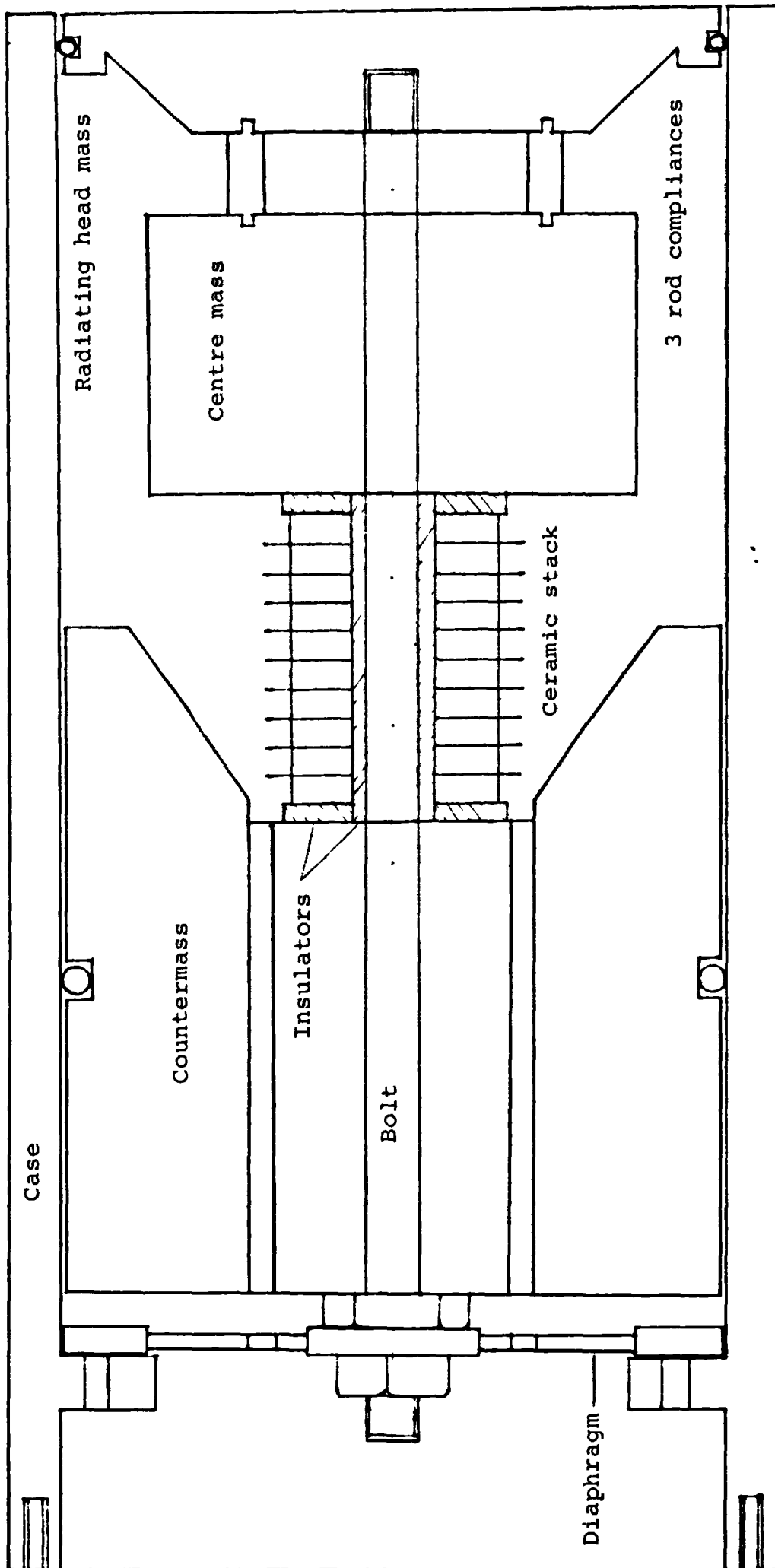
Figure 4.22- Diagram of Designed Broadband Transducer
Scale- Full size

$$C_3 = C_1{}^m = 1.368 \times 10^{-9} \text{ m/Nw}$$

$$L_2 \qquad = 2.310 \text{ kg}$$

$$C_2 \qquad = 976 \times 10^{-12} \text{ m/Nw} \qquad .$$

The above transformation presents all the circuit elements referred to the mechanical side. This is indicated on the electrical elements by the superscript 'm'.

Constructional features of Broadband Design

The mechanical realization of the circuit of Figure 4.20 is given in Figure 4.22. In this circuit R is the effective radiation resistance and L the sum of the radiating head mass and the mass equivalent of the radiation reactance. C_3 is clearly a series compliance between the radiating head mass L and the centre mass L_2. C_3 is most conveniently realized as three cylindrical rods positioned symmetrically as depicted in Figure 4.22. $C_1{}^m$, C_2 represent the ceramic stack which is anchored on one side to the countermass (described in section 3.3). The ceramic stack consists of a number of cylindrical rings bonded together by gauze-resin joints. The stack is insulated from the countermass and the centre-mass by two rings and from the centre bolt by an insulating sheath of a highly compliant material (see section 2.5 for details of stack construction). All transducer components are of circular cross-section.

The whole assembly is held together in compression by the centre bolt and adjacent elements are bonded to ensure good mechanical contact. The transducer assembly is supported in the case by a highly compliant diaphragm and

rubber rings, so as to effective isolate it, vibration-wise, from the case. The rubber ring on the head mass also serves as a seal. The electrical connections to the ceramic stack are led out through the two holes in the countermass and out of the case via a watertight gland and cable.

Design of the Ceramic Stack

From equation (3.28) the effective compliance of the ceramic stack is given by

$$C_2 = (\sin \omega p X / c_e M) / \rho c_e A M \quad .$$

Since X has already been fixed at 0.5 cm, the only controllable parameters in this expression are the area A and the number of segments p. In section 3.3 it was shown that the length of a PZT-type ceramic stack should not exceed 5 cm for approximately 'linear' behaviour up to 7.5 kHz. Thus p is conveniently fixed at 10 and A is adjusted such that C_2 is equal to the design value at 2.23 times the centre frequency (see section 3.3).

If A is 8.53 cm^2 it is found that

$$C_2 = 976 \times 10^{-12} \text{ m/Nw} \quad \text{at} \quad 5.13 \text{ kHz} \quad (2.23 \text{ } f_o)$$

$$C_2 = 1023 \times 10^{-12} \text{ m/Nw} \quad \text{at} \quad 2.30 \text{ kHz} \quad (f_1)$$

$$C_2 = 926 \times 10^{-12} \text{ m/Nw} \quad \text{at} \quad 7.00 \text{ kHz} \quad (f_2) \quad .$$

Thus the maximum variation about the design value is 5%. Further this value of A corresponds to an effective electromechanical transformation ratio ϕ' of 2.86 and an effective electrical capacitance (pC_o') of 10950 pF. The value of C_1 required by the designed circuit is however

$$C_1 = (\phi')^2 C_1^m = 11180 \text{ pF} \quad .$$

The difference of 230 pF is made up in the capacitance of the connecting cable. Since the electrical supply and the inductor L_g are located at some distance from the transducer, the capacitance of the connecting cable is appreciable.

In practice the design value of K is also treated as a controllable parameter and adjusted for a satisfactory design.

The above value of ceramic area A is obtained by making the inner and outer diameters of each segment equal to 1.430 cm and 3.598 cm respectively. The inner diameter is made large enough to accommodate the centre bolt and the insulating sheath.

The mass of the ceramic stack (ρAXp) works out to 0.327 kg. Half of this value plus the mass of the steatite insulating ring is effectively added onto the masses on either side of the ceramic stack. For the dimensions indicated in the diagram each steatite insulator has a mass of 0.005 kg and an effective compliance of 44×10^{-12} m/Nw inclusive of the bonding on either side.

The values of the electrical elements are obtained by inserting the electromechanical transformer appropriately to yield the equivalent circuit of Figure 4.21 where

$$L_g = 83 \text{ mH}$$

and $$R_g = 1832 \text{ } \Omega.$$

L_g is realized as a ferrite pot-core inductor.

Design of the other mechanical elements

The rod compliances are realized in three identical rods of diameter 0.635 cm. The total compliance of the

joints on either side of the rods is estimated at 143×10^{-12}
m/Nw. Thus the design value of $C_3 = 1368 \times 10^{-12}$ m/Nw is
satisfied if the total compliance of the three rods is
1225×10^{-12} m/Nw. This value is realized for a rod length
of 1.443 cm assuming the rods are constructed of beryllium
copper of density 8.33 gr/cm^3 and Young's modulus 0.124×10^{12}
Nw/m. The mass of the rods which is effectively added
onto the masses on either side in equal proportion, is
0.0114 kg.

Thus the required value of centre mass corrected for
the masses added from either side is 2.135 kg. This value
is realized in a cylindrical steel block of outer diameter
8.5 cm and thickness 4.84 cm, allowing for a cylindrical
cavity of 0.96 cm diameter to accommodate the bolt. The
thickness is kept close to 4.3 cm in view of the limits
derived in section 3.1.

From equation (3.54) the mass equivalent of the
radiation reactance of a piston of radius 5.71 cm works out
to 0.1272 kg. Correcting for this value and for the added
masses of the rod compliances and the bolt the radiating
head mass is required to be 0.4874 kg. The radiating
head is constructed of aluminium.

The countermass is generally constructed of steel
and its value made as large as possible. Its length,
however, is restricted to about 9 cms (see section 3.1) and
its outer diameter is conveniently made equal to the diameter
of the radiating head to facilitate insertion into the case.
For the construction depicted in the figure, the effective
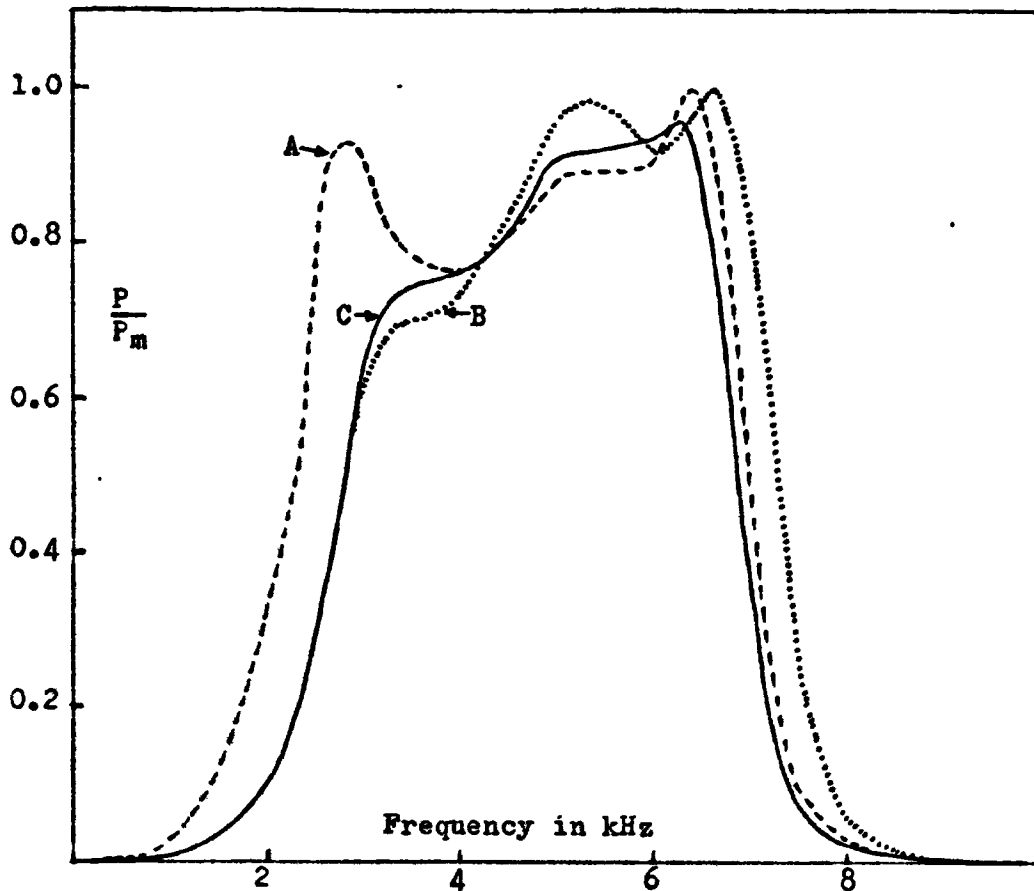
Figure 4.23- Computed Amplitude Characteristic of Designed Broadband Transducer
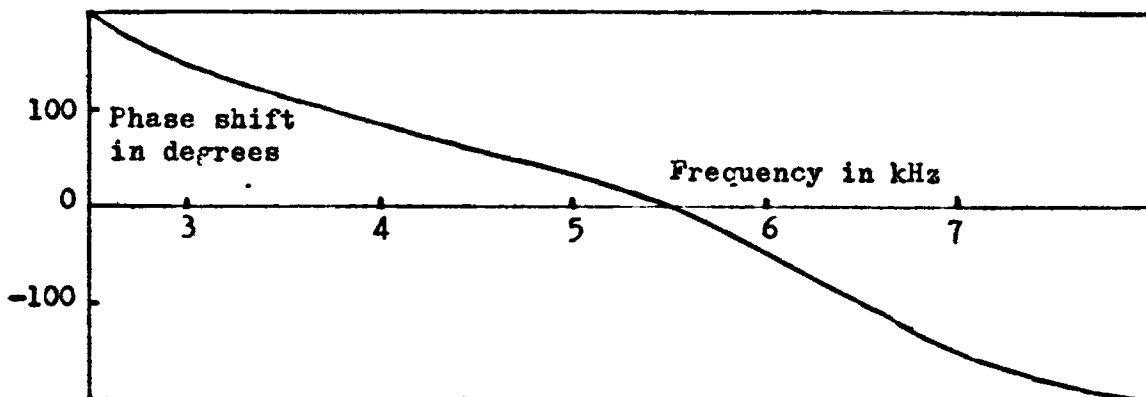
Figure 4.24- Computed Phase Shift of Designed Transducer
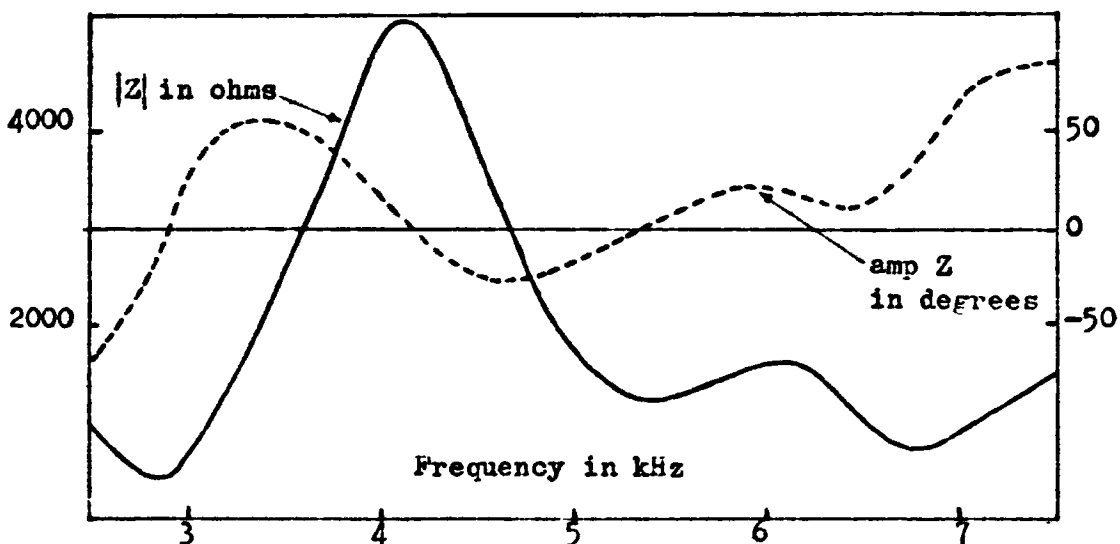
Figure 4.25- Computed Input Impedance of Designed Transducer

value of the countermass inclusive of the added masses, is 8.07 kg.

The centre bolt is a steel rod of diameter 0.952 cm and length of approximately 21 cm. Its mass is 0.112 kg and its low-frequency compliance is approximately 15,000 × 10^{-12} m/Nw. This value is large enough to justify its exclusion from the design circuit as it is an order of magnitude greater than the other circuit compliances. Its normalized value (for insertion in the circuit of Figure 5.15) is 7.42.

The compliance of the supporting diaphragm is even higher, at 275,000 × 10^{-12} m/Nw. This value is thus sufficient to effectively isolate the transducer assembly from the case.

Computed characteristics of the designed transducer

The computed characteristics of the designed transducer are depicted in Figures 4.23 to 4.25. P is the power radiated by the device and P_m is defined in equation (4.2). In Figure 4.23 curve A is the power characteristic computed from the normalized 'design' circuit of Figure 4.19. Curve B is calculated from the circuit of Figure 5.15 in which modifications are made for the inclusion of the countermass and the bolt. The countermass appears as a shunt inductor of value 17.7 between C_2 and L_2 (see Figure 5.15) and the bolt can be accounted for by a series capacitor of value 7.42 between C_3 and L. Curve C is calculated from the complete equivalent circuit by the analysis technique described in section 5.2. So also are the phase shift and impedance characteristics of the transducer.

It is observed that the characteristic A computed from the design circuit of Figure 4.19 does not closely agree with the more accurate curve C. Thus the values of $\bar{\omega}$ and β derived from the design circuit do not accurately represent the performance of the corresponding practical transducer. They are, however, adequate as a guide to design. A somewhat better approximation is effected by curve B which includes the effects of the countermass and the bolt.

According to curve C the designed transducer has a passband of 2.7 - 6.85 kHz. This corresponds to a centre frequency of 4.3 kHz and a bandwidth of 96.5%. It is also observed that while the phase shift of the device is reasonably linear in the passband, the input impedance characteristic is somewhat less than satisfactory.

CHAPTER 5

ANALYSIS

In this Chapter a technique is developed for the time and frequency analysis of extensional type piezoelectric sonar transducers. The analysis technique is based on the accurate equivalent circuits derived in Chapter 3. In section 5.1 the complete equivalent circuit is formulated for the specific case of the designed transducer of Figure 4.22. It is shown, however, that the resultant equivalent circuit is representative of conventional transducers as well, with simple modifications which do not affect the analysis theory. In section 5.2 the special structural features of the complete equivalent circuit are exploited to derive a method of frequency analysis which is particularly suitable for extensional type transducers. This is followed in section 5.3 by the description of a general method for the determination of the time responses from the frequency characteristics.

Finally, a technique applicable to the analysis of any ladder type filter network consisting of conventional electrical elements is described in section 5.4.

Computer programs for the execution of the above analysis techniques are presented in Appendices III and IV. The computed time and frequency characteristics of the designed broadband transducer and the conventional transducer of Figure 2.7 are also included.

5.1. Formulation of the Complete Equivalent Circuit

The design theory of Chapter 4 was developed on the

a. Impedance T-analogue   b. Mobility Π-anologue
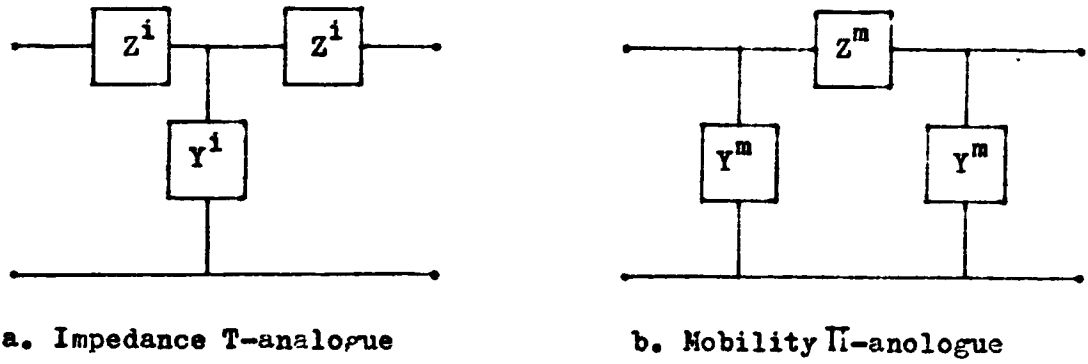
<u>Figure 5.1</u>- Equivalent Circuits of Uniform Mechanical line
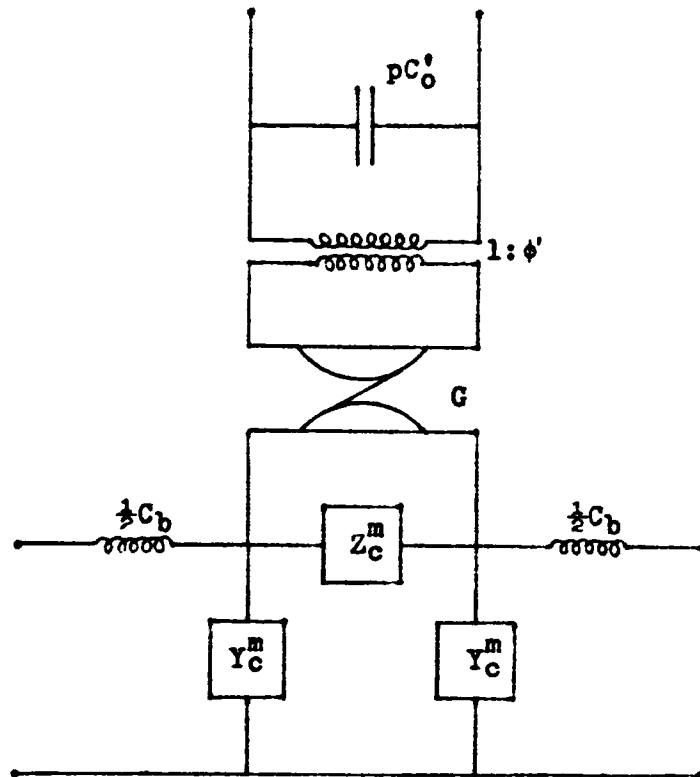
<u>Figure 5.2</u>- Mobility Representation of a Ceramic
Stack

basis of the approximate LC representation of transducer
components.   For the purposes of analysis it is necessary to
use instead the more accurate equivalents which allow for
the distributed mass and compliance wherever necessary.
The accurate equivalents of individuals components derived in
Chapter 3, are all formulated in the impedance analogy.   The
complete equivalent circuit of a transducer assembly is,
however, best formulated in the mobility analogy, on account
of the topological similarity between the mechanical circuit
and its mobility analogue (see section 2.2).   The rules
for interconversion between the two representations are
given in section 2.2.

The uniform mechanical line of Figure 3.1 is exactly
represented in the impedance and mobility analogies by
the dual networks of Figure 5.1 in which

$$Y^i = Z^m = jZ_o/\sin kX$$

$$\text{and} \quad Z^i = Y^m = jZ_o\tan kX/2$$

<div align="right">(5.1)</div>

Z_o, etc. are defined in section 3.1.   The superscripts i
and m indicate the analogy in which the equivalence is
formed.   The alternative impedance-Π representation of
Figure 3.2b or its dual the mobility-T, are not considered
here as it is not used in this Chapter.

Similarly the ceramic stack could be represented by
the mobility analogy equivalent of Figure 5.2 which is easily
derived from the impedance representation of Figure 3.14.
In this circuit the symbols Z_c^m and Y_c^m are defined in terms
of Z_{1p} and Z_{2p} of equations (3.22) as follows

Figure 5.3- Complete Mobility Equivalent of Designed Transducer

$$Z_c^m = 1/Z_{2p}, \quad Y_c^m = Z_{1p} \quad . \tag{5.2}$$

The network element G is a unit gyrator which is defined by the transmission matrix

$$\begin{bmatrix} A & B \\ C & D \end{bmatrix} = \begin{bmatrix} 0 & 1 \\ 1 & 0 \end{bmatrix} \quad . \tag{5.3}$$

The derivation of the mobility analogy equivalent circuit of a composite extensional type transducer is now a relatively simple matter. It is observed that the configurations depicted in Figures 2.7 and 4.22 both consist of simple mechanical 'extensions' on either side of the ceramic stack which link up again via the centre bolt. Thus the mobility analogy equivalent of the transducer of Figure 4.22 is derived by building up the circuit around the equivalent circuit of the ceramic stack to yield the result of Figure 5.3. The correspondence between mechanical elements and their circuit equivalents is indicated in the figure itself. The electrical elements R_g and L_g are left out for convenience.

The type of representation used for a particular element is determined by the criteria derived in section 3.1. Thus in the case of the designed transducer circuit the ceramic stack, the bolt, the centre mass and the rod compliances are represented by equivalent Π sections of the form shown in Figure 5.1b. The remaining components are represented by LC type elements. In the case of the rod compliances shown in Figure 4.22 an LC reduction would have been quite justifiable. The more accurate form is used
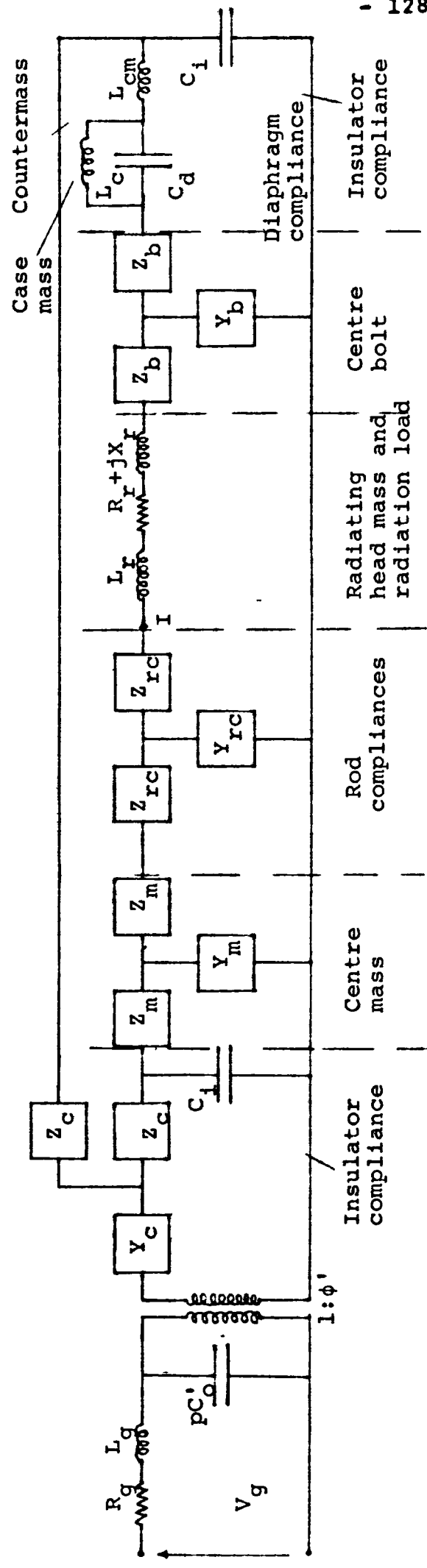
Figure 5.4- Impedance Equivalent of the Designed Transducer

however, as in some designs their length is in excess of the limiting value. The representation of the countermass by a single 'C' element in spite of its appreciable length, is justified later on in this section.

Though the mobility analogue of a transducer is much easier to derive, the impedance analogue is more convenient in analysis. As such the mobility analogy equivalent of Figure 5.3 is converted into the impedance equivalent of Figure 5.4 (according to the rules of section 2.2) before analysis. In particular, the π-sections representing the centre mass, rod compliances and bolt are converted into the T-sections of Figure 5.4. The Z, Y values of these T-sections are estimated from the dimensions of the respective mechanical elements according to equations (5.1). The elements Y_c, Z_c of the ceramic stack are obtained from Z_{1p}, Z_{2p} (of equations (3.22)) as follows

$$Y_c = 1/Z_{2p}$$

$$Z_c = Z_{1p} + j\omega L_i$$

(5.4)

where L_i is half the mass of each steatite insulator. A similar correction could be made to the Z_m nearest to C_i and to L_{cm}. Also, the insulator compliance C_i could be corrected to include the $\frac{1}{2}C_b$ shown in Figure 3.14 plus another C_b to allow for the bond on the other side of the insulator. Though these corrections are included in the analysis programme, their effects have been found to be negligible.

The radiation load $(R_r + jX_r)$ is given by equations (3.54) and L_r is the mass of the radiating head.

The compliance of the diaphragm C_d appears in parallel with a mass L_c which is some indeterminate fraction of the case mass. In practice, however, the uncertainty in the value of L_c is of little consequence, as C_d is generally large enough to constitute a virtual short circuit in the frequency range of interest.

Further, since both the impedance of L_{cm} and the admittance of Y_b is very large, the current through L_{cm} is small. Thus the error introduced by the representation of the countermass by a single constant mass L_{cm} is negligible. The effective compliance of the countermass is also negligible.

5.2. Computation of the Frequency Characteristics

The formulation of the complete equivalent circuit of the designed transducer of Figure 4.22 is discussed in section 5.1. It is clear that any extensional type transducer could be represented by a circuit similar to that of Figure 5.4. The conventional type transducer of Figure 2.7 could for instance be considered as a particular case of the mechanical configuration of Figure 4.22, in which the centre mass and the rod compliances are absent. Thus the theory developed for the analysis of the circuit of Figure 5.4 is applicable with simple modifications to any extensional transducer.

The most striking feature of the impedance equivalent of Figure 5.4 is its near ladder-like structure. On account

of this the network can be frequency analysed without recourse to a general network analysis program. A ladder structure is much simpler to handle computationally and consequently requires much less computing time.

The piston velocity is represented in the circuit of Figure 5.4 by the 'current' I. The power radiated by the transducer is then

$$P = R_r |I|^2 \qquad . \qquad (5.5)$$

The complex frequency function $G(\omega)$ which is defined by

$$I = G(\omega) V_g \qquad (5.6)$$

is referred to as the transfer function of the system. Eliminating I between these two equations

$$P = R_r |G(\omega)|^2 |V_g|^2 \qquad . \qquad (5.7)$$

The radiated power P is commonly expressed as a fraction of the maximum power P_m defined in equation (4.2). Thus

$$P/P_m = 4R_r |G(\omega)|^2 /R_g \qquad . \qquad (5.8)$$

The other frequency functions of interest are the phase shift $\bullet$ and the input impedance Z_{in} of the transducer which are defined as

$$\bullet(\omega) = \text{amp } G(\omega) \qquad (5.9)$$

and $\qquad Z_{in} = V_g/I_g - R_g \qquad . \qquad (5.10)$

The frequency functions $G(\omega)$, $\bullet$ and Z_{in} are derived as follows. The complete impedance equivalent of Figure 5.4 is first summarized by the circuit of Figure 5.5. In this circuit T is a simple ladder network of transmission matrix $\begin{bmatrix} A & B \\ C & D \end{bmatrix}$. It is then very easily demonstrated that
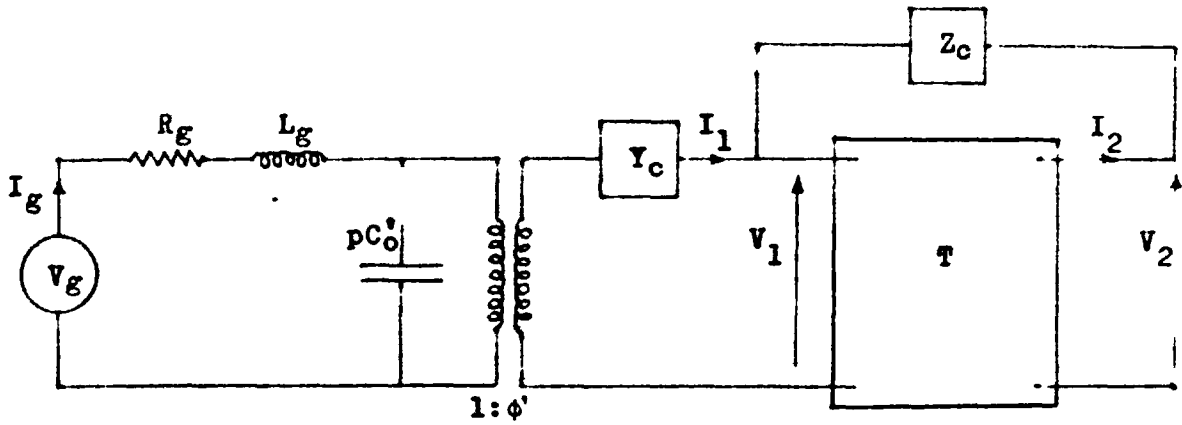
Figure 5.5- Contracted Form of the Equivalent Circuit of Figure 5.4

a. Assimilation of a shunt admittance

b. Assimilation of a series impedan
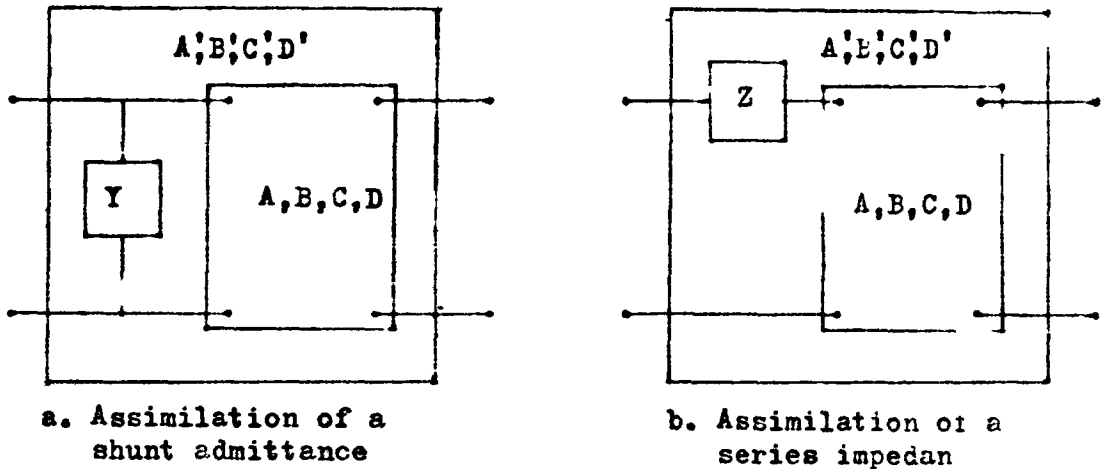
Figure 5.6- Computation of the Transmission Matrix of T
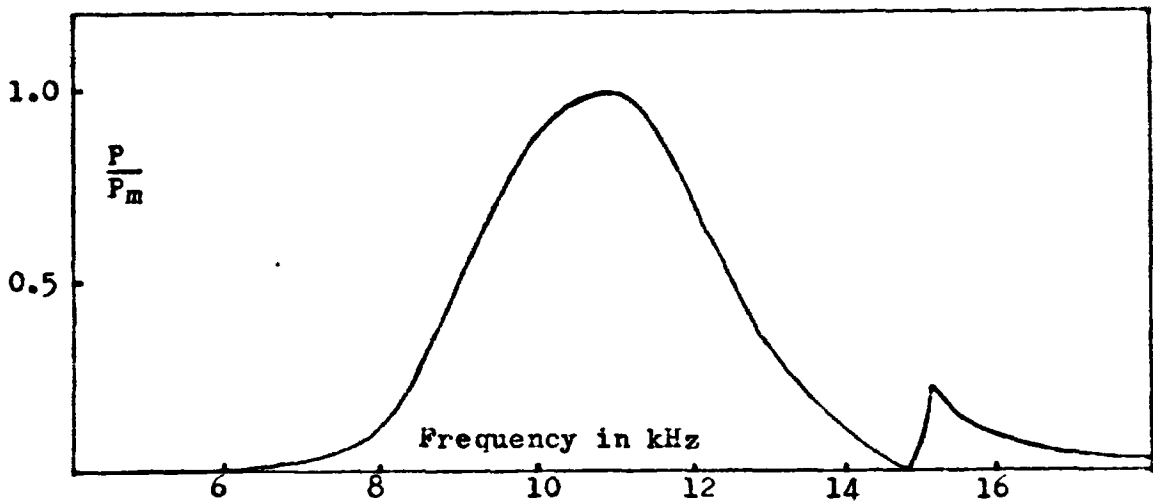
Figure 5.7- Frequency Response of Unbaffled Conventional Transducer

$$V_1 = AV_2 + BI_2 \qquad (5.11)$$

$$I_1 = CV_2 + (D-1)I_2 \qquad (5.12)$$

$$V_1 = V_2 - Z_c I_2 \qquad . \qquad (5.13)$$

Also, if Z_2 is the impedance of the series arm containing Z_b, L_{cm} and the parallel combination of C_d and L_c ,

$$I = (j\omega C_i + Y_b + j\omega C_i Y_b Z_2)V_2 + (1 + Z_2 Y_b)I_2 \qquad . \qquad (5.14)$$

But from equations (5.11) and (5.13)

$$V_2 = (B + Z_c)I_2/(1-A) \qquad . \qquad (5.15)$$

Therefore by substituting for V_2 in the above equations, V_1, I_1 and I are obtained as linear functions of I_2. Now V_g and I_g are related to V_1 and I_1 by

$$I_g = \{(\phi')^2 + j\omega p C_o'/Y_c(\phi')^2\}I_1 + \{j\omega p C_o'/(\phi')^2\}V_1 \qquad (5.16)$$

and

$$V_g = (V_1 + I_1/Y_c)/(\phi')^2 + I_g(R_g + j\omega L_g) \qquad . \qquad (5.17)$$

It is clear that I_g and V_g are also linear functions of I_2. Thus I_2 is eliminated in the formation of the ratios I/V_g, V_g/I_g. $G(\omega)$, Z_{in} are obtained (from equations (5.6) and (5.10)) as functions of the network elements alone.

In actual computation, however, (Appendix III) I, I_g and V_g are most conveniently calculated from the above equations (in the order indicated) with I_2 arbitrarily fixed at unity.

The frequency functions A, B, C, D are estimated by the stepwise procedure indicated in Figure 5.6. Thus a shunt

admittance Y is assimilated by the transformation

$$
\begin{bmatrix} A' & B' \\ C' & D' \end{bmatrix} = \begin{bmatrix} A & B \\ C+YA & D+YB \end{bmatrix} \tag{5.18}
$$

and a series impedance Z by

$$
\begin{bmatrix} A' & B' \\ C' & D' \end{bmatrix} = \begin{bmatrix} A+ZC & B+ZD \\ C & D \end{bmatrix} . \tag{5.19}
$$

Computational Details

A program for the computation of the frequency characteristics of the designed transducer circuit of Figure 5.4 is given in Appendix III under the subroutine title FRERES. This program executes the operations described above at 100 equally spaced frequency values in the range 0 - 10 kHz (or any other upper limit). Specific values of the circuit parameters for a particular transducer are fed into the program as a series of DATA statements.

The radiation load is computed by the sub-programs ARRAY, INFBAF and UNBAF, depending on whether the load termination chosen is that of an array or of a single piston source in infinitely baffled or unbaffled conditions. ARRAY is based on equations (3.54) and INFBAF on equations (3.38) - (3.40). The 'unbaffled load' values, on the other hand, are obtained from the graph of Figure 3.15 which is 'written' into the subroutine UNBAF. Provision is also made in the FRERES routine for computing the response of the transducer in air.

The parallel combination of C_d and L_c is not included in the subroutine FRERES as in practice it constitutes a

virtual short circuit (see section 5.1). The program is also modified to allow for mechanical loss at the rubber rings and for dielectric loss at low operating fields.

FRERES computes P/P_m according to equation (5.8) and displays its frequency dependence graphically by means of the subroutine GRAPH. The functions ϕ, $|Z_{in}|$ and $ampZ_{in}$ are also displayed graphically. The results of such computations for the designed transducer of Figure 4.22 are given in Figures 4.23 - 4.25. The result of a computation of P/P_m for the conventional transducer of Figure 2.7 is displayed in Figure 5.7. In this case it is assumed that the transducer is fed from a voltage source of internal impedance 10000Ω, with a tuning inductor included in the circuit.

5.3. Evaluation of the Time Responses

In addition to the frequency characteristics it is necessary to evaluate the response of the transducer to electrical and mechanical excitation which is specified in the time domain. The commonly employed exciting signals are step, steady sinusoidal and steady square-wave voltages applied suddenly (at t = 0 say). The output variable in the case of voltage inputs is chosen as the piston velocity. The voltage generated across R_g as a consequence of an explosion in the vicinity of the transducer is also of interest.

The above time responses are computed in this study from the frequency characteristics by means of the numerical Fourier transform technique described below. The technique is applicable to any linear, time-invariant network and its validity is unaffected by the nature of the frequency dependence.

The numerical technique is particularly useful in handling complex systems, such as composite transducers whose time responses cannot be derived analytically. The method is also applicable to physical systems whose frequency characteristics are known as a set of measured data.

Theory

If an input $v(t)$ is applied at $t = 0$ to a linear, passive, two-port physical system, the output $f(t)$ is obtained by time domain convolution of the input with the impulse response of the system. Thus

$$f(t) = \int_0^t g(\tau).v(t-\tau)d\tau \qquad (5.20)$$

where $g(t)$ is the response of the system to a unit impulse $\delta(0)$ applied at $t = 0$.

Now if

$$g(t) = \mathcal{J}^{-1}G(\omega) \qquad (5.21)$$

it can be shown that

$$f(t) = \mathcal{J}^{-1}[G(\omega).\mathcal{J}v(t)] \qquad (5.22)$$

where $\mathcal{J}$, $\mathcal{J}^{-1}$ are the Fourier transform and inverse Fourier transform operators respectively. In the special case when both f, v are steady sinusoidal signals, capable of representation as complex phasors F, V, the above equation becomes

$$F = G(\omega)V \qquad . \qquad (5.23)$$

Thus $G(\omega)$ is the transfer function of the system which can be derived from its 'steady-state' circuit representation. The computation of $G(\omega)$ f r the transducer equivalent circuit

of Figure 5.4 is dealt with in section 5.2. $G(\omega)$ is usually a complex function of ω. For all systems of interest it can be shown that

$$G(-\omega) = \overline{G(\omega)} \quad . \tag{5.24}$$

Thus two alternative methods of computing the time responses are evident. The one used by Liou[33] involves the application of equation (5.22); the Fourier transformation of the input followed by multiplication by $G(\omega)$ and an inverse Fourier transformation. The other method consists of the determination of the impulse response by inverse Fourier transformation (equation (5.21)) followed by time domain convolution with the input signal (according to equation (5.20)). The latter method is preferred as it is generally more comprehensive and convenient.

In this study a variation of the latter technique is employed. On account of certain computational considerations which are elaborated on below, convolution from the impulse response is found to be unsatisfactory. The response of the system to a general input can also be derived from the step response. Thus from equation (5.22)

$$f(t) = \mathfrak{F}^{-1}[\{G(\omega)/j\omega\}\{j\omega\,\mathfrak{F}v(t)\}] \tag{5.25}$$

But

$$j\omega\,\mathfrak{F}v(t) = \mathfrak{F}(dv/dt) \tag{5.26}$$

and

$$\mathfrak{F}^{-1}\{G(\omega)/j\omega\} = \int_0^t g(t)dt = u(t) \tag{5.27}$$

where $u(t)$ is the response of the system to a unit step

input applied at t = 0. Therefore in the time domain equation (5.25) is equivalent to

$$f(t) = \int_0^t u(\tau) . \frac{dv(t-\tau)}{d\tau} . d\tau \qquad . \qquad (5.28)$$

Thus f(t) emerges as the result of the convolution of u(t) with the derivative of the input. The step response is obtained by the inverse Fourier transformation of $G(\omega)/j\omega$ (according to equation (5.28)). The derivative of a general input specified numerically in the time domain can, of course, be computed numerically. For the inputs considered here, however, the derivative is specified just as easily as the input itself.

In the case of the transducer circuit of Figure 5.4 it can be demonstrated from reciprocity considerations that a force function $\theta(t)$ incident on the piston face produces a voltage $v_m(t)$ across R_g (with V_g shorted) such that

$$v_m(t) = \mathfrak{J}^{-1}[R_g G(\omega) \mathfrak{J}\theta(t)] \qquad . \qquad (5.29)$$

If $\theta(t)$ is caused by an explosion in the vicinity of the transducer, its waveform is described approximately by

$$\theta(t) = \theta_o e^{-\alpha t} \qquad (5.30)$$

where θ_o is the maximum force in Nw and α is the time constant.

Since

$$\mathfrak{J}\theta(t) = \theta_o/(\alpha + j\omega) \qquad (5.31)$$

$$v_m(t) = \theta_o R_g \mathfrak{J}^{-1}[G(\omega)/(\alpha + j\omega)] \qquad . \qquad (5.32)$$

The voltage response to a mechanical input is thus obtained by an inverse Fourier transformation alone.

Numerical inverse Fourier Transformation (after Liou[33])

The general inverse Fourier transformation problem of

$$f(t) = \mathcal{J}^{-1} F(\omega) \tag{5.33}$$

is expressed explicitly as

$$f(t) = (1/2\pi) \int_{-\infty}^{\infty} F(\omega) e^{j\omega t} d\omega \quad . \tag{5.34}$$

In principle, for the solution of this equation $F(\omega)$ must be known for the full range of ω. In practice, however, it is sufficient if $F(\omega)$ is known up to a certain maximum frequency ω_m. Since equation (5.24) is satisfied for all frequency functions of interest, the range of integration is thus shortened to $0-\omega_m$. $F(\omega)$ itself is approximated in the integration by a piecewise linear function built up of the values of $F(\omega)$ calculated at a finite set of frequencies in the range $0-\omega_m$ and spaced $\Delta\omega$ apart. The values of ω_m and $\Delta\omega$ necessary to achieve a specified degree of accuracy is considered later.

In the case of the functions considered here, both the real and imaginary parts of $F(\omega)$ are continuous, finite functions of ω which are readily capable of piecewise linear approximation. $F(\omega)$ is calculated at N equally spaced frequencies in the range $0-\omega_m$ and stored in two $N \times 1$ dimensional arrays F_1 and F_2 such that

$$F_1(M-1) + jF_2(M-1) = F(\Delta\omega.M), \quad M = 1, N \quad . \tag{5.35}$$

Since equation (5.24) is satisfied for $F(\omega)$, F_1 and F_2 are respectively even and odd in ω. If $F(\omega)$ is continuous and piecewise linear in ω and $|F(\omega)| \to 0$ as $\omega \to \infty$, it is easily shown that

$$\mathcal{J}^{-1}(dF(\omega)/d\omega) = -jt\,\mathcal{J}^{-1}F(\omega) \quad . \tag{5.36}$$

From equations (5.33) and (5.35) it can be further demonstrated that

$$f(t) = -[\,\mathcal{J}^{-1}F''_1(\omega) + j\,\mathcal{J}^{-1}F_2''(\omega)]/t^2 \tag{5.37}$$

where F_1'', F_2'' are the second derivatives of F_1, F_2 with respect to ω. Now F_1, F_2 are respectively even and odd and piecewise linear in ω. Therefore it follows that F_1'', F_2'' are also respectively even and odd and consist of sets of delta functions distributed regularly at intervals of $\Delta\omega$. Let the magnitudes of the delta functions be represented by the $N \times 1$ arrays D_1, D_2 where

$$F_i(\omega) = \sum_1^N D_i(M)\delta[\omega-(M-1)\Delta\omega], \quad i = 1, 2 \quad . \tag{5.38}$$

Then

$$D_i(M) = [F_i(M+1)-2F_i(M)+F_i(M-1)]/\Delta\omega,$$

$$i = 1, 2, \quad M = 2, N$$

and $\tag{5.39}$

$$D_1(1) = [F_1(2) - F_1(1)]/\Delta\omega , \quad D_2(1) = 0 \quad .$$

Since F_1'', F_2'' consist only of delta functions distributed regularly on the frequency axis it is possible to convert the continuous integral transformation of equation (5.34) into the sum of the finite series;

$$f(t) = -(1/\pi t^2)\sum_{1}^{N}[D_1(M).\cos(M-1)\Delta\omega.t -$$

(5.40)

$$D_2(M).\sin(M-1)\Delta\omega t] .$$

The time function $f(t)$ is computed at discrete intervals of time Δt up to a required maximum t_m. For accurate time information up to t_m, however, the frequency interval $\Delta\omega$ should be less than π/t_m. Also no detail which can be shown on a time scale division of Δt is missed out if the computation is extended to $\omega_m \geq \pi/\Delta t$. These rules are very easily extracted from the above equation; since for a given t_m, Δt, the argument of the trigonometric expressions $(M-1)\Delta\omega.t$ need not be greater than π for the limiting values of M and ω (see Bracewell[34] for details).

The signals normally applied to a 5kHz transducer have periods of around 200 µs. Consequently, if $f(t)$ is required at 10 µs intervals up to 1000 µs, $\Delta\omega/2\pi$ must be less than 500 Hz and $\omega_m/2\pi$ greater than 50 kHz. The transducer equivalent circuits from which the frequency information is calculated are, however, unreliable beyond 15 kHz. Fortunately in the case of the broadband transducers, $|F(\omega)|$ is effectively zero beyond 10 kHz for a 5 kHz transducer (see Figure 4.23). Therefore no information is lost if the computation is not taken beyond 10 kHz. The conventional transducers on the other hand exhibit multiple resonances, some of which are close to or beyond 15 kHz (see Figure 5.7). The above method is thus not applicable to the determination of the impulse response of conventional transducers. The step response can, however, be determined accurately, even in this case, for here

$$|F(\omega)| = |G(\omega)|/\omega \qquad . \qquad\qquad (5.41)$$

The division by ω reduces to insignificance the high
frequency resonances and $|F(\omega)|$ is again effectively zero
beyond 15 kHz. Consequently in the analysis of conventional
transducers at least, the use of the step response for
convolution is mandatory. Since the impulse response is
not of much interest in any case, 'step response convolution'
is used in the time analyses of both broadband and conventional
transducers.

Since the high frequency components in g(t) are
eliminated by the integral transformation to u(t) (equation
(5.27)), the latter function is much smoother than the
former. Consequently convolution from the step response
is computationally much simpler than 'impulse convolution'.

Further Computational Details

The numerical inverse Fourier transformation is
effected by the subroutine INFTRA (Appendix III) according
to equation (5.40). The necessary frequency information
is calculated by the subroutine FRERES, as described in
section 5.2. INFTRA is used to obtain the step response
(according to equation (5.27)) and the voltage response to
a mechanical input caused by an explosion. The latter is
calculated from equation (5.32) with θ_o = 1.0 and $\alpha = 10^4$
which corresponds to a waveform of time constant 100 μs.

The responses to sinusoidal and square-wave voltage
inputs applied at t = 0 are obtained by convolution with
u(t) from equation (5.28). The convolution integral is
evaluated numerically by means of the subroutine CONVOL
(Appendix III). The integration process is based on the
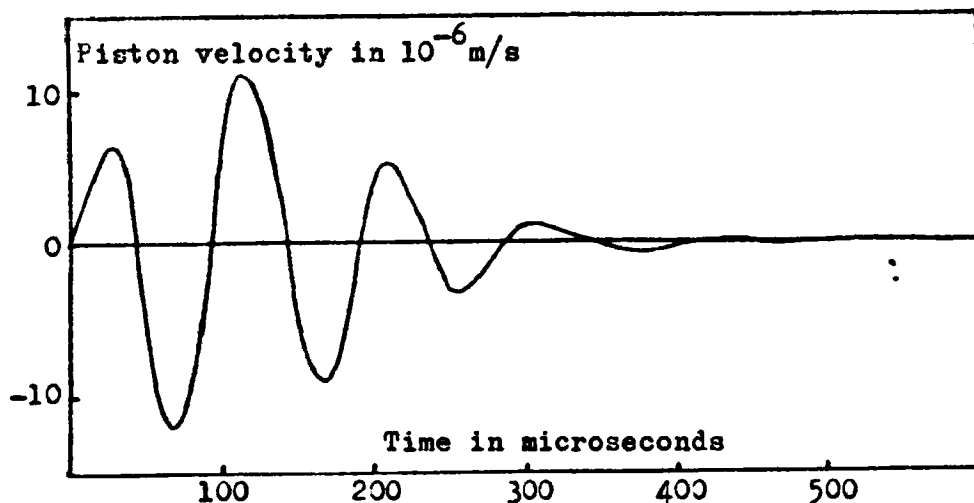
Figure 5.8- Step Response of Conventional Transducer
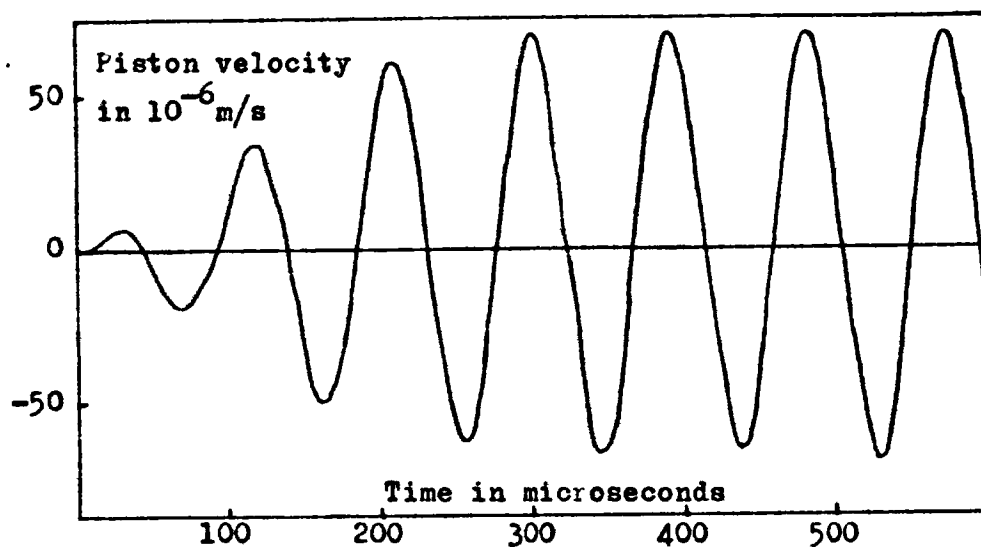
Figure 5.9- 'Sinestep' Response of Conventional
Transducer
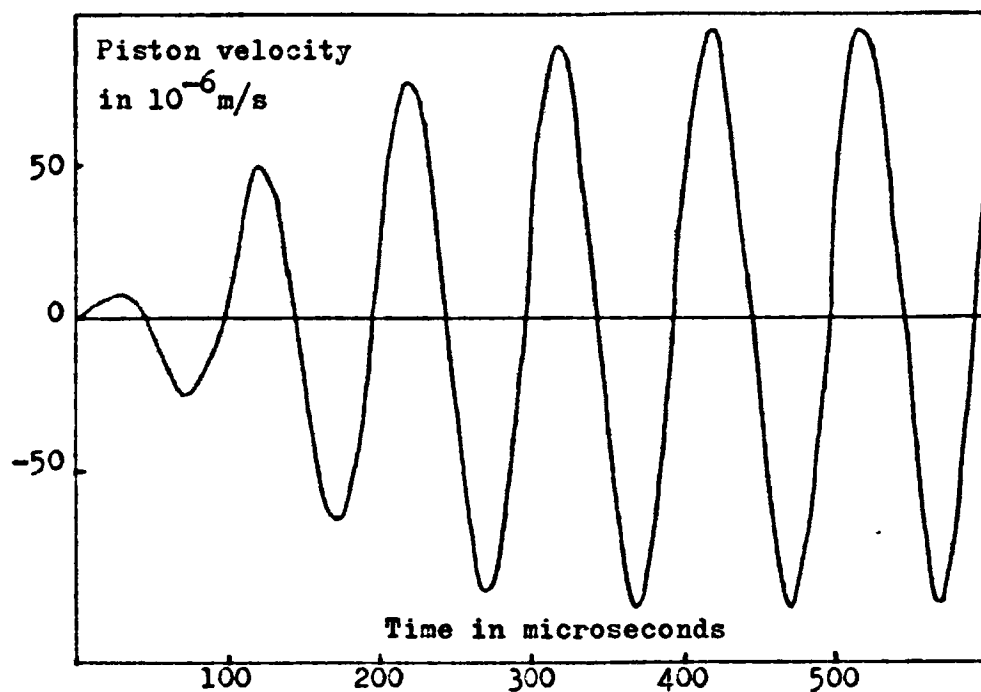
Figure 5.10- 'Square-wave' Response of Conventional
Transducer
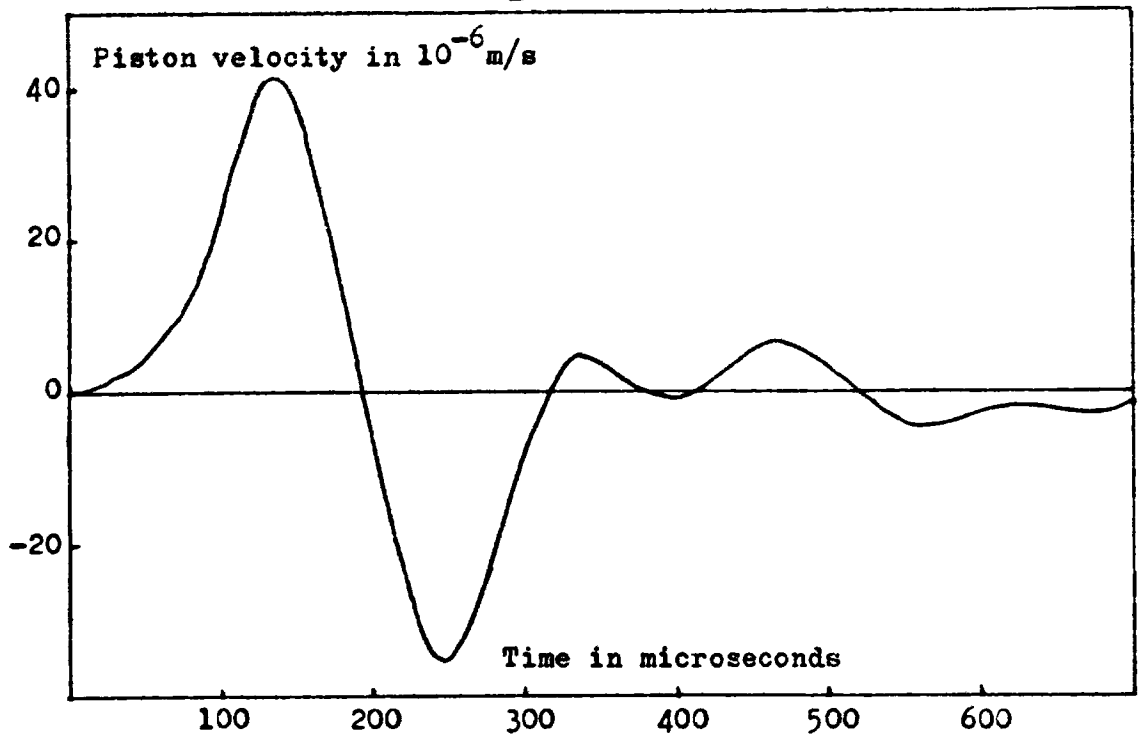
Figure 5.11- Step Response of Designed Transducer
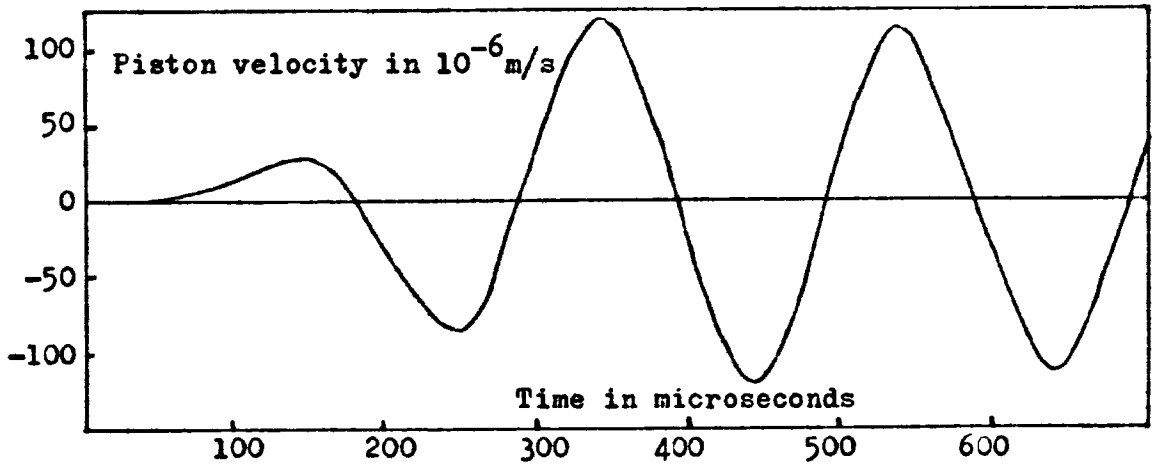
Figure 5.12- 'Sinestep' Response of Designed Transducer
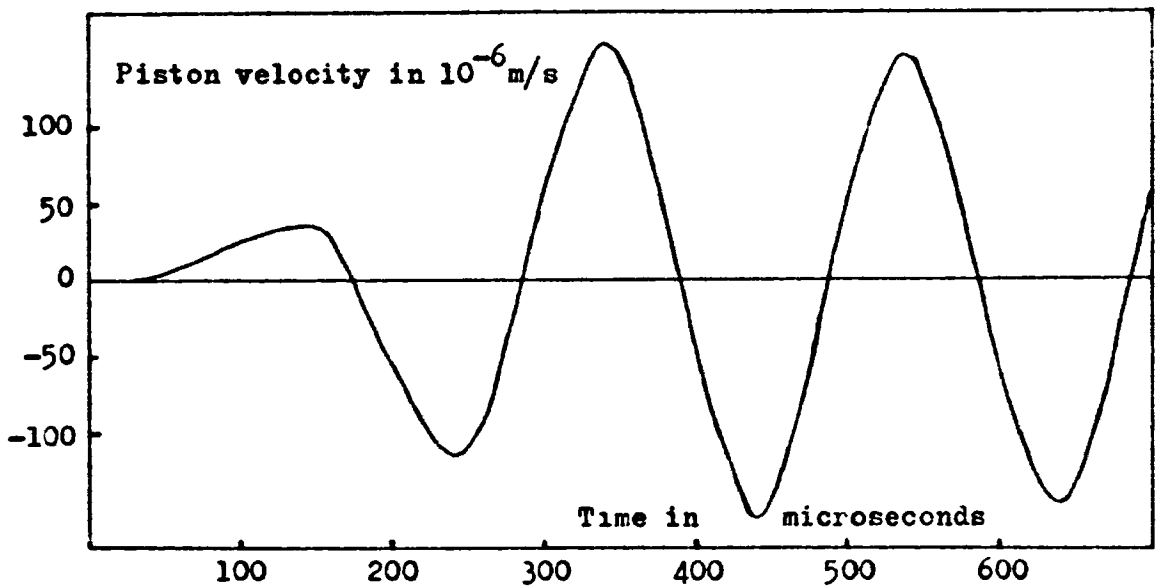
Figure 5.13- 'Square-wave' Response of Designed Transducer

trapezium rule with both functions assumed to be linear and piecewise continuous in intervals Δt. For accurate convolution the interval Δt must be small compared to the period of the highest frequency components present in either function. Consequently the time responses are calculated at 10 μs intervals up to 1000 μs.

In the case of a square-wave input, convolution is unnecessary for the derivative of a square wave is given by

$$dv/dt = \delta(0) - 2\delta(t-t') + 2\delta(t-2t') - \ldots \qquad (5.42)$$

where $2t'$ is the period of the square wave. Substituting for dv/dt in equation (5.28), the response to a square wave is

$$f(t) = u(t) - 2u(t-t') + 2u(t-2t') \ldots$$
$$\pm 2u(t-mt') \qquad (5.43)$$

where m is such that $mt' \leq t$ and $(m+1)t' > t$.

The computed time responses of the conventional transducer depicted in Figure 2.7 are given in Figures 5.8 to 5.10. The time responses of the designed broadband transducer of Figure 4.22 are displayed in Figures 5.11 to 5.14. In these figures the responses to sinusoidal and square-wave inputs applied at $t = 0$ are referred to as the 'sinestep' and 'square-wave' responses respectively. In both cases the input waveform is assumed to be of unit amplitude. The response of the designed transducer to an explosion, depicted in Figure 5.14, is calculated from equation (5.32) with $\theta_o = 1.0$ and $a = 10^4$.

It is observed that the sinestep and square-wave responses of the designed transducer build up to their
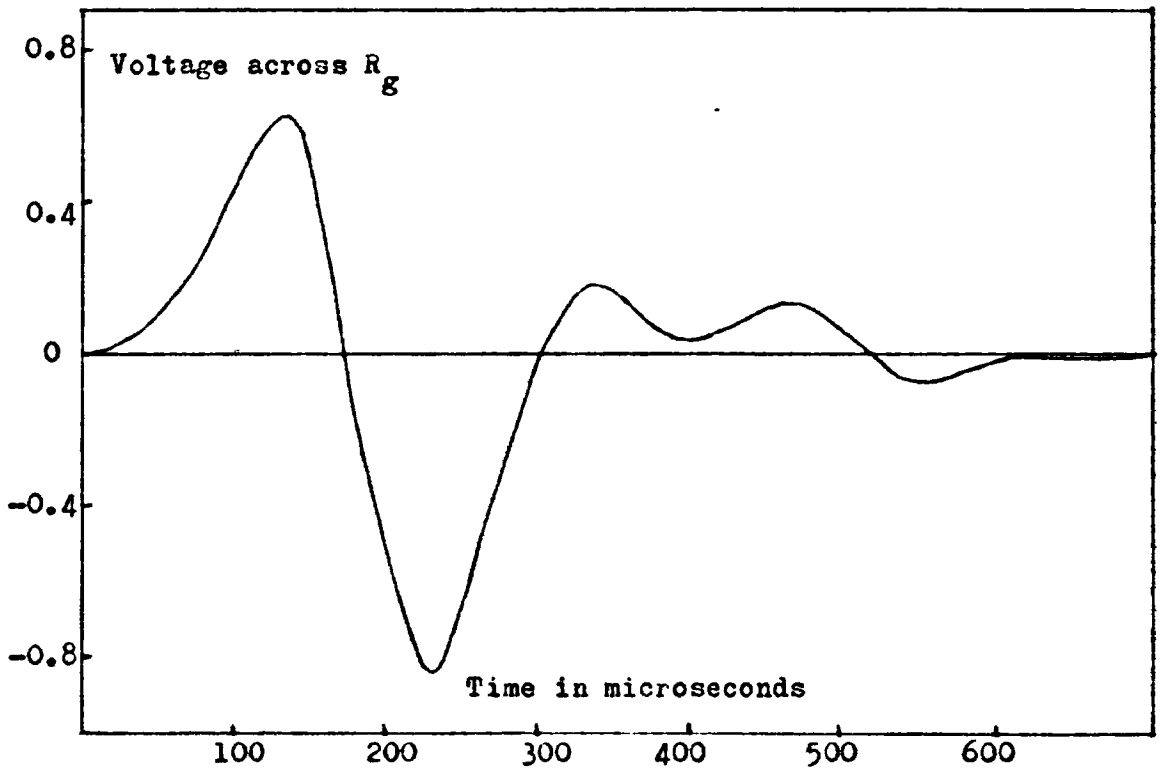
Figure 5.14- Response of Designed Transducer to an
'Explosion' Input
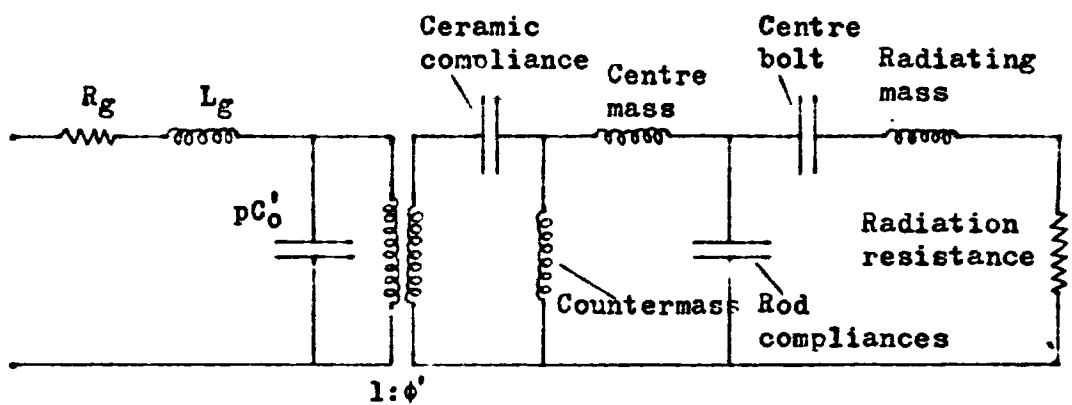
Figure 5.15- LC Approximation of the Impedance Equivalent
of the Designed Transducer

steady state values within a cycle. The corresponding interval in the case of the conventional transducer is three cycles. The faster rise time of the designed transducer is consequent on its larger bandwidth.

It is also observed that the shape of the response to a mechanical explosion input is very similar to that of the step response of the transducer.

5.4. Analysis of Ladder Networks

In addition to the analysis techniques described in sections 5.2 and 5.3, a technique was developed for the analysis of ladder type circuits consisting of conventional electrical elements. The technique was used to compute the characteristics of the normalized filter circuits (of Chapter 4), on which the design was based.

A computer program incorporating this method of analysis is given in Appendix IV. In this program, details of the constitution of the ladder network to be analysed are fed into the subroutine LAPLACE as DATA statements. This subroutine then computes the transmission matrix of the network by means of the stepwise assimilation process indicated in Figure 5.6 and defined by equations (5.18) and (5.19). Unlike in section 5.2, however, the elements Y, Z are assimilated as sC, sL, etc., and the functions A, B, C, D are built up as a set of polynomial functions in the Laplace transform variable s. The transfer function relating the output I to the input V_g is obtained from the transmission matrix in the form

$$I(s) = \frac{N(s)}{D(s)} V_g(s) \qquad (5.44)$$

where $N(s)$, $D(s)$ are polynomial functions in s. The frequency response of the system is then obtained by simply substituting $j\omega$ for s in the above equation.

Some of the time responses of the system can also be determined from the above equation. If the input signal is a voltage step of unit magnitude

$$V_g(s) = 1/s \qquad . \qquad (5.45)$$

Alternatively, if the input is a sine wave of unit magnitude

$$V_g(s) = \omega_o/(s^2 + \omega_o^2) \qquad (5.46)$$

where ω_o is the angular frequency of the wave. In either case the output $I(s)$ is obtained as a rational polynomial function of s, with a denominator of higher order than the numerator. The corresponding time domain solution is then obtained by inverse Laplace transformation.

In the program of Appendix IV the resulting rational polynomial functions are inverse Laplace transformed by the state variable technique given by Liou[33].

By the above method it is found possible to compute the response of the system to any input which can be expressed as a rational polynomial function in s. Examples of such computations are not, however, included in this study since the time responses of the filter networks analysed are not of much interest.

The program was also used to analyse the approximate LC formulation of the designed transducer. Thus if the elements of Figure 5.4 are approximated by their low frequency values and sophistications such as the compliance of the centre mass and C_i are ignored, the complete equivalent circuit

reduces to that of Figure 5.15. This circuit is clearly a conventional type ladder network which can be analysed by the method described above. It is also observed that the original design circuit of Figure 4.21 is a further simplification of the above circuit in which the countermass and the bolt have been excluded. The transducer performance as predicted by the LC approximations of Figures 4.21 and 5.15 are compared with the results of the more accurate analysis in Figure 4.23.

CHAPTER 6

EXPERIMENTAL RESULTS AND CONCLUSIONS

In this Chapter the input admittance measurements carried out on a test transducer are presented. They are compared with the corresponding computed characteristics predicted by the analysis routine.

Finally the major conclusions arrived at in this study are stated and discussed.

6.1. Characteristics of the Test Transducer

A test transducer was designed and constructed for the purpose of verifying the equivalent circuit representation. The transducer was derived from a Butterworth three pole coupled resonator bandpass circuit and is similar in construction to the transducer designed in section 4.6. The transducer was designed to have a bandwidth of around 100% at a centre frequency of 4.5 kHz, when operating in a regular array.

Since it was necessary to construct the test transducer within a limited period of time, the design specifications were not closely adhered to in construction. Further it was necessary to use a ceramic whose properties were somewhat different from the one designed for. The resulting deterioration of performance was not considered to be of much account since the primary purpose was the verification of the equivalent circuit representation.

Consequently, the original design specifications are not included in the text. A full scale sectional diagram of the test transducer, as constructed, is however given in
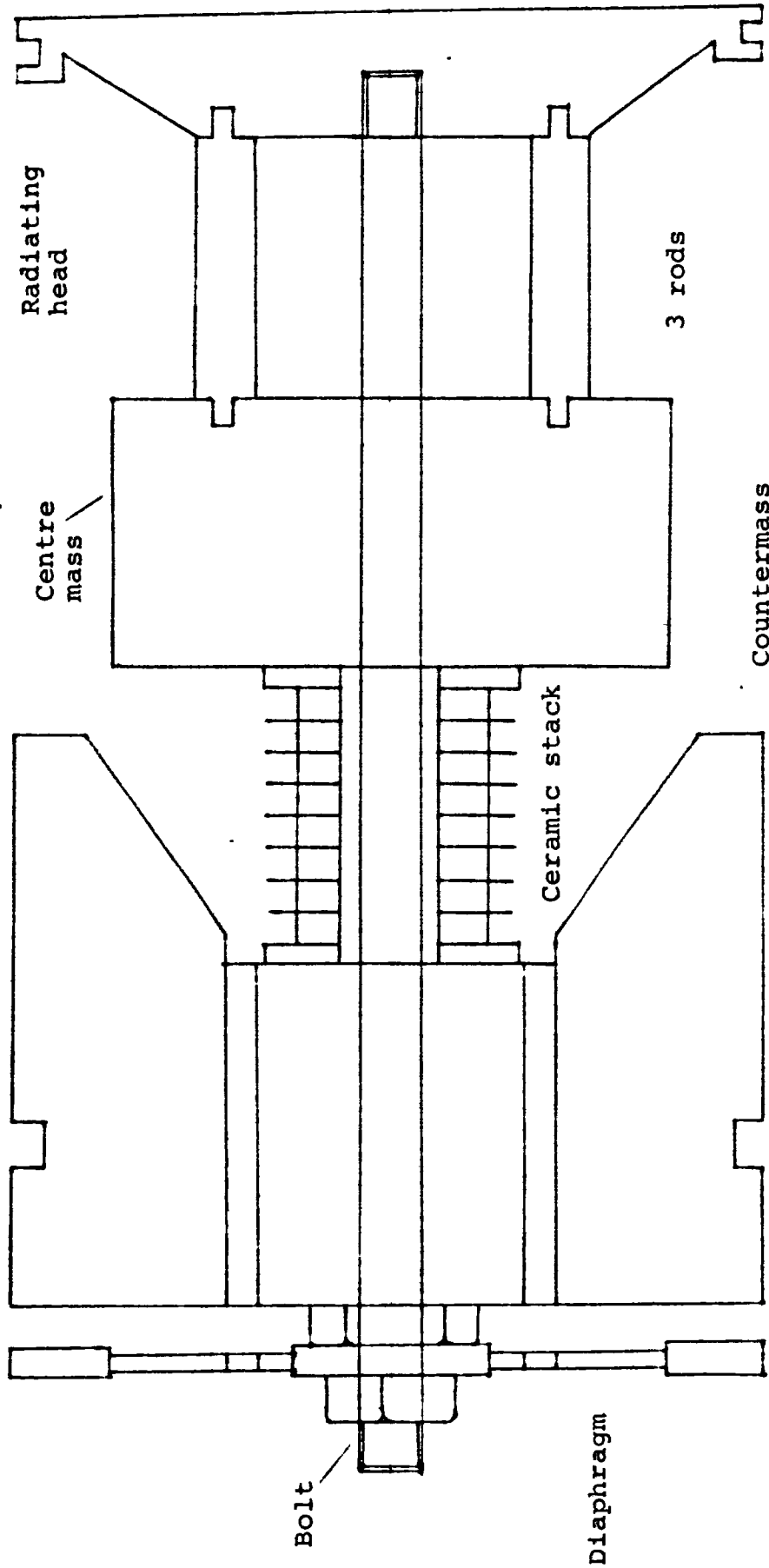
Figure 6.1- Diagram of the Test Transducer Without the Case

Scale - Full size
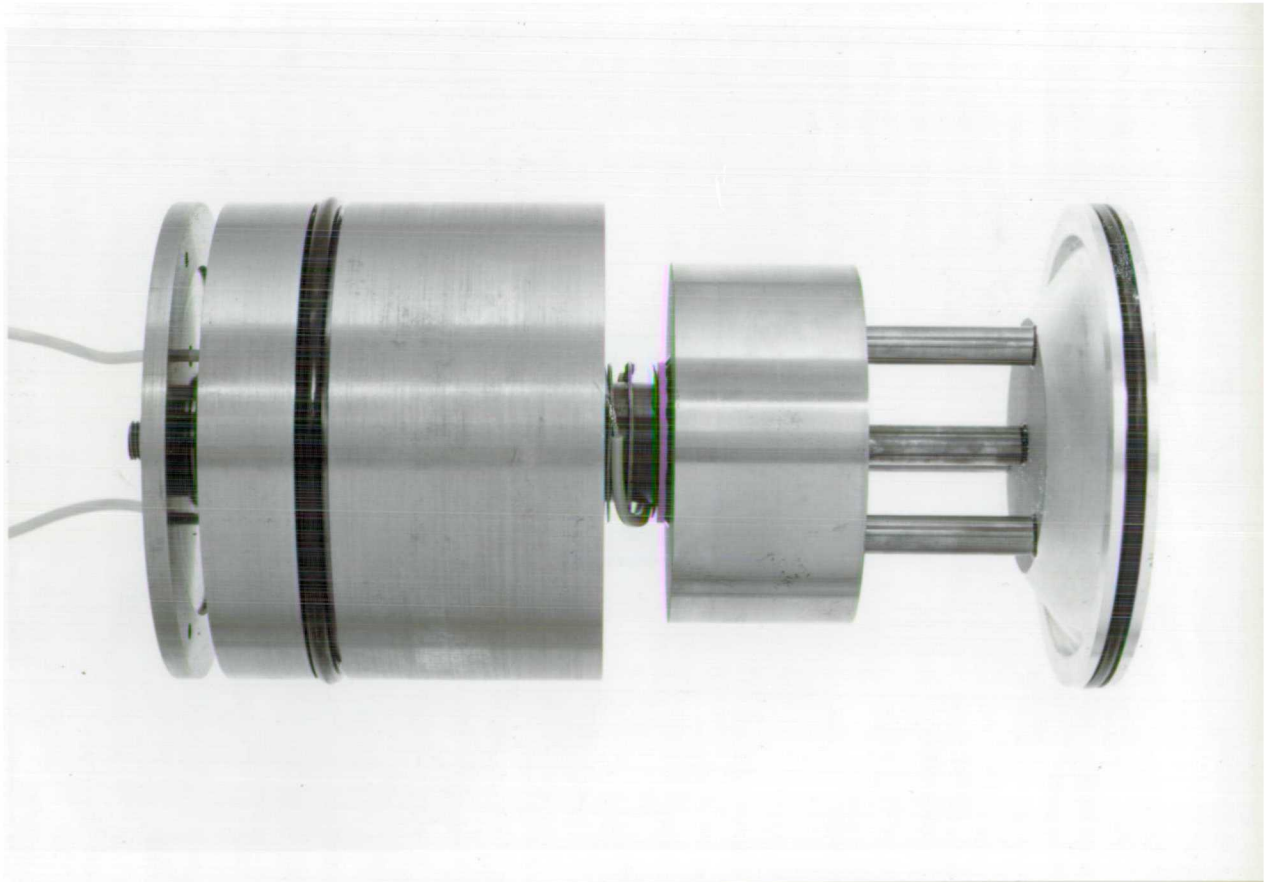
Figure 6.2- Photographs of Test Transducer with
case removed

Figure 6.1.   Two photographs of the transducer assembly
with the case removed are included in Figure 6.2.   The
electrical elements needed to complete the transducer circuit
are shown in Figure 6.3.   The resistance R_g, shown in this
Figure, would under ordinary operating conditions be the
internal resistance of the supply.

The test transducer differs from that designed in
section 4.6 only as regards the geometric dimensions and the
ceramic used.   The materials used for the other elements
are the same in both transducers.   Further the diaphragm
construction and the lateral dimensions of the piston, the
centre mass, the countermass and the bolt are the same in
both cases.   The designed transducer, however, incorporates
a larger ceramic section and countermass and shorter rod
compliances than the test transducer.   This is mainly a
result of improvements to the mechanical design which were
inferred from the performance of the test transducer and,
subsequently, incorporated in the transducer designed in
section 4.6.

The test transducer was constructed and tested at the
Admiralty Underwater Weapons Establishment in Portland,
Dorset.   The tests consisted of input admittance measure-
ments at the terminals T_e (in Figure 6.3) of the complete
transducer circuit.   In all three sets of measurements were
taken;   firstly with the encased and unbaffled transducer
supported freely in air, secondly in an acoustic tank and
finally at about 20 yards depth in the Portland Harbour.
Since the measurements in the tank agreed very closely with
the measurements taken in the harbour, the two sets are not
differentiated and reffered to jointly as the 'water
measurements'.

$$T_e \quad \underset{R_g}{\mathrm{www}} \quad \underset{L_g}{\mathrm{mmm}} \quad - - - - - - - - \rightarrow$$

Connecting cable

To electrical terminals of test transducer

$$Y \longrightarrow$$

$$T_e \longleftarrow - - - - - - - - \rightarrow$$

R_g = 4270 ohms , L_g = 0.169 henries
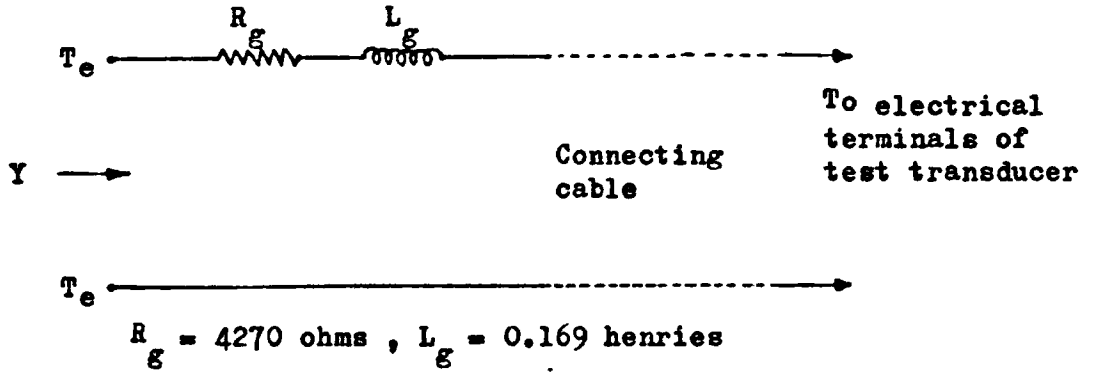
Figure 6.3- Test Transducer Circuit for Admittance Measurement
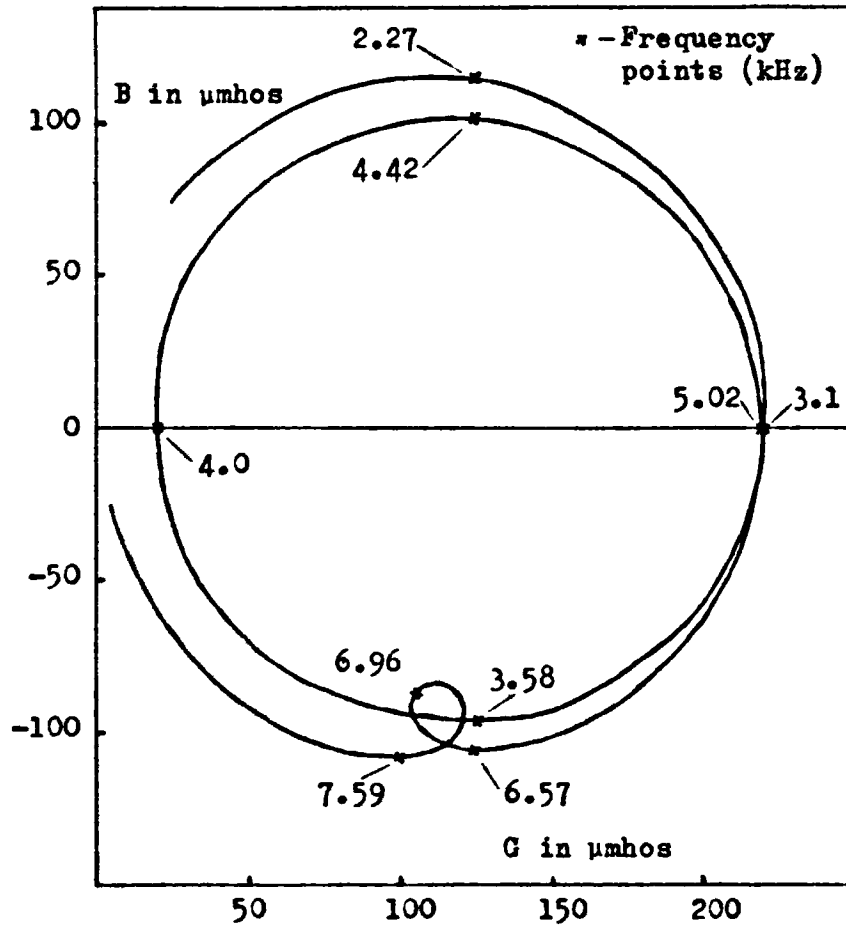
Figure 6.4- Measured Input Admittance of Test Transducer in Air
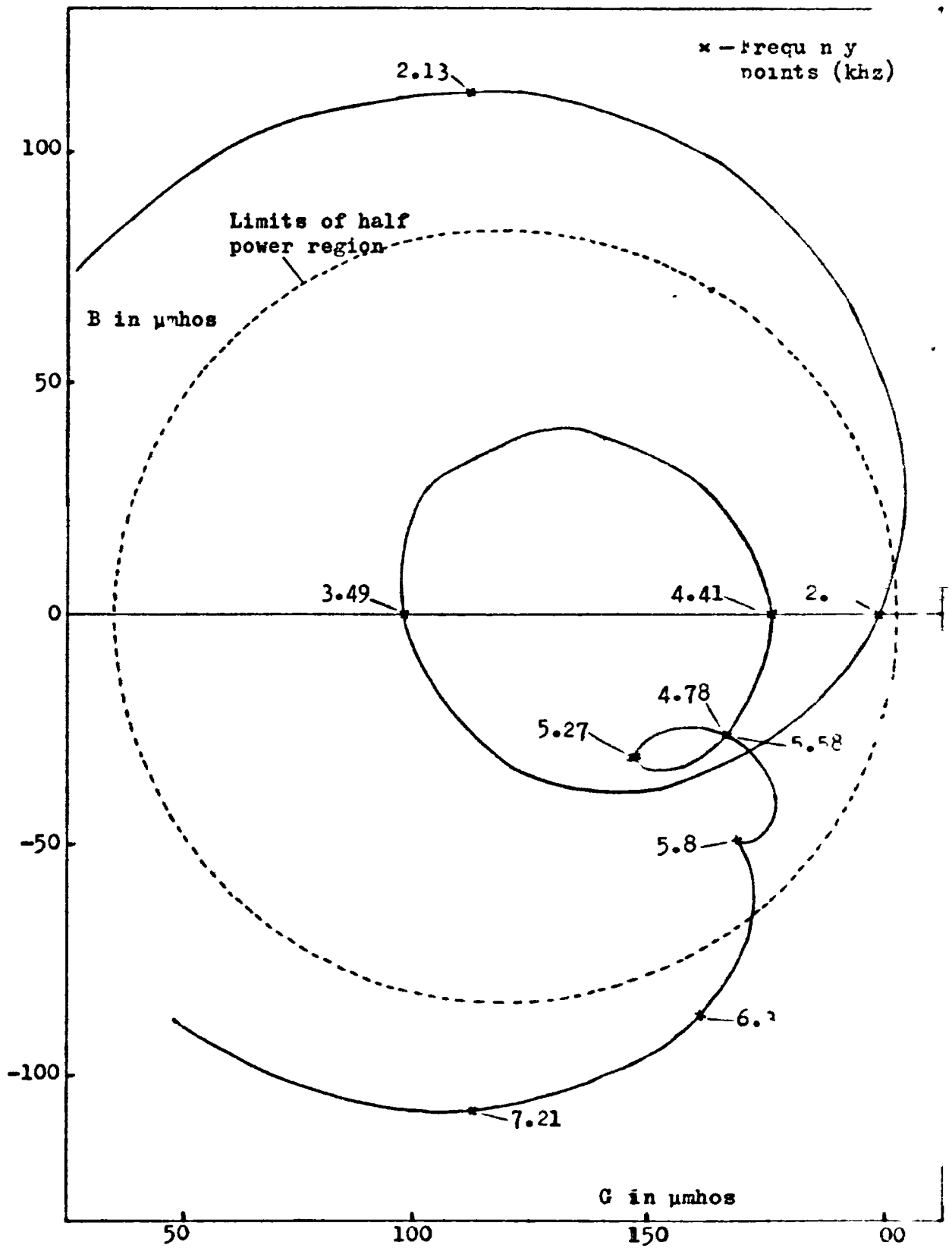
Figure 6.5- Measured Input Admittance of Test Transducer in Water
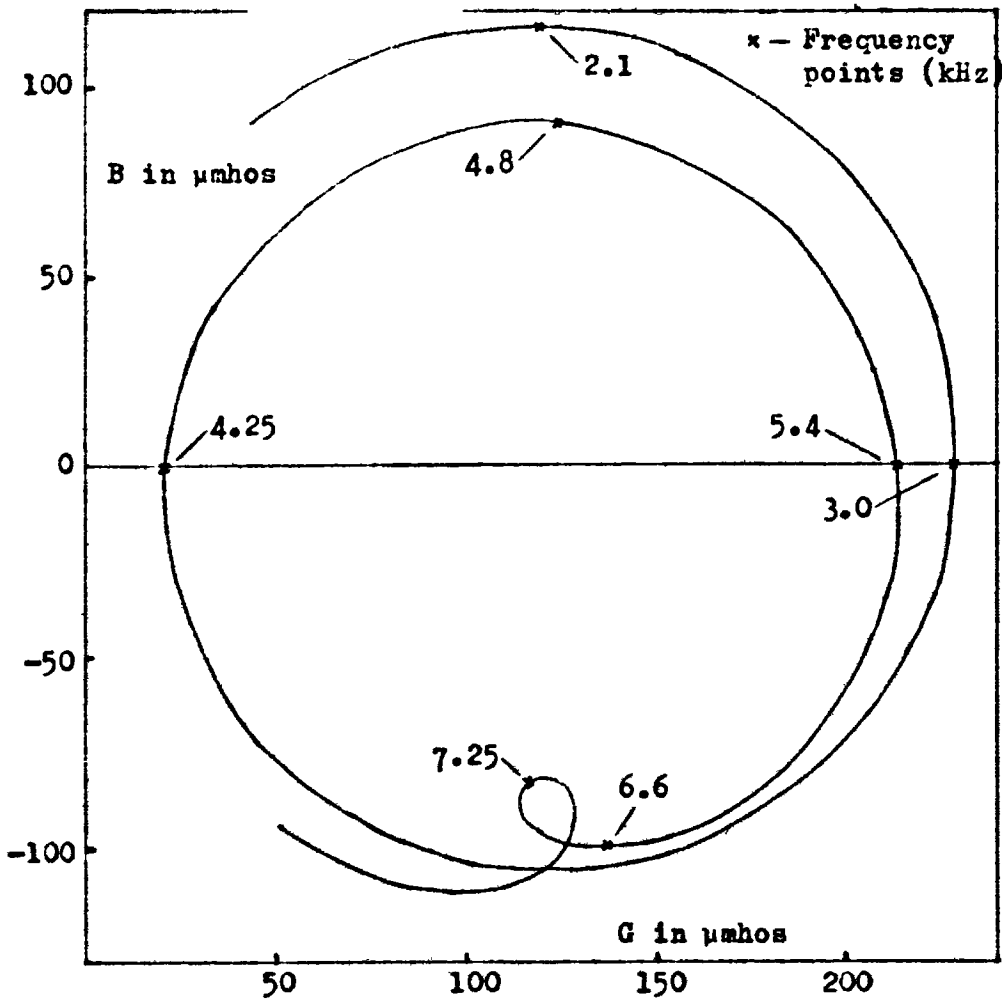
Figure 6.6- Computed Input Admittance of Test
Transducer in Air
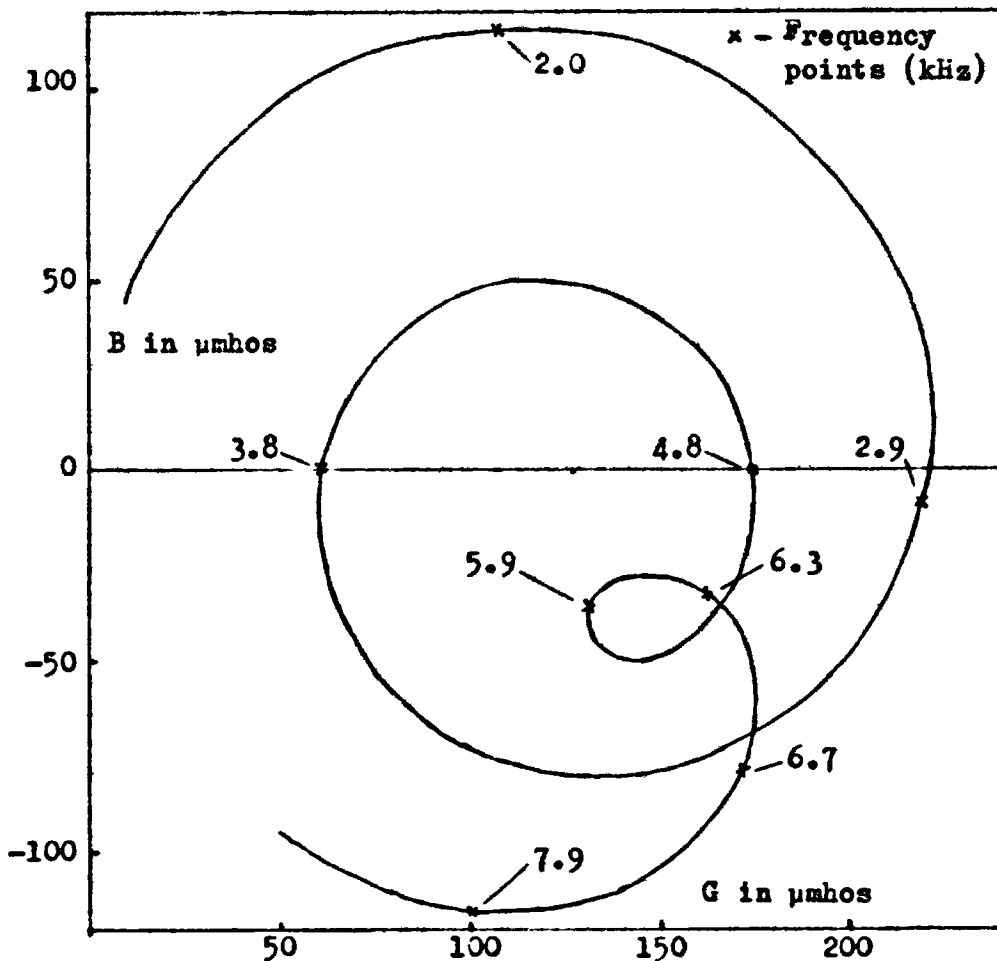
Figure 6.7- Computed Input Admittance of Test
Transducer in Water

In both cases the admittance diagrams were first obtained on an XY-recorder linked to a Dranetz impedance bridge and subsequently checked at individual frequency points by independent bridge measurements. The admittance diagrams obtained in air and water are displayed in Figures 6.4 and 6.5 respectively. The frequencies corresponding to certain points on the diagrams, are indicated in kilohertz. In all cases the diagrams were obtained in the range 2-7 kHz.

The admittance diagrams of the test transducer were also computed by means of the analysis technique described in sections 5.1 and 5.2. In the computation allowance was made for mechanical loss at the rubber rings and for the appreciable capacitance of the connecting cable. It is important to note that in the case of the test transducer, the rod compliances require the full representation indicated in Figure 5.3. The computed admittance diagrams are displayed in Figures 6.6 and 6.7.

The power absorbed by the transducer circuit, exclusive of R_g, is easily inferred from the admittance characteristic. When operating in water, the power absorbed is approximately equal to the power radiated. Thus if Y is the input admittance measured at the terminals T_e in Figure 6.3 where

$$Y = G + jB \qquad . \qquad (6.1)$$

The power P, absorbed for a particular operating voltage V_g, is given by

$$P/P_m = 4R_g(G - R_g G^2 - R_g B^2) \qquad (6.2)$$

where P_m, the maximum power that can be delivered from a supply V_g of internal resistance R_g, is given by equation
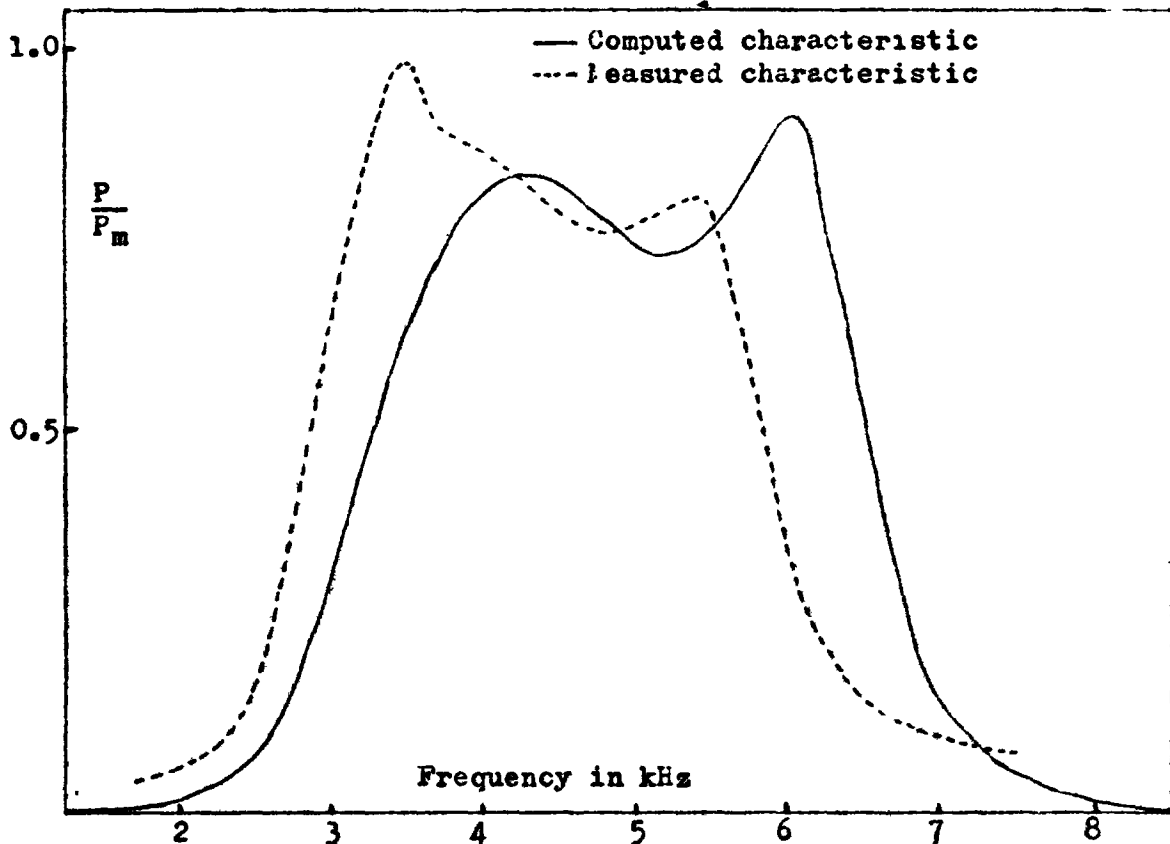
Figure 6.8- Power Absorbed by Unbaffled Test Transducer
in Water
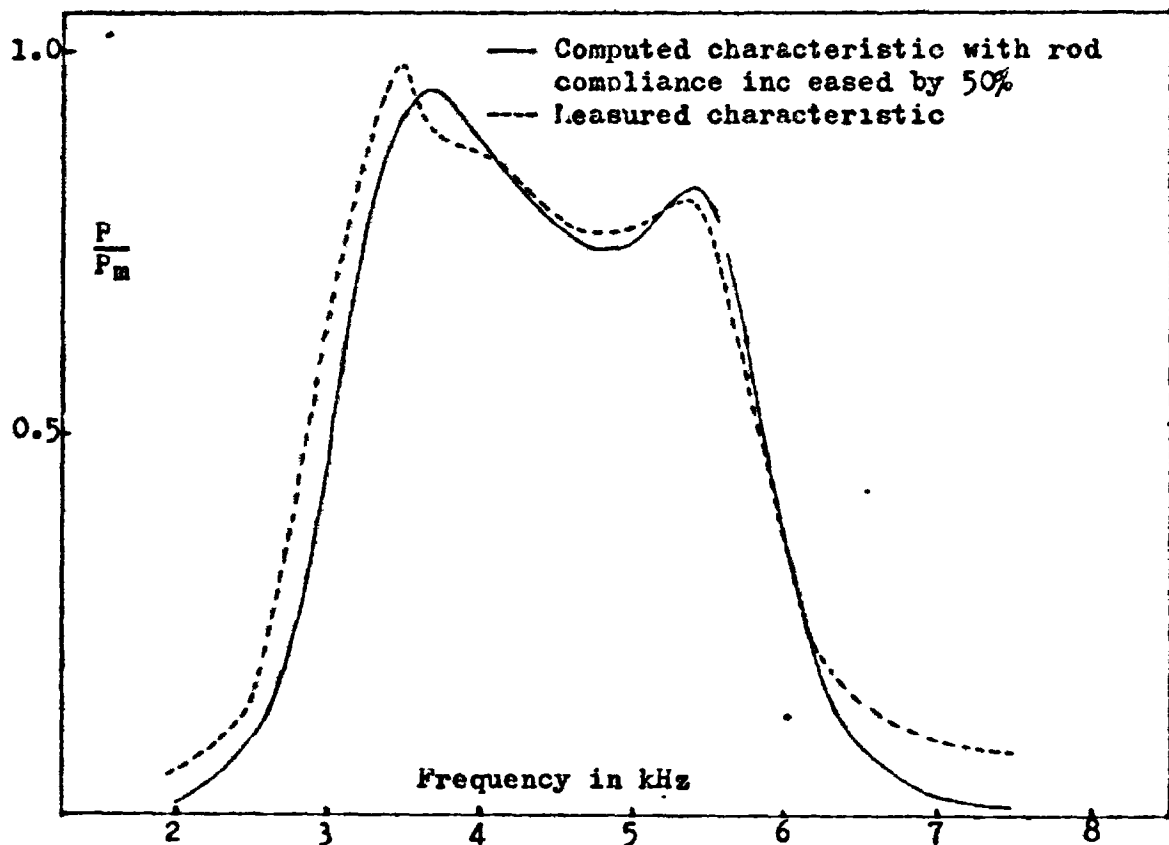
Figure 6.9- Power Absorbed   by Unbaffled Test Transducer
in Water

(4.2). Consequently the passband could be located on the admittance diagram as the region defined by

$$(G-1/2R_g)^2 + B^2 \leq 1/8R_g{}^2 \qquad . \qquad (6.3)$$

The boundary of the passband (or half-power region) is indicated in Figure 6.5.

The power absorbed by the unbaffled test transducer in water, as estimated by the measured and computed results are compared in Figure 6.8. In both cases P/P_m is calculated from equation (6.2).

6.2. Comparison of the Measured and Computed Characteristics

An examination of the computed and experimentally determined admittance characteristics, reveals that the two sets agree closely as regards general form. Each diagram consists of three loops which correspond to the resonance-antiresonance pairs the three pole circuit. The resonances and antiresonances are displayed with greater clarity in the $|Y|$ vs frequency plot of Figure 6.10.

It can be shown that the diameter of each loop is inversely proportional to the resistance associated with the corresponding resonance. Thus it is found that the size of the first loop of all diagrams and of the second loop in the air diagrams alone is largely governed by the resistance R_g. The second loop of the water diagrams is reduced by the increased dissipation in the radiation load. The size of the third loop of the air diagrams is mainly dependent on the internal power dissipation in the transducer.

The cusp that appears at 5.8 kHz in the measured diagram in water (Figure 6.5) is absent in the corresponding

computed characteirstic (Figure 6.7). It has been established
that the cusp is a reflection of the lowest flexural mode of
the piston, which falls at 5.8 kHz. Clearly the presence of
this spurious mode in the passband has little effect on the
shape of the admittance characteristic. This is probably on
account of the mode being inhibited by the constructional
form of the transducer. It is also inferred that other
spurious modes fall outside the frequency range covered by
the experimental diagrams or are too weak to affect the
performance.

A comparison of the air diagrams with the water
diagrams shows that the characteristic frequencies are
depressed when operating in water. This is a result of the
extra reactance introduced into the circuit by the water load.

It is observed, however, that the computed character-
istic frequencies differ from the experimentally determined
values. The discrepancy is somewhat regular in the case of
the water diagrams; the measured frequencies being
approximately 10% lower than the computed values. The
difference is less, but irregular, in the case of the air
diagrams. The discrepancy in the water diagrams is also
reflected in the power vs frequency characteristics of
Figure 6.8.

Clearly the magnitude of the discrepancy is too large
to be understood within the margin of error inherent in the
analysis technique. For instance, a 5% increase in the
electrical capacitance and compliance of the ceramic stack,
results in a 2.5% drop in the characteristic frequencies.
It is obvious however that the discrepancy is a result of a
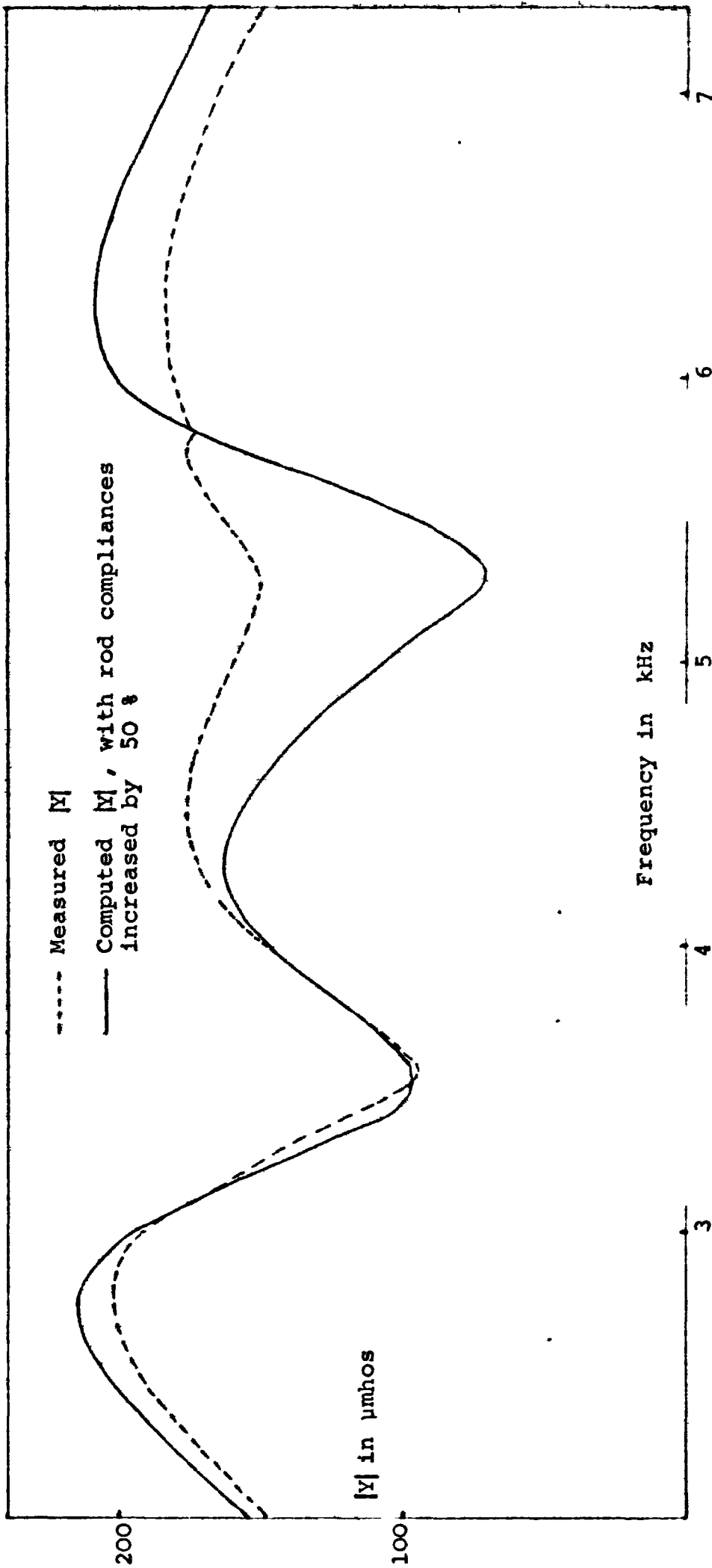
Figure 6.10— Measured and Computed Values of |Y| as a Function of Frequency

higher compliance value or a higher mass value somewhere in the circuit from that assumed in the computation. Since the mass values were calculated and subsequently checked by weighing, a large error in them is extremely unlikely. It has also been established that likely errors in the assumed value of radiation reactance are too small to cause a 10% drop of frequency. Further the ceramic compliance is determinate to within 5%. Thus the most probable source of error is an increase of the effective value of the rod compliances, above that assumed in the computation.

It has been established, by a computational trial-and-error procedure, that a 50% increase in the compliance value of the rods reduces the characteristic frequencies almost uniformly by 10% to about the values obtained by experiment. The modified power characteristic resulting from this increase in compliance is compared in Figure 6.9 with the characteristic inferred from experiment. Further, the modulus of the input admittance of the equivalent circuit incorporating this modification is compared with the experimentally determined $|Y|$ in Figure 6.10. Clearly the agreement is close in both Figures.

Consequently, it is inferred that the value of the rod compliances is raised by about 50% from that predicted by the longitudinal mode theory. The increased compliance of the rods could plausibly be traced to bending of the rods induced by their slenderness, especially under heavy loading.

6.3. Summary and Conclusions

The main objectives of this study, which are stated in section 1.1, have been achieved. The analysis technique

developed is adequate for the determination of all the
time and frequency responses of interest.   It is also
sufficiently general to be applied to any extensional
transducer.   As regards design it has been possible to
develop a transducer with a bandwidth of about 100%.   This
transducer is not only greatly superior to the conventional
designs bandwidth-wise but it is also less sensitive to
variations of the individual element values.

It is found that the equivalent circuits developed
are adequate to accurately represent transducer for the
purpose of analysis, subject to the proviso that
longitudinal mode operation is approximated to by all
mechanical elements.   Thus the unusually large divergence
of 10% between the analytically determined and measured
frequencies of the test transducer is attributed to a
breakdown of the longitudinal wave model for the rod
compliances.   In the absence of such a contingency the
analysis technique is capable of predicting the transducer
characteristics to an accuracy of a few percent.

In any case the analysis technique used is a
considerable improvement on the conventional method employing
a simplified equivalent circuit.   The graphs of Figure 4.23
indicate that the simplified circuit of Figure 5.15 is a
reasonable guide to the performance of the designed trans-
ducer up to the centre frequency.   This result is not
unexpected as the values of the simplified circuit elements
are clearly more accurate at the lower frequencies.   Further
the circuit does include the bonding correction and the
effects of the bolt and countermass, albeit in a lumped and

frequency invariant form. Thus the simplified circuit is
adequate, provided frequency information beyond the centre
frequency and time information is not desired. Even then,
only the radiation termination of a regular array element
can be handled by the simplified model.

The only bandpass filter circuit that is practically
realizable as an acceptable transducer design is the
predominantly mechanical three pole coupled resonator circuit
derived from a Butterworth or low-ripple Chebychev prototype.
Since the values of a low-ripple Chebychev circuit are
slightly different from those of a Butterworth, the broadband
design is variable within certain narrow limits. A
Chebychev circuit is easier to realize mechanically than a
Butterworth. The increase in realizability is, however,
offset by a deterioration of characteristic.

It is observed that the designed broadband transducer
is not much more complex than the conventional designs and
in any case raises no significant constructional problems.
The 'weak spot' in the broadband design has been revealed
as the slenderness of the rod compliances by the performance
of the test transducer. Consequently, in the broadband
design of section 4.6, the slenderness ratio of the rods
has been reduced by shortening them. Further, since the low
frequency side of the characteristic is adversely affected
by a low countermass, the transducer of section 4.6 is
designed with a larger countermass than the test transducer.
The former is also capable of handling about twice as much
power for the same input than the latter, on account of a
larger ceramic stack.

The broadband designs developed in this study possess output Q factors which are generally much less than what is common in conventional designs. The values employed in both designs are not, however, low enough to result in radiating heads which are appreciably non-rigid in the passband.

The resiliance of the transducer characteristic to variation of the element values is illustrated by a comparison of the computed characteristics of Figures 6.8 and 6.9. Thus a 50% variation of the rod compliance value shifts the pass-band down by 10% without appreciably affecting the pass-range. It has also been found that the characteristic is most sensitive to variations of the electrical capacitance of the ceramic and the compliance of the rods.

APPENDIX I

Radiated Power and Bandwidth of Shunt
Tuned Elementary Transducer
(with reference to section 2.4)

The basic circuit of a shunt tuned elementary composite transducer, with all elements referred to the electrical side, is given in Figure A.1. The transducer is fed from a constant voltage source V through the resistance R_o. If P is the power dissipated in the resistance R, it is easily demonstrated that

$$P/|V|^2 = R/(R_o|T|)^2 \qquad \text{(A.1)}$$

where

$$T = 1 + Z(Y + 1/R_o) \qquad \text{(A.2)}$$

$$Z = R + j\omega L - j/\omega C \qquad \text{(A.3)}$$

$$Y = j\omega C_o - j/\omega L_o \qquad . \qquad \text{(A.4)}$$

Now the shunt inductor L_o is such that

$$L_o C_o = LC = 1/\omega_r^2 \qquad \text{(A.5)}$$

and the input and output Qs are defined as

$$Q_o = 1/d_o = \omega_r C_o R_o \qquad \text{(A.6)}$$

and
$$Q_m = 1/d_m = \omega_r L/R \qquad . \qquad \text{(A.7)}$$

Also
$$L_o/L = C/C_o = K^2 \qquad . \qquad \text{(A.8)}$$

From equations (A.2) - (A.7) it can be shown that

$$T = 1 + (d_m + j\Omega)(d_o + j\Omega)/K^2 \qquad \text{(A.9)}$$
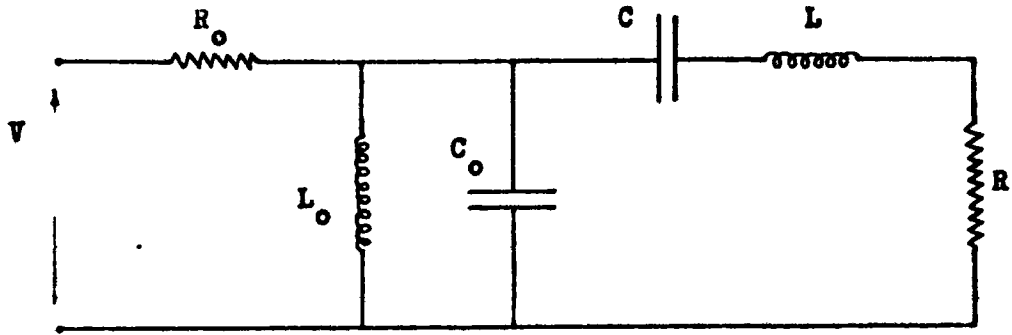
Figure A.1- Shunt Tuned Elementary Transducer Circuit

where $\Omega = \omega / \omega_r - \omega_r / \omega$. (A.10)

From which

$$K^4 . |T|^2 = \Omega^4 + (b^2 - 2a)\Omega^2 + a^2 \qquad \text{(A.11)}$$

where $\quad a = (K^2 + d_m d_o)$

(A.12)

and $\quad b = (d_m + d_o)$.

From equation (A.1) it is clear that the shape of the power-frequency characteristic is completely determined by the behaviour of $|T|^2$. From equation (A.11) the condition for a single resonance at $\omega = \omega_r$ is

$$b^2 \geq 2a \qquad . \qquad \text{(A.13)}$$

Assuming that this condition is always satisfied, the half-power points are obtained from the solution of

$$\Omega^4 + (b^2 - 2a)\Omega^2 - a^2 = 0 \qquad . \qquad \text{(A.14)}$$

This equation has a positive and negative root of Ω^2. If β^2 is the positive root (the negative one being inadmissible) the half-power frequencies are given by

$$\omega_1 . \omega_2 = \omega_r, \qquad (\omega_2 - \omega_1)/\omega_r = \beta \qquad . \qquad \text{(A.15)}$$

Thus β is the fractional bandwidth as well. Equation (A.14) has a relatively simple solution (for Ω^2) under two different conditions. Thus if $b^2 \geq 5a$, β^2 is given to within 5% of the exact value by

$$\beta^2 \quad a^2/(b^2 - 2a) \qquad . \qquad \text{(A.16)}$$

This is equivalent to a fractional bandwidth β_1 of

$$\beta_1 = (K^2 + d_m d_o)/(d_m^2 + d_o^2 - 2K^2)^{\frac{1}{2}} \qquad \text{(A.17)}$$

The solution being valid for values of d_m, d_o such that

$$5K^2 \leq d_m^2 + d_o^2 - 3d_m d_o \qquad . \qquad \text{(A.18)}$$

The second solution, which is valid for $b^2 = 2a$, yields a fractional bandwidth β_2 of

$$\beta_2 = (K^2 + d_m d_o)^{\frac{1}{2}} \qquad . \qquad \text{(A.19)}$$

The condition of validity is equivalent to

$$d_m^2 + d_o^2 = 2K^2 \qquad . \qquad \text{(A.20)}$$

From equations (A.17) and (A.18) it can, however, be shown that

$$\beta_1 \leq (K^2 + d_m d_o)^{\frac{1}{2}}/\sqrt{3} < \beta_2 \qquad . \qquad \text{(A.21)}$$

Thus in practical design the second condition (that of equation (A.20)) is aimed at, as it yields a higher fractional bandwidth. It can, however, be further demonstrated that β_2 is a maximum for

$$d_m = d_o = K \qquad \text{(A.22)}$$

when $(\beta_2)_{max} = \sqrt{2}K$.

But the condition of equation (A.22) can only be achieved in practice with barium titanate ceramic. For realizable designs in PZT-type ceramics, Q_m has to be greater than about 4.5 (see section 4.7).

The maximum power delivered to the load is obtained from equations (A.1) and (A.11), for $\Omega^2 = 0$. Thus

$$P_{max}/|V|^2 = RK^4/R_o^2(K^2 + d_m d_o)^2 \qquad\qquad (A.23)$$

$$\text{or} \quad P_{max}/|V|^2 = d_m d_o K^2/R_o(K^2 + d_m d_o)^2 \quad . \qquad\qquad (A.24)$$

.

APPENDIX II

Program for the Determination of the Average
Radiation Impedance in a Regular Array

```
*FORTRAN  OJRCE
      DIM NSIO  F1(101),F2(101)
      TEXT A/'MOR IS'/
      CLEAR F1(1),F2(1)
      PM=100.0
      PM=50.0
      PO=2500.0
      DO 11 RR=0.03,0.061,0.01
      DO 12 J=2,101
      F=(J-1)*PM+PO
      W=2.0*3.1415926*F
      CALL RADIMP(RR,W,SR,SX)
      F1(J)=SR
   12 F2(J)=SX/W
      CALL GRAPH(101,F1,A)
      CALL GRAPH(101,F2,A)
   11 CONTINUE
      END
```

```
*FORTRAN SOURCE
      SUBROUTINE RADIMP(RR,W,SR,SX)
      REAL M
      RD=2.5*RR
      N=15
      N=10
      RK=W/1500.0
      CLEAR SR,SX,RD1,RD2
      X=2.0*RR*RK
      M=(X/3.1)*4.0/3.1415926
      T=X*X/8.0
      DO 103 I=2,100
      SR=SR+T
      SX=SX+M
      T=-T*X*X/(4.0*I*(I+1.0))
      M=-M*X*X/(4.0*I*I-1.0)
  103 CONTINUE
      RN1=1.0-0.0411*RR*RK+0.138*(RR*RK)**2
      RN2=1.0+0.009*RR*RK+0.118*(RR*RK)**2
      DO 104 I=1,( -1)
      DO 104 JI=1,(I+1)
      J=JI-1
      XD=I*I+J*J
      XD=RK*RD*SQRT(XD)
      RF=6*(N-I)*(N-J)
      IF(J.EQ.I. R.J.E .0)RF=RF/2.0
      RD1=RD1+RF*SIN(XD)/XD
  104 RD2=RD2+RF*COS(XD)/XD
      SX=SX+S *R 2/(RN2*  *V)
      SR= R+SR*RD1/(RN1*  * )
      RETRN
      END
```

```
FORTRAN  OURCE
      SUBROUTINE GRAPH(N1,FX,A)
      TEX  F4,FS(101)/101*'-'/
      TEXT A,F3,F(101)
      DIMENSION FX(N1)
      N=N1/100
      CLE'R F,FXL,FXG
      DO 80 I=1,J1
      IF(FX(I).GT.FXG)FXG=FX(I)
      IF(FX(I).LT.FXL)FXL=FX(I)
 80   CONTINUE
      GFX=FXG-FXL
      L=-100.0*FXL/GFX+1.5
      DO 81 K=L,101,10
 81   F(K)='.'
      DO 82 K=L,1,-10
 82   F(K)='.'
      F(L)='I'
      WRITE(6,83)A,FXL,FXG
 83   FORMAT(1H1,'RESPONSE TO'3X,A8,5X,'FXL=',E1),3,3X,'FXG=',F10.
      FS(L)='I'
      IM=0
      DO 85 I=1,N1,N
      IM=IM+1
      J=100.0*(FX(I)-F(L)/GFX+1.5
      IF(IM.NE.1)GO TO 86
      F4=FS(J)
      FS(J)='*'
      WRITE(6,84)FS
      FS(J)=F4
      GO TO 85
 86   F3=F(J)
      F(J)='*'
      WRITE(6,84)F
 84   FORMAT(1H ,101A1)
      F(J)=F3
 85   IF(IM.EQ.10)IM=0
      FS(L)='-'
      RETURN
      END
```

APPENDIX III

Program for the Analysis of a Piezoelectric Sonar Transducer

```
FORTRAN
      BEGIN
      N1=101
      AL=1.0E4
      M1=100
      FM=10000.0
    . TT=1.0E-3
      BEGIN
      DIMENSION F1(M1+1),F2(M1+1),F(N1),PH(N1)
      DIMENSION F3(M1+1),F4(M1+1)
      DIMENSION FF(N1)
      TEXT A
      DT=TT/(N1-1)
      D2=2.0*DT
      D2=DT
      DW=2.0*3.1415926*FM/M1
      CALL FRERES(M1,FM,F1,F2)
      R=FM
      DO 11 I=2,(M1+1)
      W=DW*(I-1)
      F3(I)=R*(AL*F1(I)+W*F2(I))/(AL*AL+W*W)
      F4(I)=R*(AL*F2(I)-W*F1(I))/(AL*AL+W*W)
      FFF=-F1(I)/W
      F1(I)=F2(I)/W
   11 F2(I)=FFF
      CALL INFRA(M1,N1,F1,F2,FF,DW,D2)
      A='STEP'
      CALL GRAPH(N1,FF,A,5.0E-5,-5.0E-5)
      WS=50.0*DW
      L=3.1415926/(WS*D2)+0.5
      TF=D2*WS
      DO 14 I=1,M1
      WT=TF*(I-1)
   14 PH(I)=COS(WT)*WS
      CALL CON CL(FF,PH,M1,D2,'STIFSTEP')
      CLEAR PH
      DO 13 I=2,N1
      C1=1.0
      DO 15 J=1,I,L
      DG=2.0*FF(I-J+1)*C1
      C1=-1.0*C1
   15 PH(I)=PH(I)+DG
   13 PH(I)=PH(I)-FF(I)
      CALL GRAPH(N1,PH,'SQ WAVE',2.5E-4,-2.5E-4)
      CALL INFRA(M1,N1,F3,F4,PH,DW,D2)
      XM=0.1
      CALL GRAPH(N1,PH,'EXPLOS',XM,-XM)
      END
      END
```

```fortran
FORTRAN
      SUBROUTINE FRERES(M1,FM,F1,F2)
      DIMENSIO  F1(M1+1),F2(M1+1)
      DIMENSION FP(M1+1),F3(M1+1),F4(M1+1),F5(M1+1)
      REAL  M,MZC
      TEXT  A
      IMPLICIT REAL(L)CCMPLEX(Z,Y)
      DATA C70,TC,FI,PCC/15590.0,1.84E-5,2.51,9.606E-9/
      DATA LI,CI,MZO,TM/0.005,4.6E-11,2.28E5,8.2E-6/
      DATA LR,LF/0.4(4.8.07/
      DATA BZO, B,SZO,TS/2897.0,4.06E-5,3050.0,4.77E-6/
      DATA RR,LG,RC/0.C571,0.0947,2380.0/
      TAMB=0.014
      ZU-(0.0,1. )
      RC=4.84E6*PR*RR
      CLEAR F1(1),F2(1),FP(1),F3(1),F4(1),F5(1)
      PM=FM/M1
      DO 102 J=2,(M1+1)
      F=(J-1)*FM
      W=2.0*3.1415926*F
      AF=RR*F
      RC=0.3*F
      CLEAR SR,SX
      X=2.0*RR*W/15(0.C
      CALL ARRAY(AF,SR,SX)
      GO TO 101
      CALL LABAF(AF,SR,SX)
      SR=2.78E-4
      CALL IMFRAF(X,SR,SX)
  101 R=FC*SF
      XR=RC*SX
      R=R+FC
      CLEAR ZB,ZC
      ZA=(1.0,C.0)
      ZF=(1.0,0.0)
      ZZ=ZL*CZC*TAM(TC*W/2.0)
      ZF=ZZ+ZU*W*LI
      YI=W*CI*ZL
      Y=YI
      ZA=ZA+ZB*Y
      ZC=ZC+ZD*Y
      ZF=ZL*FZC*TAN(W*TM/2.0)
      Z=ZF+ZL*F*LI
      ZB=ZF+Z*ZA
      ZD=ZF+Z*ZC
      Y=SIN(W* M)*ZU/MZC
      ZA=ZA+ZB*Y
      ZC=ZC+ZD*Y
      ZZS=ZL*SZC*TAN(W*TS/2.0)
      Z=ZZS+ZM
      ZB=ZF+Z*ZA
      ZC=ZF+Z* C
      Y=ZL*SIN(W*TS)/SZC
      ZA=ZA+ZB*Y
      ZC=ZC+ZD*Y
      ZZB=ZL*BZC*TAN(W*TB/2.0)
      Z=ZL*W*LF+F+ZU*XR+ZZB+ZZS
      ZB=ZE+Z*ZA
      ZD=ZD+Z*ZC
      Y=ZU*SIN(W*TB)/BZO
      YB=Y
```

```
      ZA=ZA+ZB*Y
      ZC=ZC+ZD*Y
      Z=ZL*W*(LF+LI)+ZZB+RC
      ZB-ZI+Z*ZA
      ZD-ZI+Z*ZC
      Y-YI
      ZA=ZA+ZB*Y
      ZC=ZC+ZD*Y
      ZVR=(ZZ+/L*W*LI+ZB)/(1.0-ZA)
      ZVS=ZA*ZVR+Z
      ZI=ZC*ZVR+ZD-1.0
      ZIC=ZVR*(YI+YB*(1.0+YI*Z))+1.0+Z*YB
      YT=W*FCO*(ZU+TAND)
      YC=ZL*SIN(W*TC)/CZO
      ZVT=(ZVS+ZI/YC)/FI
      ZIN=ZI*FI+ZVT*YT
      ZVN=ZVT+ZIN*(RC+ZL*W*LG)
      ZZZ=ZVT/ZII+ZU*W*LG
      Z6=1.0E6*ZIN/ZVN
      G=REAL(Z6)
      B=AIMAG(Z6)
      CIN=AIMAG(1.0E12*ZIN/(ZVT*W))
      WRITE(6,111)F,G,B,CIN
111   FORMAT(1H ,4(2X,F7.1))
      YVN=ZIO/ZVN
      F1(J)=REAL(YVN)
      F2(J)=AIMAG(YVN)
      FP(J)=R*1.0E6*(F1(J)**2+F2(J)**2)
      F3(J)=CABS(ZZZ)
      IF(F3(J).GT.10000.0)F3(J)=10000.0
      F4(J)=ATAN2(AIMAG(ZZZ),REAL(ZZZ))*180.0/3.14159265
      F5(J)=ATAN2(F2(J),F1(J))*180.0/3.14159265
102   CONTINUE
      A='H P IMV'
      FXC=0.25E6/RG
      CALL GRAPH(101,FP,A,FXG,0.0)
      A='IN IMF M'
      CALL GRAPH(101,F3,A,10000.0,0.0)
      A='IN IMF P'
      CALL GRAPH(1 1,F4,A,100.0,-100.0)
      A='TF IMF P'
      CALL GRAPH(101,F5,A,200.0,-200.0)
      FM=RG
      RETURN
      END
```

```
FORTRAN
      SUBROUTINE INFTRA(M1,N1,F1,F2,F,DW,DT)
      DIMENSION F1(M1+1),F2(M1+1),F(N1)
      CLEAR T,F(1)
      DO 32 N=2,N1
      T-DT*(N-1)
      TS=F1(2)-F1(1)
      DO 31 M=2,M1
      TEM=DW*(M-1)*T
      FD1=F1(M+1)+F1(M-1)-2.0*F1( )
      FD2=F2(M+1)+F2(M-1)-2.0*F2(M)
   31 TS=TS+FD1*COS(TEM)-FD2*SI (TEM)
   32 F(N)=-TS/(DW*T*T*3.141593)
      RETURN
      END




FORTRAN
      SUBROUTINE GRAPH(N1,FX,A,FXG,FXL)
      TEXT F4,FS(101)/101*'-'/
      TEXT A,F3,F(101)
      DIMENSION FX(N1)
      N=N1/100
      CLEAR F
      DO 80 I=1,N1
      IF(FX(I).GT.FXG)FXG=FX(I)
      IF(FX(I).LT.FXL)FXL=FX(I)
   80 CONTINUE
      GFX=FXG-FXL
      L=-100.0*FXL/GFX+1.5
      DO 81 K=L,101,10
   81 F(K)='.'
      DO 82 K=L,1,-10
   82 F(K)='.'
      F(L)='I'
      WRITE(6,83)A,FXL,FXG
   83 FORMAT(1H1,'RESPONSE TO'3X,A8,5X,'FXL=',E10.3,3X,'FXG=',E10,
      FS(L)='I'
      IM=0
      DO 85 I=1,N1,N
      IM=IM+1
      J=100.0*(FX(I)-FX )/GFX+1.5
      IF(IM.NE.1)GO TO 86
      F4=FS(J)
      FS(J)='*'
      WRITE(6,84)FS
      FS(J)=F4
      GO TO 85
   86 F3=F(J)
      F(J)='*'
      WRITE(6,84)F
   84 FORMAT(1H ,101A1)
      F(J)=F3
   85 IF(IM.EQ.10)IM=0
      FS(L)='-'
      RETURN
      END
```

FCRTRAN

```
      SULRCLTIFE UNRAF(AF,SR,SX)
      DIMENSIO  AR(8),AX(8)
      CATA AR/C.0,0.C3, .1,0.21,0.39,0.55,0.72,0.89/
      CATA AX/0.0,0.2,0.4,0.58,n,65,0.62,0.5,0.4/
      I=INT(AF/75.0)+1
      R=AF/75.0+1.0-I
      IF(I.CE.P)CO TO 32
      SR=AR(I)+(AR(I+1)-AR(I))*R
      SX=AX(I)+(AX(I+1)-AX(I))*P
      GC TC 33
  32  SR=1.0
      SX=0.0
  33  SR=1.0*SR
      RETLRN
      END
```

FCRTRAN

```
      SUERCUTINE INFRAF(X,SR,SX)
      REAL M
      M=(X/3.0)*4.0/3.1415926
      T=X*X/2.C·
      CO 103 I=2,100
      SR=SR+T
      SX=SX+M
      T=-T*X*X/(4.0*I*(I+1.0))
      M=-M*X*X/(4.0*I*I-1.0)
 103  CONTINUE
      ENC
```

FCRTRAN

```
      SUERCUTINE ARRAY(AF,SR,SX)
      SR=0.475
      SX=0.06+(2.5E-6)*AF*AF
      IF(AF.GT.600.0)SX=0.0
      IF(AF.CT.600.0)SR=1.)
      RETLRN
      END
```

FORTRAN

```
      SUPRCLTIFE CONVOL(F,PH,N1,CT,A)
      CIMENSION F(N1),PH(N1),C(N1)
      TEXT A
      CLEAR C(1)
      CC 42 N=2,N1
      CLEAF C,C1,G2
      CC 41 M=1,(N-1)
      PA=PH(M)
      PB=PH(M+1)
      FA=F(N-M+1)
      FP=F(N-M)
      G1=G1+(PE-PA)*(FB-FA)
      G2=G2+(FA*(PE-PA)+PA*(FB-FA))
  41  G=C+PA*FA
  42  C(N)=CT*(G+G2/2.0+G1/3.))
      CALL GRAFH(N1,C,A,2.5F-4,-2.5E-4)
      RETLRN
      END
```

APPENDIX IV

Program for the Analysis of
Ladder Networks

```
FORTRAN
      BEGIN
      TEXT C(7),CC(7)/'F','I','S','W','E','Q','R'/
      TEXT CF(7)/' ','ELEC.IMP','D.C.STEP','SI ESTEP','XPLOSION',2*
      READ(5,11)M,C
  11  FORMAT(I2,1X,7A1)
      BEGIN


      TEXT INF1(M),INF2(M)
      DIMENSION A1(M+1),A2(M+1),A3(M+1),A4(M+1),VAL(M)
      DIMENSION AD(M+6),AN(M+6),BD(M+6),BN(M+6)
      CLEAR AD,AN,BD,BN
      DO 21 I=1,M
  23  FORMAT(2A1,F12.4)
  21  READ(5,23)INF1(I),INF2(I),VAL(I)
      DO 22 I=1,M
  20  FORMAT(1H ,2A1,F12.6)
  22  WRITE(6,20)INF1(I),INF2(I),VAL(I)
      R1=VAL(M)
      R2=VAL(1)
      CALL LAPLACE(M,INF1,INF2,VAL,A1,A2,A3,A4,IB,N)
      CALL WRITE(I,A1,A2,A3,A4,NB,N)
      TRACE L
      FC=5.C
      WC=FC*2.0*3 41.59265
      Z=1.0E-5
      DO 24 I=1,N
  24  AD(I)=A2(I)
      AN(NB+1)=1.
      DO 25 I=N,1,-1
      L=I
      IF(AN(I).GT.Z)GO TO 225
      IF(AD(I).GT.Z)GO TO 250
  25  CONTINUE
 250  DO 26 J=1,L
      AN(J)=AN(J)/AD(L)
  26  AD(J)=AD(J)/AD(L)
  27  IF(AD(1).LT.Z.AND.AN(1).LT.Z),29
      DO 28 J=1,L
      AD(J)-AD(J+1)
  28  AN(J)=AN(J+1)
      L=L-1
      GO TO 27
      TRACE BN,BD,N1,TT
  29  DO 214 K=1,7
      TT=WL/1000.0
      N1=100
      DO 210 J1=1,7
      J-J1
      IF(C(K).EQ.CC(J))GO TO 211
  21  CONTINUE
      GO TO 214
 211  GO TO(215,216,218,221,223,291,292),J
 215  CALL STEADY(AN,AD,L,R1,R2,2)
```

```
          G  TC 214
216   DC 217 I=1,L
      B (I)-AN(I)
217   BC(I) AC(I)
      I=L
      GO TO 212
 292  CALL STE CY(A2,A4,N,R1,R2,1)
 291  GC TC 214
218   IF(AN(1).LT.Z)CC TO 220
      DO 219 I=1,L
      BD(I+1)=AC(I)
219   BN(I)=AN(I)
      BD(1)-0.0
      I=L+1
      GO TC 212
220   DO 202 I=1,L
      BN(I)-AN(I+1)
202   BD(I)=AC(I)
      I=L
      GO TC 212
221   DC 222 I=1,L
      BN(I)=AN(I)
222   BD(I+2)=AC(I+2)+AC(I)
      BD(2)=AC(2)
      BC(1)-AC(1)
      I=L+2
      GO TC 212
223   DO 224 I=1,L
      BN(I)=AN(I)
224   BC(I+1)=0.265*AC(I+1)+AD(I)
      BD(1)-0.265*AC(1)
      I=L+1
212   T=TT*1 0000 .N/WC
      WRITE(6,213)CF(J),T
213   FCRMAT(1H1,'TRANSIENT RESPO'SE TO UNIT ',A8,'---------------
     1---TCTAL TIME = ',F6.1,' MICROSECS----------------------')
      CALL TRA SIENT(I,BN,BD,N ,TT)
      CLEAR BN,BC
214   CCNTINUE
225   CONTINUE
      END

      END
 FCRTRAN
      SLBRCUTINE CRAPH(N1,FX,F L,FXG)
      DIMENSICN FX(N1)
      TEXT F3,F(1 1)
      CLEAR F
      GFX=FXC-FXL
      L--100.0*FXL/CFX+1.5
      DO 81 K=L,1 1,10
 81   F(K)='.'
      DC 82 K=L,1,-10
 82   F(K)='.'
      F(L)='I'
      DO 85 I=1,N1
      J=10 .0*(FX(I)-FXL)/GFX+1.5
      F3=F(J)
      F(J)='*'
      WRITE(6,84)F
 84   FCRMAT(1H , 01A1)
 85   F(J)=F3
      RETURN
```

```
FORTRAN
      SUB OUTINE STEADY(A,B,M, 1,R2,1)
      DIMENSION A(N),P(N),FX(1J ),FY(1 0)
      COM LEX WI,XN,XD,Z
      CLEAR FXG,W,RM
      RR=1.C
      PI-3.141592653⁶6
      IF(M.EQ.1)RM=R1
      IF( .EC.2)RF=4.C*R1*R2
      DO 102 J=1, 00
      W=M+0.C2
      CLEAR XN,XD
      WI=(1.0,0.0)
      DC 1 1 I=1,M
      XN=XN+WI*A(I)
      XD=XD+WI*E(I)
101   WI=WI*CMFLX(0.0,W)
      Z=XN/XD-RM
      FX(J)=RR*(CABS(Z))**M
      IF(FX(J).CT.FXG)FXG=FY(J)
102   FY(J)=ATAN2(AIMAG(Z),PEAL(Z))
      WRITE(6,1C3)
103   FORMAT(1H1,'NCRMALIZED FREQUENCY RESPONSE FROM  0.0 KHZ TO 1
     1Z IN C.1 KHZ STEPS------------------------------------------')
      IF(M.EC.2)FXG=1.0
      CALL CRAFF(100,FX,0.0,FXG)
      WRITE(6,133)FXG
133   FORMAT(1H ,'FXG=',E12.4)
      WRITE(6,1C4)
104   FORMAT(1H1,'PHASE AS PERCENT OF PI-----------------------------
     1---------------------------------------')
      CALL CRAFF(100,FY,-PI,PI)
      RETURN
      END
FORTRAN
      SUBROUTINE TRANSIENT(N,CA,CB,N1,TT)
      DIMENSION CA(N),CB(N),X (N-1),A((N-1),(N-1)),FX( 1),XO(N-1)
      M=N-1
      CLEAR A,FXL,FXG
      DO 92 I=1,M
      A(M,I)=-CB(I)
      XC(I)=CA(N-I)
      IF(I.EC.1)GO TO 92
      A((N-I),(N-I+1))=1.0
      DO 91 J=1,(I-1)
91    XC(I)=XC(I)-XC(J)*CB(N-I+J)
92    CONTINUE
      T=TT/N1
      CALL CEAT(T,M,A)
      DC 95 I=1,N1
      CLEAR X
      DC 93 J=1,M
      DC 93 K=1,M
93    X(J)=X(J)+A(J,K)*XO(K)
      DC 94 J=1,M
94    XC(J)=X( )
      IF X(1). T.FXC)FXC=X(1)
      IF(X(1).LT.FXL)FXL=X(1)
95    FX(I)=X(1)
      CALL CRAFF(N1,FX,FXL,FXG)
      WRITE(6,96)FXL,FXG
96    FORMAT(1H ,'LEAST VALUE=',E10.3,45X,'GREATEST VAL E=', 1 .3)
      RETURN
      END
```

```fortran
FORTRAN
      SUBROUTINE LAPLACE(M,INF1,INF2,VAL,A1,A2,A3,A4,NB,N)
      TEXT INF1(M),INF2(M)
      DIMENSION A1(M+1),A2(M+1),A3(M+1),A4(M+1),VAL(M)
      CLEAR A1,A2,A3,A4,NB
      A1(1),A4(1)-1.0
      N=1
      DO 42 I=1,M
      A=VAL(I)
      IF (INF1(I).EG.'R') GO T  38
      N=N+1
      IF (INF2(I).EG.'P') GO TO 34
      IF (INF1(I).EG.'C') GO T) 32
      DO 31 J=2,N
      A1(J)=A1(J)+A3(J-1)*A
31    A2(J)=A2(J)+A*A4(J-1)
      GO TO 42
32    A=1.0/A
      NB=NB+1
      DO 33 J=N,2,-1
      A1(J)=A*A3(J)+A1(J-1)
      A2(J)=A*A4(J)+A2(J-1)
      A3(J)=A3(J-1)
33    A4(J)=A4(J-1)
      A1(1)=A*A3(1)
      A2(1)=A*A4(1)
      A3(1),A4(1)=0.0
      GO TO 42
34    IF (INF1(I).EG.'L') GO TO 36
      DO 35 J=2,N
      A3(J)=A3(J)+A*A1(J-1)
35    A4(J)=A4(J)+A*A2(J-1)
      GO TO 42
36    A=1.0/A
      NB=NB+1
      DO 37 J=N,2,-1
      A3(J)=A3(J-1)+A*A1(J)
      A1(J)-A1(J-1)
      A4(J)=A4(J-1)+A*A2(J)
37    A2(J)=A2(J-1)
      A3(1)=A*A1(1)
      A4(1)=A*A2(1)
      A1(1),A2(1)=0.0
      GO TO 42
38    IF (INF2(I).EG.'P') GO TO 4
      DO 39 J=1,N
      A1(J)=A1(J)+A*A3(J)
39    A2(J)=A2(J)+A*A4(J)
      GO TO 42
40    A=1.0/A
      DO 41 J=1,N
      A3(J)=A3(J)+A*A1(J)
41    A4(J)=A4(J)+A*A2(J)
42    CONTINUE
      RETURN
      END
```

```
FORTRAN
      SUBROUTINE F CEAT(T, M, )
      DIMENSION A(M,M),AB(M,M),ABY(M,M)
      CLEA  AM
      DO 61 I=1,M
      DO 61 J=1,M
 61   AM=AM+A(I,J)*A(I,J)
      AM=S RT(AM)
      AMT=AM*T
      K=AINT(AMT)
      Y=AMT-FLOAT(K)
      DO 62 I=1,M
      DO 62 J=1,M
      AB(I,J)=A(I,J)/AM
 62   AB (I,J)=Y*AB(I,J)
      CALL CEAB(M,ABY)
      CALL CEAB(M,AB)
      DO 65 KI=1,K
      CLEAR A
      DO 63 I=1,M
      DO 63 J=1,M
      DO 63 N=1,M
 63   A(I,J)=A(I,J)+AB(I,N)*ABY(N,J)
      DO 64 I=1,M
      DO 64 J=1,M
 64   ABY(I,J)=A(I,J)
 65   CONTINUE
      RETURN
      END

FORTRAN
      SUBROUTINE CEAB(M,B)
      DIMENSION A(M,M),B(M,M),BT(M,M)
      INTEGER X
      DO 71 I=1,M
      DO 70 J=1,M
      A(I,J)=B(I,J)
 70   B(I,J),BT(I,J)=0.0
.71   B(I,I)=1.0
      DO 75 X=30,1,-1
      DO 73 I=1,M
      DO 72 J=1,M
      DO 72 K=1,M
 72   BT(I,J)=BT(I,J)+A(I,K)*B(K,J)/X
 73   BT(I,I)=BT(I,I)+1.0
      DO 74 I=1,M
      DO 74 J=1,M
      B(I,J)=BT(I,J)
 74   BT(I,J)= .0
 75   CONTINUE
      RETURN
      END

FORTRAN
      SUBROUTINE WRITE(M,A1,A2,A3,A4,NB,N)
      DIMENSION A1(M+1),A2(M+1),A3(M+1),A4(M+1)
      WRITE(6,50)
 50   FORMAT(1H ,'              TRANSFER MATRIX OF SYSTEM')
      WRITE(6,51)NB
 51   FORMAT(1H ,.5X,'A',12X,'B',12X,'C',12X,'D',6X,'N3=',I2)
      DO 53 I=1,N
      J=I-1
 52   FORMAT(4 ,'S',I2,5X,4(F1 .3,2X))
 53   WRITE(6,52)J,A1(I),A2(I),A3(I),A4(I)
      RETURN
      END
```

REFERENCES

1. D.G.Tucker and B.K.Gazey, Applied Underwater Acoustics, (Pergamon Press, Oxford, 1966), Chapters 5 and 6.

2. D.Schofield, 'Transducers', in Underwater Acoustics, Vol.1, (V.M.Albers, ed.), (Plenum Press, New York, 1963), Chapter 1.

3. D.A.Berlincourt, D.R.Curran and H.Jaffe, 'Piezoelectric and Piezomagnetic Materials' in Physical Acoustics, Vol.1, pt.A (W.P.Mason, ed.). (Academic Press Inc., New York, 1964), pp.169-256.

4. R.S.Woollett, 'Effective Coupling Factor of Single Degree of Freedom Transducers', J.Acoust.Soc.Am., 40, pp.1112,1966.

5. F.Rosenthal and V.D.Mikuteit, 'Vibrations of Ferro-electric Transducer Elements loaded by Masses and Acoustic Radiation', IRE Natl.Conv.Record 7, part 6, pp.252, 1959.

6. B.A.Becken, 'Sonar' in Advances in Hydroscience, vol.1, (Ven Te Chow, ed.), (Academic Press Inc., New York, 1964), section IV, pp.55-78.

7. J.van Randeraat (ed.), Piezoelectric Ceramics (Mullard, London, 1968).

8. A.Block, 'Electro-mechanical Analogies and their Use for the Analysis of Mechanical and Electro-mechanical Systems', J.Inst.Elec.Eng., 92, pp.157-169, 1945.

9. F.A.Fischer, Fundamentals of Electroacoustics. (Interscience Publishers Inc., New York, 1955), Chapter 1.

10. L.L.Beranek, Acoustics (McGraw-Hill, New York, 1954), Chapter 3.

11. F.A.Firestone, 'A New Analogy between Mechanical and Electrical Systems', J.Acoust.Soc.Am., 4, pp.249, 1933.

12. G.J.O'Hara, 'Mechanical Impedance and Mobility Concepts', J.Acoust.Soc.Am., 41, pp.1180, 1967.

13. R.N.Thurston, 'Effect of Electrical and Mechanical Terminating Resistances on Loss and Bandwidth according to the Conventional Circuit of a Piezoelectric Transducer', I.R.E.Nat.Convention Record, Vol.7, part 6, pp.260, 1959.

14. M.Redwood, 'Transient Performance of a Piezoelectric Transducer', J.Acoust.Soc.Am., 33, pp.527-536, 1961.

15. E.J.Skudrzyk, Simple and Complex Vibratory Systems. (The Pennsylvania State University Press, University Park, Pennsylvania, 1968), Chapters 5 and 14.

16. W.P.Mason, Electromechanical Transducers and Wave Filters (D.van Nostrand Company, Inc., Princeton, New Jersey 1948), pp.200, 399.

17. G.E.Martin, 'Vibrations of Longitudinally Polarized Ferroelectric Cylindrical Tubes', J.Acoust.Soc.Am., 35, pp.510-520, 1963.

18. G.E.Martin, 'On the Theory of Segmented Electro-mechanical Systems', J.Acoust.Soc.Am., 36, pp.1366-1370, 1964.

19. G.E.Martin, 'Vibrations of Co-axially Segmented, Longitudinally Polarized Ferroelectric Tubes', J.Acoust.Soc.Am.36, pp.1496-1506, 1964.

20. J.S.Arnold and J.G.Martner, 'Description of the Resonances of Short Solid Barium Titanate Cylinders', J.Acoust.Soc.Am.31, pp.217-226, 1959.

21. E.P.Golubkov, 'Vibrations in Piezoceramic Tubes', Soviet Physics - Acoustics, Vol.12, No.1, July-September 1966, pp.18, 19.

22. L.E.Kinsler and A.R.Frey, Fundamentals of Acoustics, (John Wiley and Sons Inc., New York 1962), Chapter 7.

23. R.W.B.Stephen and A.E.Bate, Acoustics and Vibrational Physics. (Arnold, London, 1966), Appendices 35, 36.

24. P.H.G.Crane, 'Method for the Calculation of the Acoustic Radiation Impedance of Unbaffled and Partially Baffled Piston Sources', J.Sound Vib., 5, pp.257-277, 1967.

25. C.H.Sherman, 'Analysis of Acoustic interact'ons in Transducer Arrays', IEEE Transactions on Sonics and Ultrasonics, SU-13, 1, pp.9-15, 1966.

26. A.Freedman, 'Approximations for the Mutual Radiation Impedance Coefficients between Baffled and Unbaffled Circular Pistons', A.U.W.E.Technical Note 320/68, Oct.1968.

27. W.J.Toulis, 'Radiation Load on Arrays of Small Pistons', J.Acoust.Soc.Am., 29, pp.346, 1957.

28. J.C.Morris, 'Average Radiation Impedance of Circular Pistons in a Broadside Array', A.U.W.E.Technical Note 326/68, Dec.1968.

29. H.G.Baerwald, 'A Limit Theorem on Passive Reactance Two Ports with Constraints', IRE International Convention Record, Pt.4, pp.244, 1961.

30. Reference Data for Radio Engineers (International Telephone and Telegraph Corp., New York, 1956).

31. E.Green, Amplitude-Frequency Characteristics of Lad er Networks (Marconi's Wireless Telegraph Co., Chelmsford, Essex, 1954).

32. A.I.Zverev, Handbook of Filter Synthesis (John Wiley and Sons, Inc., New York, 1967), Chapter 6.

33. M.L.Liou, 'Time and Frequency Domain Analysis of Linear Time-Invariant Systems' in Systems Analysis by Digital Computer (F.F.Kuo and J.F.Kaiser, eds.), (John Wiley and Sons, Inc., New York, 1966), Ch pter 4.

34. R.Bracewell, ihe Fourier Transform and Some of Its Applications (McGraw-Hill, New York, 1965).